Effects of intracranial stimulation and the involvement of the human parahippocampal cortex in perception

Dissertation

zur

Erlangung des Doktorgrades (Dr. rer. nat.)

der

Mathematisch-Naturwissenschaftlichen Fakultät

der

Rheinischen Friedrich-Wilhelms-Universität Bonn

vorgelegt von

Simeon Knieling

aus

Cuxhaven

Bonn 2019

Angefertigt mit Genehmigung der Mathematisch-Naturwissenschaftlichen Fakultät der Rheinischen Friedrich-Wilhelms-Universität Bonn

1. Gutachter: Prof. Dr. Dr. Florian Mormann
2. Gutachter: Prof. Dr. Horst Bleckmann

Tag der Promotion: 16.09.2019
Erscheinungsjahr: 2019

Summary

How the human brain translates photons hitting the retina into conscious perception remains an open question. Throughout the medial temporal lobe (MTL), there are neurons (called concept cells) that change their firing rate when that neuron's preferred concept, e.g., a specific person or object, is seen. The firing rate of concept cells is correlated with perception. Nevertheless, it remains unclear whether or to what extent concept cells are involved in perceptogenesis, i.e., the creation of conscious percepts. Inferring from studies in monkeys, concept-specific neurons involved in perceptogenesis would be expected along the ventral and dorsal stream of visual processing (also called the *what* and *where* pathway, respectively). Various regions that are part of the dorsal stream are connected to the parahippocampal cortex (PHC), a region within the MTL. Compared to other MTL regions, lower selectivity, the absence of multimodal responses, and especially the shorter response latencies do not exclude an involvement of the PHC in perceptogenesis. In fact, damage to the parahippocampal place area (PPA, a part of the PHC) results in topographical disorientation. The goal of this thesis is to test the involvement of the PHC in perception by using electrical stimulation during a forced-choice categorization task involving landscapes versus animals.

First, we determined effective parameters for intracranial stimulation of brain tissue in epilepsy patients implanted with depth-electrodes for seizure monitoring. We investigated the effects of amplitude, phase width, frequency, and pulse-train duration on neuronal firing, the local field potential (LFP), and behavioral responses to evoked percepts. Frequency and charge per phase were the most influential parameters on all three signals. Both parameters showed a positive effect on event-related potentials (ERPs) in the LFP. Higher frequencies (especially around 200 Hz) lead to a short-term inhibition of neuronal firing, while higher charge per phase can have an inhibitory or excitatory effect on neuronal firing. All parameters had a positive effect on the reports of evoked percepts; on reports of phosphenes in response to stimulating close to the optic radiation as well as on reports of auditory verbal hallucinations in response to stimulating Heschl's gyrus.

Using functional magnetic resonance imaging (fMRI), we found that the PPA, i.e., the part of the PHC that is most selective towards images of landscapes, is rather small (up to 1‰ of total brain volume per hemisphere) with varying degrees of hemispheric laterality. Stimulating the PHC outside of the PPA - using a 100 ms high-frequency pulse train delivered at the natural response latency of the PHC - had no effect on categorizing landscapes. However, stimulating inside the PPA, close to the peak activation of the fMRI cluster, resulted in a 7% to 10% increase in landscape responses to ambiguous stimuli. Furthermore, stimulating the PPA also led to an increase in behavioral response time, especially to images with a predominant landscape component. None of our patients reported visual hallucinations of places or scenes in response to our stimulation protocols. Our data suggests that the PPA is involved in the perceptogenesis of landscapes at a stage that does not reach awareness, while the rest of the PHC is unlikely to be involved in perceptogenesis, at least not as it pertains to the perception of landscapes or animals.

We also developed an online spike sorting algorithm and an adaptive screening procedure for concept cells to pave the way for new paradigms involving informed feedback.

Contents

1. Introduction

Since the early beginnings of cognitive neuroscience, with people like Hans Berger (who pioneered EEG in 1929), Wilder Penfield (who pioneered ablative therapy for epilepsy in 1936) or Athur Ward (who pioneered micro-electrode recordings in humans in 1955), there has been great progress in our understanding of the human brain. Yet, it remains unclear how neurons cause complex functions such as emotions, memory, or conscious perception.

A candidate for contributing to the instantiation of conscious perception are neurons in the medial temporal lobe (MTL) that respond to stimulus categories (Kreiman et al. 2000; Mormann et al. 2011, 2017) or even more fine-grained concepts (Quian Quiroga et al. 2005, 2009). Many of these neurons only respond to a small subset of presented stimuli (high selectivity) and in most cases, the majority of the response-eliciting stimuli represent the same semantic concept (high invariance). Hence, these neurons have been termed *concept cells*. A concept cell would, e.g., reliably increase its firing rate shortly after the subject saw a picture of one particular person (e.g., the subject's spouse) but not in response to other people or objects. Other frequently found examples include broader concepts like "any presented flower" or even "any presented natural scenery".

1.1 Medial temporal lobe epilepsy

The discovery of concept cells was enabled by a diagnostic procedure (see Section 1.2) for epilepsy patients that allows to record the activity of individual neurons. A modern definition of epilepsy is given by Fisher et al. (2005):

> "Epilepsy is a disorder of the brain characterized by an enduring predisposition to generate epileptic seizures and by the neurobiologic, cognitive, psychological, and social consequences of this condition. The definition of epilepsy requires the occurrence of at least one epileptic seizure."
> "An epileptic seizure is a transient occurrence of signs and/or symptoms due to abnormal excessive or synchronous neuronal activity in the brain."

Seizures can originate in a rather local area or within widely distributed networks. Seizures originating in a local region or a network limited to one hemisphere are called *focal* (formerly *partial*), whereas seizures that originate within (and rapidly engage) bilaterally distributed networks are called *generalized* (Berg et al. 2010; Fisher et al. 2017). Depending on the afflicted brain regions, seizure symptoms may include subjective sensory or psychic phenomena (so called *auras*), changes in awareness or consciousness, and involuntary motor symptoms (Berg et al. 2010).

A region or network in which seizure activity originates is commonly referred to as *epileptic focus*. Some authors distinguish between a *seizure onset zone* and an *epileptogenic zone* (Rosenow and Lüders 2001). A seizure onset zone is where seizure activity starts, while an epileptogenic zone encompasses all tissue that is required for an epileptic seizure to occur. Here, we use the term epileptic focus similarly to seizure onset zone, meaning a brain region where seizure activity originates from. A patient can have more than one epileptic focus, resulting in different or similar seizure symptoms (Engel 2001). In addition, a single focus may give rise to multiple manifestations of seizure symptoms. For example, a patient may experience auras prior to only some seizures. Likewise, a focal seizure may terminate or it may progress into a secondarily generalized seizure (Engel et al. 2008).

In medial temporal lobe epilepsy (MTLE), an epileptic focus is located within (or rapidly recruits) structures in the medial part of the temporal lobe. MTLE is one of the most common forms of human epilepsy and it is often intractable to antiepileptic drugs (Engel 2001). In many cases, surgical disconnection or removal of the epileptic focus remains the only option for curative treatment. Encouragingly, Wiebe et al. (2001) found that patients who underwent surgical resection have fewer seizures and a better quality of life compared with patients receiving antiepileptic medication. Improved seizure control also leads to a reduction in seizure-mediated cognitive decline (Helmstaedter et al. 2003). Cognitive decline may be stopped and sometimes even partly reversed by successful surgery (Elger et al. 2004). Yet, there are cases in which surgery would be inadequate:

a) If the epileptic focus cannot be determined, there will be no target to resect.

b) If symptoms conform with MTLE but the true focus is located somewhere else, resection of MTL structures might yield poor results (Williamson, Boon, et al. 1992; Salanova et al. 1992; Palmini et al. 1993; Ho et al. 1994).

c) If seizures originate from both (left and right) MTL, adverse effects of surgery will usually outweigh the expected benefits. A removal of both hippocampi would leave

the patient with severe anterograde amnesia (Scoville and Milner 1957). Thus, until current efforts of creating a hippocampal prothesis (Berger et al. 2012; Song et al. 2017; Geng et al. 2018) are successful, the only surgical option remaining is to resect unilaterally. However, resecting unilaterally when a bilateral focus is diagnosed is less common, since seizure freedom may not be achieved while a risk of cognitive decline due to the resection persists. Unilateral resection is typically reserved for cases in which the majority of seizures originate from the same side.

1.2 Invasive presurgical evaluation

For the majority of patients, non-invasive diagnostics provide enough evidence to identify the epileptic focus for surgical resection. Yet, in some patients non-invasive diagnostics are insufficient or inconclusive. In those cases, depth-electrode recordings can be of great value. Spencer (1981) reviewed that compared with scalp EEG, depth EEG "could have enabled selection of 36% more patients for surgery by defining otherwise unidentifiable single epileptogenic foci" and "prevented surgery in another 18% by demonstrating different or additional epileptogenic foci in patients otherwise thought to have a single discharging focus amenable to resection".

Typically, depth electrodes are chronically implanted for 3 to 10 days to record invasive EEG (also called depth EEG or stereotactic EEG) from various regions of interest as part of an extensive presurgical evaluation (Rosenow and Lüders 2001). The duration for which the electrodes stay implanted largely depends on how frequently seizures are occurring. Clinicians typically wait until — ideally — at least 3 naturally occurring seizures are recorded before explantation. Occurrence of seizures is usually facilitated by carefully tapering off the antiepileptic medication the patients are on. If no seizures occur naturally, clinicians can try to induce seizures via electrical stimulation and might compare different regions with respect to the amplitude and duration of stimulation required to provoke a seizure (Bernier et al. 1990).

The implantation of depth electrodes at the University of Bonn Medical Center is based on Crandall et al. (1963); a laterotemporal approach, requiring one burr hole per electrode (see Figure 1.1). Modern improvements include magnetic-resonance imaging (MRI) assisted planning of electrode trajectories and magnetic-resonance compatible recording electrodes.

Precise electrode placement is achieved by coregistering (aligning) the MRI scan used for surgical planning with a computed tomography (CT) scan after attaching the head-mounted part of a Leksell stereotactic frame to the patient, moments before the surgery.

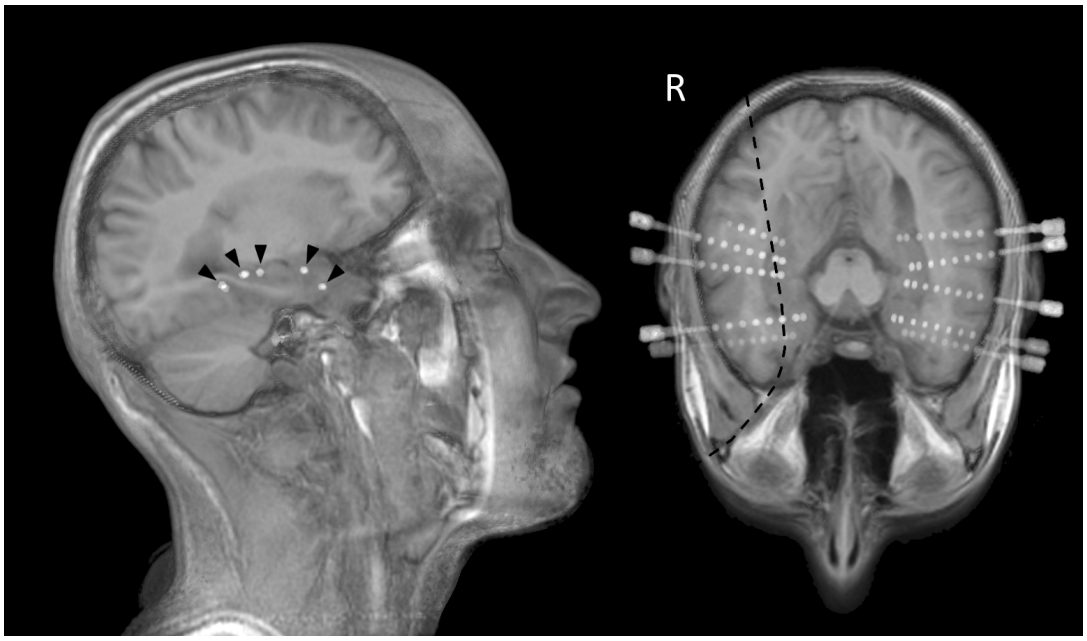

Figure 1.1: **Example of a typical depth-electrode placement in MTLE**. Fusion of a pre-operative structural MRI and a coregistered post-operative CT rendered by using volumetric ray casting. From anterior to posterior, electrodes were placed bilaterally in the entorhinal cortex, the amygdala, the anterior and middle hippocampus, as well as the parahippocampal cortex. Arrow heads point to the electrodes' macro-contacts. The dashed line in the axial view reflects the cut in the sagittal view.

Based on this alignment, a software calculates the rectangular and polar coordinates required by the Leksell apparatus for correct electrode placement.

Compared to scalp EEG, depth electrodes offer a greater spatial (and possibly also temporal, see Burle et al. 2015) resolution. Disadvantages include surgical risks and decreased spatial coverage. For each electrode, neurosurgeons carefully plan a trajectory to the target region that avoids larger blood vessels. Yet, small residual risks of brain hemorrhage and infection accumulate across electrodes. Thus, one important task of the neurologist is to determine a small number of target regions still sufficient to discover individual pathology. These targets are determined by each patient's clinical symptoms and history, considering findings from scalp-EEG-video monitoring, neuropsychological test profiles, and neuroimaging.

The standard implantation scheme for MTLE in Bonn includes bilateral placement of electrodes in the hippocampus, entorhinal cortex (ERC), amygdala, and parahippocampal cortex (PHC). They are all part of a network depicted in excerpts in Figure 1.2.

Epileptic foci in MTLE most commonly reside in the hippocampus (Engel 1998). Less often, epileptic foci are found in the entorhinal cortex (Spencer and Spencer 1994; Bartolomei et al. 2004) which nevertheless plays an important role in seizure pathogenesis.

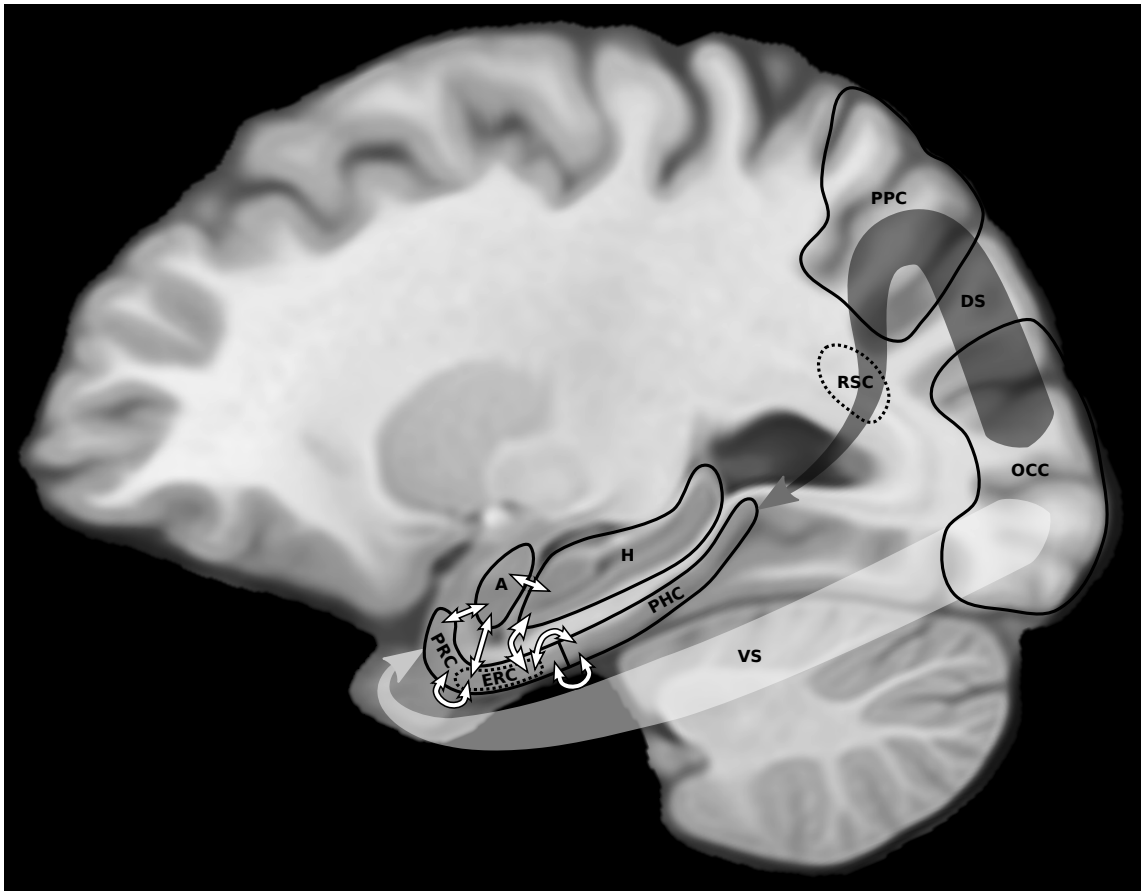

Figure 1.2: **Medial temporal lobe network**. The MTL is composed of distinct anatomical regions: the amygdala (**A**), the hippocampus (**H**), and the parahippocampal gyrus (PHG). The PHG is further segmented into entorhinal (**ERC**), perirhinal (**PRC**) and parahippocampal cortex (**PHC**). Visual information processing is separated into two paths: the ventral stream (**VS**, also known as *object stream* or *what pathway*) and the dorsal stream (**DS**, also known as *spatial stream* or *where pathway*) (Mishkin et al. 1983; Goodale and Milner 1992; Ranganath and Ritchey 2012). The ventral stream connects to the perirhinal cortex, while the dorsal stream connects to the parahippocampal cortex (Haan et al. 2006; Schultz et al. 2015). Along the dorsal stream, the parahippocampal cortex is connected to occipital regions (**OCC**), posterior parietal cortex (**PPC**), and retrosplenial cortex (**RSC**) (Squire and Wixted 2011; Kveraga et al. 2011; Libby et al. 2012; Aminoff et al. 2013; Miller et al. 2014). Parahippocampal and perirhinal cortices are the major sources of cortical input to the entorhinal cortex (Insausti et al. 1987; Suzuki and Amaral 1994) and the entorhinal cortex is the major source of cortical input to the hippocampus (Squire et al. 2004). Various connections are omitted for clarity; especially the amygdala is highly connected to a variety of other regions, including unimodal and polymodal association areas (Young et al. 1994; Suzuki 1996). Dotted lines represent regions medial to the presented sectional plane.

Siegel et al. (1990) found a positive correlation between good postoperative outcome and the amount of ERC tissue removed. Epileptic foci rarely reside in the amygdala (Wieser 1998; Eschle et al. 2002) but the amygdala is connected to a myriad of other regions (Young et al. 1994) and often suffers from epilepsy-related damage (Yilmazer-Hanke et al. 2000). While the epileptic focus could be restricted to one of these regions, the fact that shared pathologies between hippocampal and extrahippocampal structures (Moran et al. 2001) are often observed, indicates that they frequently recruit each other. The variability of pathologies further suggests various possible seizure pathways (Yilmazer-Hanke et al. 2000).

The PHC is connected to parietal and occipital regions (Libby et al. 2012; Aminoff et al. 2013). The PHC is targeted to identify cases of asymptomatic (silent) seizure onset in parietal (Williamson, Boon, et al. 1992; Ho et al. 1994) or occipital (Williamson, Thadani, et al. 1992; Salanova et al. 1992; Palmini et al. 1993) regions that quickly recruit MTL structures. At this stage they become symptomatic and are identified as MTLE seizures (Foldvary et al. 2001; Andermann 2003; Harroud et al. 2012).

To summarize, by identifying the onset of neuronal seizure activity in depth EEG and following its propagation over various electrodes in different regions of interest, clinicians can determine if a resection would be feasible and where as well as how much tissue should be removed. If a resection is feasible, clinicians often decide between a unilateral *amygdalohippocampectomy* (removal of the amygdala and hippocampus) and a unilateral (anterior) *temporal lobectomy*, depending on how much tissue needs to be removed to likely obtain seizure freedom (Siegel et al. 1990; Wiebe et al. 2001). Over 60% of these surgeries result in seizure freedom and over 90% result in a seizure reduction by at least 50% (Helmstaedter et al. 2003; Harroud et al. 2012; Engel 1998).

1.3 Intracranial micro-electrode recordings

In order to combine invasive presurgical monitoring with clinical as well as basic research on the activity of individual neurons, a few institutions worldwide (including the center in Bonn) routinely use *Behnke–Fried electrodes* (Fried et al. 1999). The hollow lumen of this clinical macro-electrode allows for the insertion of a micro-wire bundle that extends beyond the tip of the macro-electrode (see Figure 1.3); a technique introduced by Babb et al. (1973). Insertion of micro-wires through clinical macro-electrodes adds a negligible risk to the patient. The micro-wire bundle encompasses 8 insulated wires and 1 uninsulated wire intended to be used as a local reference electrode.

The signal measured in electrophysiological recordings is the difference in electric

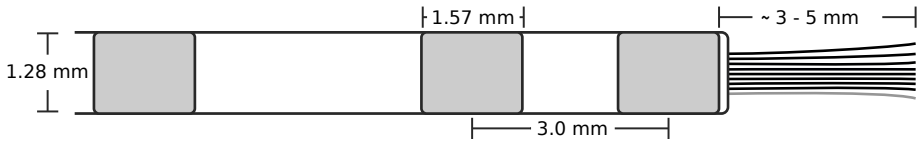

Figure 1.3: **Schematic of a Behnke–Fried electrode with micro-wire bundle**. Micro-wire tips are cut during surgery to ensure that impedances of free surfaces are not altered during the sterilization process.

potential between two electrodes. Consequently, it is measured in volts. The measurement is performed by a data acquisition system (also called recording system or amplifier). The signal is amplified, converted from analog to digital, and sent to a computer for display and storage purposes.

Recording systems pick up electrophysiological signals around the electrodes, but also unwanted signals like electronic noise (continuous signal distortions) from surrounding electronic devices and artifacts (short signal disturbances) from cable movements or other sources. To reduce noise, two electrodes with similar physical properties (including electrical impedance) can be placed in close proximity to each other. In such a bipolar setup, the influence of electromagnetic noise on the electric potential picked up by both electrodes is similar. Hence, when measuring the difference, noise (as well as neuronal signals from further away) is largely removed. One disadvantage of a bipolar setup is the difficulty to ascribe the origin of a signal component to one or the other electrode.

To restrict the signal (or at least certain components of it) to one electrode (called the recording electrode), changes in the electric potential picked up by the other electrode (called the reference electrode) should ideally be absent or at least be of significantly lower frequency or amplitude. Such a monopolar recording is implemented by decreasing the reference's impedance and/or by increasing its surface area. As a result, the reference picks up the electric potential of a larger field and high-frequency components mostly average out. Hence, in a monopolar recording, high-frequency components typically reflect activity close to the recording electrode.

In micro-electrode recordings (MER), the high impedance of micro-wires (typically 100 to 800 kΩ) allows to pick up high frequency components (e.g., spikes caused by action potentials) only in the immediate vicinity of the electrode's surface. Given the small surface of micro-electrodes (e.g., the cross section of a 40 µm wire), only action potentials from a few neurons close to the tip will cause spikes in the signal.

1.4 Screening for concept cells

Once depth electrodes and micro-wires are implanted and signals are being recorded, a unique setting for cognitive neuroscience is established that allows to record action potentials of individual neurons from within the brain of an awake and behaving human being. A hallmark finding originating from this setting is the discovery of concept cells in the human MTL (Quian Quiroga et al. 2005). Concept cells are neurons that temporarily increase their firing rate in response to their preferred concept but not (or to a lesser extent) in response to other concepts. One famous example is the *Jennifer Aniston neuron* described in Quian Quiroga et al. (2005) that would temporarily increase its firing rate in response to various images depicting the actress Jennifer Aniston but not in response to images of other people (including other blonde actresses), animals, or objects.

Concept cells are found by screening for response-eliciting stimuli. These stimuli can be images, written words, or auditory stimuli (Quian Quiroga et al. 2009). A response-eliciting stimulus reliably causes a neuronal response (i.e., a transient increase in a neuron's firing rate) a certain time after the subject has been presented with the stimulus. The time between stimulus presentation and the neuron's response is called response latency. The average latency varies across regions of the MTL (Mormann et al. 2008).

In animals, screenings are often conducted by repeatedly presenting the animal with a small number of stimuli while moving the recording electrode until a cell is found that responds to one of the stimuli. In humans, this method can be used in an intra-operative environment, since micro-electrodes (especially targeting electrodes) can be moved during surgery. However, Behnke–Fried electrodes do not provide the functionality to move them after implantation. Even if this were to become a possibility in the future, repetition suppression (Pedreira et al. 2010; Rey et al. 2015) could render this type of screening less effective: The number of action potentials fired by a concept cell in response to a stimulus decreases with repeated presentation of the same stimulus. When the micro-electrode reaches the spatial proximity of a responding concept cell only after multiple previous presentations, a weakened neuronal response could decrease the chance of correctly identifying the stimulus as response-eliciting.

Another way to screen for response-eliciting stimuli is to present the subject with a multitude of different stimuli while leaving the electrode in place. Due to the fixed electrode positions, this has become the standard screening procedure in concept-cell research.

The expected yield of a screening, i.e., the number of response-eliciting stimuli, increases with the amount and variety of presented stimuli as well as with their personal familiarity and/or relevance to the individual patient (Viskontas et al. 2009). However, increasing the screening's duration has the negative effect that patients tend to get more distracted (sometimes even bored or annoyed) as experimental durations increase. Distractions lead to a larger number of missed presentations and, as a consequence, to a decrease in the expected yield of the screening. Chapter 2 describes an adaptive screening procedure that increases the number of presented stimuli by 30% without increasing the duration of the experimental session.

1.5 Spike sorting

Even though the micro-wires inserted through Behnke–Fried electrodes have a high impedance and a diameter of only 40 µm, they tend to pick up action potentials from more than one surrounding neuron; meaning the recorded signal often contains spikes from different neurons.

Fortunately, spike-shapes of different neurons recorded at a fixed point in space are often distinguishable. First, interneurons have a shorter spike width than principal cells (Csicsvari et al. 1998; Dannenberg et al. 2015). Second, the shape of a recorded action potential varies as a function of a neuron's position relative to the recording electrode. Thus, they can be sorted into different groups (usually called clusters) according to their shape. The goal is that each cluster corresponds to the entire activity of just one neuron.

Due to noise and movement artifacts, this goal can currently only be considered an ideal. A more practical approach is to differentiate between single and multi-units. Compared with a multi-unit, a single unit should be purer (fewer false positives) and more complete (fewer false negatives). Unfortunately, there is no generally accepted criterion for determining if a cluster should be labeled a single or a multi-unit. A reasonable suggestion for quality metrics to help distinguish between single and multi-units was made by Hill et al. (2011).

Spike-sorting algorithms can be separated into two groups: online and offline algorithms. Offline algorithms require the entire input (i.e., all recorded spike shapes) before the sorting process can start. Thus, they are unsuited for real-time analyses, since they would not have access to future input.

Online algorithms process the input sequentially as it becomes available. With less information available — especially at the beginning of the sorting process — their results are often inferior to their offline counterparts. However, their sequential processing makes

them ideal for real-time analyses.

Human micro-electrode recordings are particularly challenging to sort, due to the noisy medical equipment and movement artifacts. Quian Quiroga et al. (2004) published a spike-sorting software (Wave_Clus) particularly suited to automate this task. It has long been the standard in the field. The Wave_Clus methodology was significantly improved and extended by Niediek et al. (2016), resulting in a software called Combinato. Yet, both are limited to offline analyses. Chapter 3 describes an online spike-sorting algorithm capable of outperforming Wave_Clus.

1.6 Perception in the MTL

Using screenings and spike sorting, several studies have demonstrated a correlation between concept-cell activity and conscious perception (Kreiman et al. 2002; Quian Quiroga, Mukamel, et al. 2008; Quian Quiroga et al. 2014; Reber et al. 2017). Yet, a causal connection remains to be established.

Do concept cells instantiate perception or do they act downstream of perception, e.g., as a link between perception and memory formation? If the activity of concept cells causes perception, activating these cells artificially, e.g., via electrical stimulation, should have a noticeable influence on perception.

In the macaque monkey, a causal relationship between perception and face-selective cells in the inferior temporal (IT) cortex has been demonstrated using electrical stimulation (Afraz et al. 2006). In a forced-choice task, monkeys had to categorize noisy images as either a *face* or a *non-face*. Micro-stimulation of face-selective clusters of neurons biased monkeys towards selecting the face category. The effect size depended on various factors. First, increased face selectivity of a stimulated cluster was associated with a greater magnitude of behavioral bias. Second, a greater size of the cluster of face-selective neurons was also associated with a greater magnitude of behavioral bias. Stimulating sites that were not face-selective had no effect. Finally, timing of stimulation pulses relative to stimulus onset was also important. The greatest effect was observed when stimulation was applied with the same onset latency that these cells naturally responded with.

Afraz et al. (2006) stimulated in the lower bank of the superior temporal sulcus and in subdivision *a* of the regio temporalis propria (see von Economo and Koskinas 1925; Seltzer and Pandya 1978). Compared to face-selective cells in these regions of the macaque brain, concept cells in most regions of the human MTL do not seem to organize in clusters of semantic similarity on a microscopic level. However, responses to some

stimulus categories are more frequently found in certain macroscopic regions: Neuronal responses to animals (Mormann et al. 2011) and faces (Fried et al. 1997; Rutishauser et al. 2011) have been found to be more prevalent in the amygdala than in other MTL regions whereas neuronal responses to scenes (Mormann et al. 2017) have been found to be more prevalent in the PHC. Mormann et al. (2017) also reported that the density of scene-selective cells in the PHC is high enough to record evoked potentials in the local field potential (LFP) in response to scene presentations. Furthermore, functional MRI (fMRI) studies showed a gradient of increasing scene selectivity from anterior to posterior parts of the PHC (Litman et al. 2009), culminating in the parahippocampal place area (PPA, see Epstein and Kanwisher 1998); the part of the PHC that is most selective to scenes.

While concept cells can be found throughout the MTL, their properties vary, and so might their involvement in perception. Mormann et al. (2008) found that cells in the PHC show a significantly lower latency and less selectivity than cells in the amygdala, hippocampus, and entorhinal cortex; indicating that the PHC is involved in earlier processes (possibly related to perception) than other regions of the MTL that have been associated with declarative memory (Quian Quiroga 2012).

Another line of evidence for the notion that the PHC is involved in perception stems from lesion studies. Typically, when the PPA is damaged (e.g., due to a stroke) patients report topographical disorientation (Barrash et al. 2000). Interestingly, Henry Molaison (better known as H. M.) — who was unable to form new declarative memories after a bilateral MTL resection — had no detectable deficits in perception (Scoville and Milner 1957). The resection included (among others) the amygdalae, the entorhinal cortices and the anterior part of both hippocampi, while the parahippocampal cortices were largely left intact (Corkin et al. 1997).

Based on these findings, we hypothesize that concept cells in the PHC are involved in object recognition and perceptogenesis. In Chapter 6, we test this hypothesis by stimulating the PPA during a categorization task involving landscape and animal stimuli.

1.7 Intracranial stimulation

One method to test the causal involvement of a brain region in a certain cognitive function is to stimulate that region electrically through implanted electrodes. Electrical stimulation could be applied through the micro-wires or through the macro-contacts. Afraz et al. (2006) used micro-stimulation to stimulate microscopic clusters of face-selective neurons. They found that the degree of selectivity as well as the size of the

cluster of face-selective cells were both important factors for inducing a behavioral bias. Given the macroscopic size of the PPA, macro-stimulation appears to be more effective to excite a sufficiently large network of scene-selective cells to affect the behavior of untrained humans. Furthermore, based on the following principles, macro-stimulation is generally considered safer.

Electrical stimulation in the brain acts by depolarizing membranes of excitable cells. When a voltage is applied between two electrodes, charge is transferred from the electrode to the extracellular fluid and vice versa. Charge transfer can be capacitive or faradaic.

Capacitive charge transfer is mediated via a redistribution of ions in the extracellular fluid around the electrode. The negatively driven electrode (cathode) attracts positively charged ions (cations) while repelling negatively charged ions (anions). Consequently, the positively driven electrode (anode) attracts anions while repelling cations. This redistribution of charge is reversible.

However, if charge densities exceed a certain threshold, capacitive charge transfer is insufficient and electrons will start crossing from the electrode into the extracellular fluid and vice versa. This form of charge transfer is called faradaic and results in oxidation and reduction. These electrochemical reactions mainly result in changes in the extracellular fluid's pH and the formation of H_2 and O_2. For a comprehensive review on stimulation safety see Merrill et al. (2005) and Cogan (2008). In small doses, most of these reactions appear to be harmless. Subtle changes in pH can be compensated by diffusion, O_2 is required to maintain cellular function and H_2 may even have neuroprotective properties (Iketani and Ohsawa 2017). However, if these reaction products accumulated too quickly, they could reach neurotoxic concentrations.

The main difference between micro- and macro-stimulation is the size of the electrode and, more importantly, its surface area. In a Behnke–Fried electrode (see Figure 1.3), the surface area of a macro-contact is approximately 6 mm^2, while the surface area of a micro-wire (except for the reference wire) is approximately 0.0013 mm^2. Since charge transfer occurs at the electrode's surface, micro- and macro-stimulation require different parameter values in order to be safe but effective. Common parameters are depicted in Figure 1.4. To neutralize the redistribution of ions caused by capacitive charge transfer, stimulation pulses often have a second phase of equal charge but inverse polarity. This prevents an accumulation of charge over successive pulses that might otherwise culminate in faradaic charge transfer.

While parameter values reported for macro-stimulation vary (Benabid et al. 1987; Arzy et al. 2006; Murphey et al. 2009; Parvizi et al. 2012; Mégevand et al. 2014),

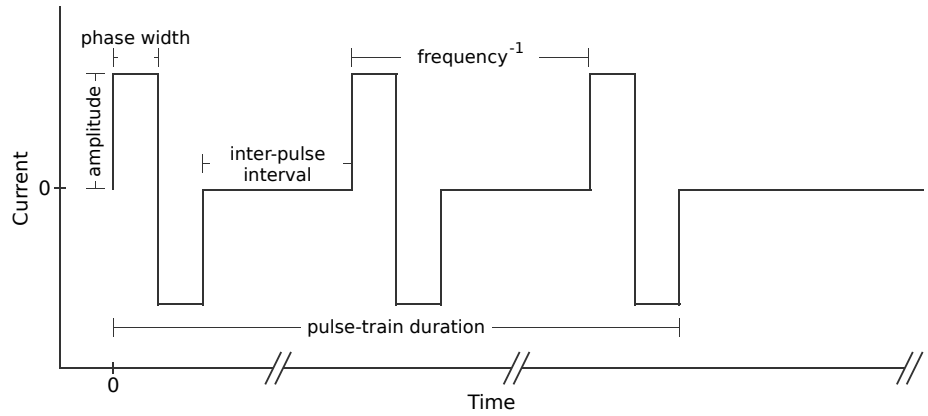

Figure 1.4: **Pulse train of charge-balanced biphasic stimulation pulses**. A pulse consists of two phases of equal but opposite charge. Typically, they are equal in their absolute *amplitude* and duration (*phase width*). Pulses are repeated at a certain *frequency* for a certain duration (*pulse-train duration*). Some protocols allow for an inter-phase interval, separating the positive and the negative phase (not shown).

they typically stay far below the threshold for faradaic charge transfer. For example, a relatively strong pulse of 3 mA and a phase width of 200 µs delivered between two macro-contacts of a Behnke–Fried electrode would cause a charge density of 10 µC/cm^2. In this case, the threshold for faradaic charge transfer would be between 50 and 100 µC/cm^2 (Rose and Robblee 1990).

The reasons for choosing specific parameter values are rarely reported. They mostly appear to be a matter of heuristics, technical capabilities, and previously reported values. A prominent example is the default frequency of 130 Hz for deep brain stimulation (DBS) in movement disorders. While short-term benefits of DBS for Parkinson's disease have long been known from intra-operative targeting, Benabid et al. (1987) was the first to report chronic DBS as a treatment option for Parkinson's disease. The authors noted that the optimal frequency seemed to be 200 Hz, but their implantable stimulator was limited to a maximum of 130 Hz.

In Chapters 4 and 5, we compare various combinations of stimulation-parameter values based on their effects on neuronal firing, event-related potentials (ERP), and evoked percepts.

1.8 Aim of this thesis

In this chapter we have reviewed the origins and basics of concept-cell research in the human MTL. Since their discovery by Kreiman et al. (2000, 2002) and Quian Quiroga et al. (2005), concept cells have been the subject of investigation in numerous studies

(see Quian Quiroga 2012 for a review). Yet, a lot of open questions remain.

The main part of this thesis focuses on the involvement of temporal lobe structures in perception. Based on the literature we discussed in Section 1.6, we hypothesize that the PHC (and in particular the PPA) is involved in perceptogenesis. We aim to test this hypothesis by inducing neuronal activity in the PPA via electrical stimulation. In Chapter 4 — to find effective stimulation parameters — we compare and rank different combinations of parameter values based on their effects on neuronal firing rates, the LFP, and evoked percepts. In Chapter 5, we reliably induce acoustic verbal hallucinations by stimulating inside the transverse temporal gyrus (Heschl's gyrus), which largely overlaps with primary auditory cortex. Lastly, in Chapter 6 we design a forced-choice categorization task for landscapes versus animals, and measure the bias induced by either amygdala or PHC stimulation.

Another open question addresses the encoding of concepts. Primarily, there have been two opposing theories: *sparse coding* versus *distributed coding* (see Quian Quiroga, Kreiman, et al. (2008) for a review). The sparse coding theory assumes that a concept is encoded in the individual activity of just a few dedicated neurons. In contrast, distributed coding assumes that a concept is encoded in the collective activity of a larger network.

While the literature is leaning towards sparse coding, a regular screening session of about 30 minutes cannot sample enough concepts to exclude the possibility that concept cells that seem invariant to one particular concept are not involved in encoding other concepts as well. Mapping the *semantic tuning curve* or *semantome* of a concept cell — i.e., the entirety of concepts that a cell responds to — would require a more elaborate approach: Once a concept cell has been identified, semantically related stimuli could be presented and their neuronal response evaluated ad-hoc. Related concepts that also elicit a response in the same neuron would inform the next iteration of semantically related candidate stimuli, etc. By evaluating the cell's response to these related stimuli, the semantic network that this cell is involved in might be uncovered.

In the next two chapters of this thesis, we lay the foundation of such an exhaustive screening procedure. An adaptive screening, capable of evaluating neuronal responses in real time, is described in Chapter 2. Ideally, the screening should also be able to evaluate neuronal responses of previously silent cells responding to a stimulus added during later iterations. This newly found neuron might be part of the initial concept-cell's network or at least could be used for follow-up experiments. This would require an online clustering algorithm capable of performing in a noisy medical environment. Such an algorithm is described in Chapter 3.

1.9 References

Afraz S.-R, Kiani R, and Esteky H (2006). *Microstimulation of inferotemporal cortex influences face categorization*. Nature 442.7103:692–695.

Aminoff EM, Kveraga K, and Bar M (2013). *The role of the parahippocampal cortex in cognition*. Trends in Cognitive Sciences 17.8:379–390.

Andermann F (2003). *Pseudotemporal vs neocortical temporal epilepsy*. Neurology 61.6:732.

Arzy S, Seeck M, Ortigue S, Spinelli L, and Blanke O (2006). *Induction of an illusory shadow person*. Nature 443.7109:287.

Babb TL, Carr E, and Crandall PH (1973). *Analysis of extracellular firing patterns of deep temporal lobe structures in man*. Electroencephalography and Clinical Neurophysiology 34.3:247–257.

Barrash J, Damasio H, Adolphs R, and Tranel D (2000). *The neuroanatomical correlates of route learning impairment*. Neuropsychologia 38.6:820–836.

Bartolomei F, Wendling F, Régis J, Gavaret M, Guye M, and Chauvel P (2004). *Pre-ictal synchronicity in limbic networks of mesial temporal lobe epilepsy*. Epilepsy Research 61.1:89–104.

Benabid AL, Pollak P, Louveau A, Henry S, and de Rougemont J (1987). *Combined (thalamotomy and stimulation) stereotactic surgery of the VIM thalamic nucleus for bilateral Parkinson disease*. Applied Neurophysiology 50.1:344–346.

Berg AT, Berkovic SF, Brodie MJ, Buchhalter J, Cross JH, Van Emde Boas W, Engel J, French J, Glauser TA, Mathern GW, Moshé SL, Nordli D, Plouin P, and Scheffer IE (2010). *Revised terminology and concepts for organization of seizures and epilepsies: Report of the ILAE Commission on Classification and Terminology, 2005–2009*. Epilepsia 51.4:676–685.

Berger H (1929). *Über das Elektrenkephalogramm des Menschen*. Archiv für Psychiatrie und Nervenkrankheiten 87.1:527–570.

Berger TW, Song D, Chan RHM, Marmarelis VZ, LaCoss J, Wills J, Hampson RE, Deadwyler SA, and Granacki JJ (2012). *A Hippocampal Cognitive Prosthesis: Multi-Input, Multi-Output Nonlinear Modeling and VLSI Implementation*. Ieee Transactions on Neural Systems and Rehabilitation Engineering 20.2:198–211.

Bernier GP, Richer F, Giard N, Bouvier G, Merrier M, Turmel A, and Saint-Hilaire J.-M (1990). *Electrical Stimulation of the Human Brain in Epilepsy*. Epilepsia 31.5:513–520.

Burle B, Spieser L, Roger C, Casini L, Hasbroucq T, and Vidal F (2015). *Spatial and temporal resolutions of EEG: Is it really black and white? A scalp current density*

view. International Journal of Psychophysiology. On the benefits of using surface Laplacian (current source density) methodology in electrophysiology 97.3:210–220.

Cogan SF (2008). *Neural Stimulation and Recording Electrodes*. Annual Review of Biomedical Engineering 10.1:275–309.

Corkin S, Amaral DG, González RG, Johnson KA, and Hyman BT (1997). *H. M.'s Medial Temporal Lobe Lesion: Findings from Magnetic Resonance Imaging*. Journal of Neuroscience 17.10:3964–3979.

Crandall PH, Walter RD, and Rand RW (1963). *Clinical Applications of Studies on Stereotactically Implanted Electrodes in Temporal-Lobe Epilepsy*. Journal of Neurosurgery 20.10:827–840.

Csicsvari J, Hirase H, Czurko A, and Buzsáki G (1998). *Reliability and state dependence of pyramidal cell-interneuron synapses in the hippocampus: an ensemble approach in the behaving rat*. Neuron 21.1:179–189.

Dannenberg H, Pabst M, Braganza O, Schoch S, Niediek J, Bayraktar M, Mormann F, and Beck H (2015). *Synergy of direct and indirect cholinergic septo-hippocampal pathways coordinates firing in hippocampal networks*. The Journal of Neuroscience: The Official Journal of the Society for Neuroscience 35.22:8394–8410.

Elger CE, Helmstaedter C, and Kurthen M (2004). *Chronic epilepsy and cognition*. The Lancet. Neurology 3.11:663–672.

Engel J, Williamson PD, Berg AT, and Wolf P (2008). *Classification of Epileptic Seizures*. Epilepsy: A Comprehensive Textbook. 2nd Edition. Vol. 1. 3 vols. Lippincott Williams and Wilkins.

Engel J (1998). *Etiology as a risk factor for medically refractory epilepsy: a case for early surgical intervention*. Neurology 51.5:1243–1244.

Engel J (2001). *Mesial Temporal Lobe Epilepsy: What Have We Learned?* The Neuroscientist 7.4:340–352.

Epstein R and Kanwisher N (1998). *A cortical representation of the local visual environment*. Nature 392.6676:598–601.

Eschle D, Siegel AM, and Wieser H.-G (2002). *Epilepsy with severe abdominal pain*. Mayo Clinic Proceedings 77.12:1358–1360.

Fisher RS, Boas WvE, Blume W, Elger C, Genton P, Lee P, and Engel J (2005). *Epileptic Seizures and Epilepsy: Definitions Proposed by the International League Against Epilepsy (ILAE) and the International Bureau for Epilepsy (IBE)*. Epilepsia 46.4:470–472.

Fisher RS, Cross JH, French JA, Higurashi N, Hirsch E, Jansen FE, Lagae L, Moshé SL, Peltola J, Roulet Perez E, Scheffer IE, and Zuberi SM (2017). *Operational classifi-*

cation of seizure types by the International League Against Epilepsy: Position Paper of the ILAE Commission for Classification and Terminology. Epilepsia 58.4:522–530.

Foldvary N, Klem G, Hammel J, Bingaman W, Najm I, and Lüders H (2001). *The localizing value of ictal EEG in focal epilepsy*. Neurology 57.11:2022–2028.

Fried I, MacDonald KA, and Wilson CL (1997). *Single Neuron Activity in Human Hippocampus and Amygdala during Recognition of Faces and Objects*. Neuron 18.5:753–765.

Fried I, Wilson CL, Maidment NT, Engel J, Behnke E, Fields TA, Macdonald KA, Morrow JW, and Ackerson L (1999). *Cerebral microdialysis combined with single-neuron and electroencephalographic recording in neurosurgical patients*. Journal of Neurosurgery 91.4:697–705.

Geng K, Shin DC, Song D, Hampson RE, Deadwyler SA, Berger TW, and Marmarelis VZ (2018). *Mechanism-Based and Input-Output Modeling of the Key Neuronal Connections and Signal Transformations in the CA3-CA1 Regions of the Hippocampus*. Neural Computation 30.1:149–183.

Goodale MA and Milner AD (1992). *Separate visual pathways for perception and action*. Trends in Neurosciences 15.1:20–25.

Haan Md, Mishkin M, Baldeweg T, and Vargha-Khadem F (2006). *Human memory development and its dysfunction after early hippocampal injury*. Trends in Neurosciences 29.7:374–381.

Harroud A, Bouthillier A, Weil AG, and Nguyen DK (2012). *Temporal Lobe Epilepsy Surgery Failures: A Review*. Epilepsy Research and Treatment 2012.

Helmstaedter C, Kurthen M, Lux S, Reuber M, and Elger CE (2003). *Chronic epilepsy and cognition: A longitudinal study in temporal lobe epilepsy*. Annals of Neurology 54.4:425–432.

Hill DN, Mehta SB, and Kleinfeld D (2011). *Quality metrics to accompany spike sorting of extracellular signals*. The Journal of Neuroscience: The Official Journal of the Society for Neuroscience 31.24:8699–8705.

Ho SS, Berkovic SF, Newton MR, Austin MC, McKay WJ, and Bladin PF (1994). *Parietal lobe epilepsy: clinical features and seizure localization by ictal SPECT*. Neurology 44.12:2277–2284.

Iketani M and Ohsawa I (2017). *Molecular Hydrogen as a Neuroprotective Agent*. Current Neuropharmacology 15.2:324–331.

Insausti R, Amaral DG, and Cowan WM (1987). *The entorhinal cortex of the monkey: II. Cortical afferents*. The Journal of Comparative Neurology 264.3:356–395.

Kreiman G, Fried I, and Koch C (2002). *Single-neuron correlates of subjective vision in the human medial temporal lobe*. Proceedings of the National Academy of Sciences 99.12:8378–8383.

Kreiman G, Koch C, and Fried I (2000). *Category-specific visual responses of single neurons in the human medial temporal lobe*. Nature Neuroscience 3.9:946.

Kveraga K, Ghuman AS, Kassam KS, Aminoff EA, Hämäläinen MS, Chaumon M, and Bar M (2011). *Early onset of neural synchronization in the contextual associations network*. Proceedings of the National Academy of Sciences 108.8:3389–3394.

Libby LA, Ekstrom AD, Ragland JD, and Ranganath C (2012). *Differential Connectivity of Perirhinal and Parahippocampal Cortices within Human Hippocampal Subregions Revealed by High-Resolution Functional Imaging*. Journal of Neuroscience 32.19:6550–6560.

Litman L, Awipi T, and Davachi L (2009). *Category-specificity in the Human Medial Temporal Lobe Cortex*. Hippocampus 19.3:308–319.

Mégevand P, Groppe DM, Goldfinger MS, Hwang ST, Kingsley PB, Davidesco I, and Mehta AD (2014). *Seeing scenes: topographic visual hallucinations evoked by direct electrical stimulation of the parahippocampal place area*. The Journal of Neuroscience: The Official Journal of the Society for Neuroscience 34.16:5399–5405.

Merrill DR, Bikson M, and Jefferys JGR (2005). *Electrical stimulation of excitable tissue: design of efficacious and safe protocols*. Journal of Neuroscience Methods 141.2:171–198.

Miller AMP, Vedder LC, Law LM, and Smith DM (2014). *Cues, context, and long-term memory: the role of the retrosplenial cortex in spatial cognition*. Frontiers in Human Neuroscience 8.

Mishkin M, Ungerleider LG, and Macko KA (1983). *Object vision and spatial vision: two cortical pathways*. Trends in Neurosciences 6:414–417.

Moran NF, Lemieux L, Kitchen ND, Fish DR, and Shorvon SD (2001). *Extrahippocampal temporal lobe atrophy in temporal lobe epilepsy and mesial temporal sclerosis*. Brain: A Journal of Neurology 124 (Pt 1):167–175.

Mormann F, Dubois J, Kornblith S, Milosavljevic M, Cerf M, Ison M, Tsuchiya N, Kraskov A, Quian Quiroga R, Adolphs R, Fried I, and Koch C (2011). *A category-specific response to animals in the right human amygdala*. Nature Neuroscience 14.10:1247–1249.

Mormann F, Kornblith S, Cerf M, Ison MJ, Kraskov A, Tran M, Knieling S, Quian Quiroga R, Koch C, and Fried I (2017). *Scene-selective coding by single neurons*

in the human parahippocampal cortex. Proceedings of the National Academy of Sciences of the United States of America 114.5:1153–1158.

Mormann F, Kornblith S, Quian Quiroga R, Kraskov A, Cerf M, Fried I, and Koch C (2008). *Latency and selectivity of single neurons indicate hierarchical processing in the human medial temporal lobe*. The Journal of Neuroscience: The Official Journal of the Society for Neuroscience 28.36:8865–8872.

Murphey DK, Maunsell JHR, Beauchamp MS, and Yoshor D (2009). *Perceiving electrical stimulation of identified human visual areas*. Proceedings of the National Academy of Sciences of the United States of America 106.13:5389–5393.

Niediek J, Boström J, Elger CE, and Mormann F (2016). *Reliable Analysis of Single-Unit Recordings from the Human Brain under Noisy Conditions: Tracking Neurons over Hours*. PloS One 11.12:e0166598.

Palmini A, Andermann F, Dubeau F, Gloor P, Olivier A, Quesney LF, and Salanova V (1993). *Occipitotemporal Epilepsies: Evaluation of Selected Patients Requiring Depth Electrodes Studies and Rationale for Surgical Approaches*. Epilepsia 34.1:84–96.

Parvizi J, Jacques C, Foster BL, Witthoft N, Withoft N, Rangarajan V, Weiner KS, and Grill-Spector K (2012). *Electrical stimulation of human fusiform face-selective regions distorts face perception*. The Journal of Neuroscience: The Official Journal of the Society for Neuroscience 32.43:14915–14920.

Pedreira C, Mormann F, Kraskov A, Cerf M, Fried I, Koch C, and Quian Quiroga R (2010). *Responses of human medial temporal lobe neurons are modulated by stimulus repetition*. Journal of Neurophysiology 103.1:97–107.

Penfield W (1936). *Epilepsy and Surgical Therapy*. Archives of Neurology & Psychiatry 36.3:449–484.

Quian Quiroga R (2012). *Concept cells: the building blocks of declarative memory functions*. Nature Reviews Neuroscience 13.8:587–597.

Quian Quiroga R, Kraskov A, Koch C, and Fried I (2009). *Explicit Encoding of Multimodal Percepts by Single Neurons in the Human Brain*. Current Biology 19.15:1308–1313.

Quian Quiroga R, Kraskov A, Mormann F, Fried I, and Koch C (2014). *Single-Cell Responses to Face Adaptation in the Human Medial Temporal Lobe*. Neuron 84.2:363–369.

Quian Quiroga R, Kreiman G, Koch C, and Fried I (2008). *Sparse but not 'Grandmother-cell' coding in the medial temporal lobe*. Trends in Cognitive Sciences 12.3:87–91.

Quian Quiroga R, Mukamel R, Isham EA, Malach R, and Fried I (2008). *Human single-neuron responses at the threshold of conscious recognition*. Proceedings of the National Academy of Sciences 105.9:3599–3604.

Quian Quiroga R, Nadasdy Z, and Ben-Shaul Y (2004). *Unsupervised spike detection and sorting with wavelets and superparamagnetic clustering*. Neural Computation 16.8:1661–1687.

Quian Quiroga R, Reddy L, Kreiman G, Koch C, and Fried I (2005). *Invariant visual representation by single neurons in the human brain*. Nature 435.7045:1102–1107.

Ranganath C and Ritchey M (2012). *Two cortical systems for memory-guided behaviour*. Nature Reviews Neuroscience 13.10:713–726.

Reber TP, Faber J, Niediek J, Boström J, Elger CE, and Mormann F (2017). *Single-Neuron Correlates of Conscious Perception in the Human Medial Temporal Lobe*. Current biology: CB 27.19:2991–2998.e2.

Rey HG, Ison MJ, Pedreira C, Valentin A, Alarcon G, Selway R, Richardson MP, and Quian Quiroga R (2015). *Single-cell recordings in the human medial temporal lobe*. Journal of Anatomy 227.4:394–408.

Rose TL and Robblee LS (1990). *Electrical stimulation with Pt electrodes. VIII. Electrochemically safe charge injection limits with 0.2 ms pulses*. IEEE transactions on bio-medical engineering 37.11:1118–1120.

Rosenow F and Lüders H (2001). *Presurgical evaluation of epilepsy*. Brain 124.9:1683–1700.

Rutishauser U, Tudusciuc O, Neumann D, Mamelak AN, Heller AC, Ross IB, Philpott L, Sutherling WW, and Adolphs R (2011). *Single-Unit Responses Selective for Whole Faces in the Human Amygdala*. Current Biology 21.19:1654–1660.

Salanova V, Andermann F, Oliver A, Rasmussen T, and Quesney LF (1992). *Occipital Lobe Epilepsy: Electroclinical Manifestations, Electrocorticography, Cortical Stimulation and Outcome in 42 Patients Treated Between 1930 and 1991 Surgery of Occipital Lobe Epilepsy*. Brain 115.6:1655–1680.

Schultz H, Sommer T, and Peters J (2015). *The Role of the Human Entorhinal Cortex in a Representational Account of Memory*. Frontiers in Human Neuroscience 9.

Scoville WB and Milner B (1957). *Loss of Recent Memory After Bilateral Hippocampal Lesions*. Journal of Neurology, Neurosurgery, and Psychiatry 20.1:11–21.

Seltzer B and Pandya DN (1978). *Afferent cortical connections and architectonics of the superior temporal sulcus and surrounding cortex in the rhesus monkey*. Brain Research 149.1:1–24.

Siegel AM, Wieser HG, Wichmann W, and Yasargil GM (1990). *Relationships between MR-imaged total amount of tissue removed, resection scores of specific mediobasal limbic subcompartments and clinical outcome following selective amygdalohippocampectomy*. Epilepsy Research 6.1:56–65.

Song D, She X, Hampson RE, Deadwyler SA, and Berger TW (2017). *Multi-resolution multi-trial sparse classification model for decoding visual memories from hippocampal spikes in human*. IEEE Engineering in Medicine and Biology Society. Annual Conference 2017:1046–1049.

Spencer SS (1981). *Depth electroencephalography in selection of refractory epilepsy for surgery*. Annals of Neurology 9.3:207–214.

Spencer SS and Spencer DD (1994). *Entorhinal-Hippocampal Interactions in Medial Temporal Lobe Epilepsy*. Epilepsia 35.4:721–727.

Squire LR, Stark CEL, and Clark RE (2004). *The medial temporal lobe*. Annual Review of Neuroscience 27:279–306.

Squire LR and Wixted JT (2011). *The Cognitive Neuroscience of Human Memory Since H.M.* Annual Review of Neuroscience 34.1:259–288.

Suzuki WA and Amaral DG (1994). *Topographic organization of the reciprocal connections between the monkey entorhinal cortex and the perirhinal and parahippocampal cortices*. The Journal of Neuroscience: The Official Journal of the Society for Neuroscience 14.3:1856–1877.

Suzuki WA (1996). *Neuroanatomy of the monkey entorhinal, perirhinal and parahippocampal cortices: Organization of cortical inputs and interconnections with amygdala and striatum*. Seminars in Neuroscience 8.1:3–12.

Viskontas IV, Quiroga RQ, and Fried I (2009). *Human medial temporal lobe neurons respond preferentially to personally relevant images*. Proceedings of the National Academy of Sciences 106.50:21329–21334.

Von Economo CF and Koskinas GN (1925). *Die Cytoarchitektonik der Hirnrinde des erwachsenen Menschen*. J. Springer. 810 pp.

Ward AA and Thomas LB (1955). *The electrical activity of single units in the cerebral cortex of man*. Electroencephalography and Clinical Neurophysiology 7.1:135–136.

Wiebe S, Blume WT, Girvin JP, and Eliasziw M (2001). *A Randomized, Controlled Trial of Surgery for Temporal-Lobe Epilepsy*. New England Journal of Medicine 345.5:311–318.

Wieser HG (1998). *Epilepsy surgery: past, present and future*. Seizure 7.3:173–184.

Williamson PD, Boon PA, Thadani VM, Darcey TM, Spencer DD, Spencer SS, Novelly RA, and Mattson RH (1992). *Parietal lobe epilepsy: Diagnostic considerations and results of surgery*. Annals of Neurology 31.2:193–201.

Williamson PD, Thadani VM, Darcey TM, Spencer DD, Spencer SS, and Mattson RH (1992). *Occipital lobe epilepsy: Clinical characteristics, seizure spread patterns, and results of surgery*. Annals of Neurology 31.1:3–13.

Yilmazer-Hanke DM, Wolf HK, Schramm J, Elger CE, Wiestler OD, and Blümcke I (2000). *Subregional Pathology of the Amygdala Complex and Entorhinal Region in Surgical Specimens From Patients With Pharmacoresistant Temporal Lobe Epilepsy*. Journal of Neuropathology & Experimental Neurology 59.10:907–920.

Young MP, Scannell JW, Burns GA, and Blakemore C (1994). *Analysis of connectivity: neural systems in the cerebral cortex*. Reviews in the Neurosciences 5.3:227–250.

2. An online adaptive screening procedure for selective neuronal responses

Author	Contribution (CASRAI Contributor Role Taxonomy)
Simeon Knieling[1]	Conceptualization, data curation, formal analysis, investigation (experiments), methodology, software, validation, visualization, writing – original draft, writing – review & editing
Johannes Niediek[1]	Supervision, investigation (experiments), writing – review & editing
Esther F. Kutter[1]	Visualization, writing – review & editing
Jan Bostroem[2]	Investigation (surgery), writing – review & editing
Christian E. Elger[1]	Resources, writing – review & editing
Florian Mormann[1]	Conceptualization, funding acquisition, investigation (surgery, experiments), project administration, resources, supervision, validation, writing – review & editing

[1] Department of Epileptology, University of Bonn
[2] Department of Neurosurgery, University of Bonn

This work was originally published in the *Journal of Neuroscience Methods*:

Knieling S, Niediek J, Kutter E, Bostroem J, Elger CE, and Mormann F (2017). *An online adaptive screening procedure for selective neuronal responses*. **Journal of Neuroscience Methods** 291:36–42. https://doi.org/10.1016/j.jneumeth.2017.08.002

Permission for embedding the published journal article was granted by Elsevier.

A precursor of this method was described in S. Knieling's Master's thesis (2012) *"On-line screening procedure for semantically selective neurons as a platform for biofeedback and Brain-Computer Interfaces"*.

2.1 Introduction

Section 1.4 briefly introduced screening experiments as a means to discover concept cells and their response-eliciting stimuli. Many concept-cell studies require identification of a minimum number of response-eliciting concepts before a session can begin. However, in some patients, screenings do not yield enough response-eliciting stimuli. Given the low number of patients that these studies can be performed with (in our institution approximately 10 per year), a poor screening yield can potentially delay research projects by months.

One way to increase a screening's yield is to present more concepts. However, increasing the screening's duration by adding more stimuli can have negative consequences. As experimental durations increase, patients often become more distracted and are less likely to consciously attend each stimulus presentation. This will weaken or (in case the patient completely misses the stimulus) eliminate any potential neuronal response. Consequently, chances of identifying response-eliciting stimuli decrease.

To reliably identify response-eliciting stimuli, each stimulus is typically presented six times. If no neuronal response can be detected in the first three presentations, it is unlikely that the presented stimulus will be considered response-eliciting after all six presentations. Removing these unlikely candidate stimuli mid-screening can save trials and enable the experimenter to start out with a larger pool of candidate stimuli without increasing the total duration of the experiment.

The ability to evaluate neuronal responses in real time can also open up new possibilities to investigate how concepts are encoded (as discussed in Section 1.8).

2.2 Summary

In the following article, we describe an adaptive screening capable of simultaneously evaluating neuronal responses on a large number of channels in real time. By removing the least response-eliciting half of the stimuli after the first half of the experiment, our method can screen 30% more stimuli in the same amount of trials. In addition, the time between the screening and the first follow-up experiment can be decreased, since no time-consuming post-hoc analysis is required to identify the response-eliciting stimuli.

Journal of Neuroscience Methods 291 (2017) 36–42

Contents lists available at ScienceDirect

Journal of Neuroscience Methods

journal homepage: www.elsevier.com/locate/jneumeth

Research article

An online adaptive screening procedure for selective neuronal responses

S. Knieling[a], J. Niediek[a], E. Kutter[a], J. Bostroem[b], C.E. Elger[a], F. Mormann[a,*]

[a] Dept. of Epileptology, University of Bonn, Germany
[b] Dept. of Neurosurgery, University of Bonn, Germany

HIGHLIGHTS

- We propose an online adaptive procedure to screen for neuronal responses to stimuli.
- Our algorithms adaptively excludes stimuli eliciting weak responses.
- It thus allows screening more stimuli per time period at higher accuracy.
- It can be universally applied across species and classes of stimuli.
- It can be easily adapted to a wide range of biofeedback applications.

ARTICLE INFO

Article history:
Received 9 February 2017
Received in revised form 1 August 2017
Accepted 2 August 2017
Available online 4 August 2017

Keywords:
Single units
Biofeedback
Online spike sorting
Neuronal response
Tuning curve

ABSTRACT

Background: A common problem in neurophysiology is to identify stimuli that elicit neuronal responses in a given brain region. Particularly in situations where electrode positions are fixed, this can be a time-consuming task that requires presentation of a large number of stimuli. Such a screening for response-eliciting stimuli is employed, e.g., as a standard procedure to identify 'concept cells' in the human medial temporal lobe.
New method: Our new method evaluates neuronal responses to stimuli online during a screening session, which allows us to successively exclude stimuli that do not evoke a response. Using this method, we can screen a larger number of stimuli which in turn increases the chances of finding responsive neurons and renders time-consuming offline analysis unnecessary.
Results: Our method enabled us to present 30% more stimuli in the same period of time with additional presentations of the most promising candidate stimuli. Our online method ran smoothly on a standard computer and network.
Comparison with an existing method: To analyze how our online screening procedure performs in comparison to an established offline method, we used the Wave_Clus software package. We did not observe any major drawbacks in our method, but a much higher efficiency and analysis speed.
Conclusions: By transitioning from a traditional offline screening procedure to our new online method, we substantially increased the number of visual stimuli presented in a given time period. This allows to identify more response-eliciting stimuli, which forms the basis to better address a great number of questions in cognitive neuroscience.

1. Introduction

Single unit recordings from the temporal lobe of the mammalian brain have greatly contributed to our understanding of the neural mechanisms involved in object recognition, perception and memory. Neurons responding selectively to certain stimulus categories (e.g., faces) by significantly increasing their firing rates have been identified both in monkeys (e.g., Gross et al., 1969, 1972) and humans (Kreiman et al., 2000a). A study by Quian Quiroga et al. (2005) has furthermore discovered neurons in the human medial temporal lobe that respond in a specific and semantically invariant manner to concrete and abstract concepts. For example, a neuron might respond to different pictures of an actress, and even to

* Corresponding author at: Department of Epileptology, University of Bonn, Sigmund–Freud–Strasse 25, 53105 Bonn, Germany.
E-mail address: florian.mormann@ukbonn.de (F. Mormann).

http://dx.doi.org/10.1016/j.jneumeth.2017.08.002
0165-0270/

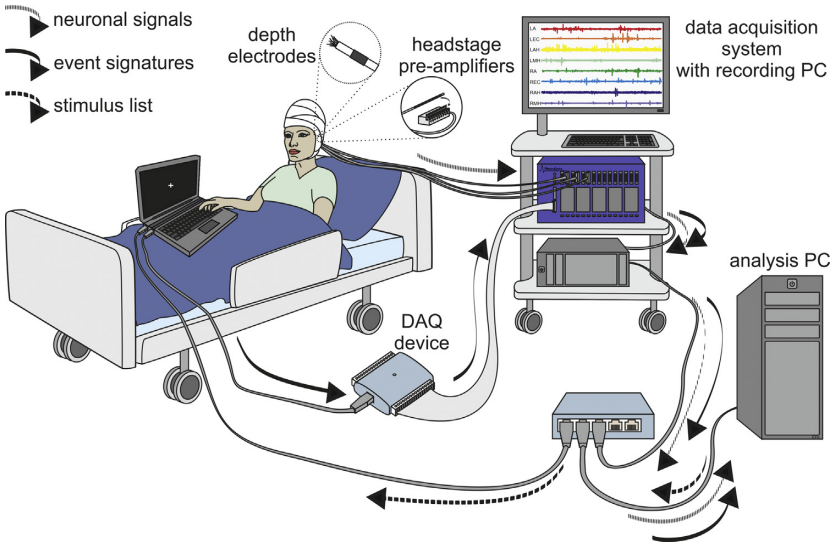

Fig. 1. Recording Setup. Neuronal signals are picked up by the micro-wires protruding from the depth electrodes and sent to the data acquisition system (amplifier) via the headstage pre-amplifiers. From there the signals are sent to the recording PC. Next, the data acquisition software streams the signal through the Ethernet connection to the analysis PC. Once this stream is established, the analysis PC sends a list of stimulus identification numbers for the first run of stimulus presentations to the presentation laptop. The presentation software on the laptop receives this list and starts presenting the stimuli. Upon distinct events (e.g. stimulus onset), the laptop sends event signatures to the amplifier. The recording PC forwards these event signatures to the adaptive screening program on the analysis PC via the previously established stream.

her written name, but not to other presented pictures of persons, animals, or objects.

These concept-specific neurons in humans have been subject to extensive research (Cerf et al., 2010; De Falco et al., 2016; Fried et al., 1997, 2002; Gelbard-Sagiv et al., 2008; Ison et al., 2011, 2015; Kamiński et al., 2017; Kornblith et al., 2017; Kraskov et al., 2007; Kreiman et al., 2000a, 2000b, 2002; Mormann et al., 2008, 2011, 2015, 2017; Niediek et al., 2016; Pedreira et al., 2010; Quian Quiroga et al., 2014; Quiroga et al., 2005, 2007, 2008b, 2008a, 2009; Quiroga, 2012; Reddy et al., 2006, 2015; Rey et al., 2014, 2015; Rutishauser et al., 2015; Steinmetz et al., 2011; Suthana et al., 2015; Valdez et al., 2015; Viskontas et al., 2009; Waydo et al., 2006) because they provide insights into the encoding and storage of abstract information in the human brain.

All of these studies are based on the identification of response-eliciting stimuli. In animal electrophysiology, researchers can either use a fixed stimulus and move the electrodes to find neurons that respond to this stimulus, or use fixed electrodes and change the stimulus until a neuron responds. In human subjects, however, moving the electrodes is currently impossible, leaving only the latter option. To maximize the number of identified response-eliciting stimuli, it is thus important to test as many different stimuli as possible.

Here, we propose an improved screening procedure that allows to better identify response-eliciting stimuli by maximizing the number of stimuli that can be presented within a given period of time. During a conventional screening procedure, aimed at identifying response-eliciting stimuli, numerous stimuli are presented to the subject in pseudorandom order. This is repeated across several runs in order to identify reliable responses. In this standard procedure, even though most presented stimuli in a screening session do not evoke a response, all of them are presented in every run. The adaptive screening procedure we describe here analyzes the neuronal responses online and excludes stimuli which do not evoke clear responses from the remaining part of the screening. This way we are able to screen more stimuli in the same amount of time, increasing the chances of finding responsive neurons along with their response-eliciting stimuli. Furthermore, follow-up experiments can be performed immediately afterwards since no time-consuming offline analysis is necessary.

2. Materials and methods

2.1. Experimental setup

Our subjects are patients with pharmacologically intractable medial temporal lobe epilepsy, who have been implanted with "Behnke-Fried" Depth Electrodes (Ad-Tech, Racine, WI) to localize the epileptic focus for possible resection. Every depth electrode is equipped with nine micro-wires (eight recording channels plus one reference) which are 40 μm in diameter and protrude from the tip of the electrode by approx. 4 mm. Patients provided written informed consent for implantation of micro-electrodes and participation in cognitive paradigms. All studies and procedures were approved by the internal review board of the University of Bonn.

The micro-wires were connected to headstage pre-amplifiers (CHET-10, Neuralynx, Bozeman, MT), which in turn were connected to the data acquisition system (amplifier) (Neuralynx ATLAS system) (Fig. 1). Data was acquired at a sampling frequency of 32 kHz. The amplifier was connected to a recording PC running Neuralynx's data acquisition software Cheetah ATLAS (version 1.1.0). The acquisition software band-pass filtered the data between 0.1 and 9000 Hz. A laptop used to present stimuli to the patient was connected to the data acquisition system via a USB DAQ Device (Measurement Computing's USB-1208FS), which was used to send event signatures (such as stimulus onset) to the recording system using TTL pulses. In addition, an analysis PC (Intel® Core™ i7-3820) was connected to the recording PC and the presentation laptop via Ethernet connection. This connection was used to receive data streams from the data acquisition software via Neuralynx's NetCom API and to send data to the presentation laptop (Fig. 1).

2.2. Experimental procedure

The presentation laptop is running our adaptive screening procedure, which is intended for experiments in cognitive neuroscience that involve repeated presentation of stimuli while acquiring micro-electrode recordings (MER). The screening procedure consists of a predefined number of runs R. During each run $r = 1, \ldots, R$, a predetermined number of N_r stimuli are presented. The idea of the adaptive screening is to evaluate the neuronal response to each stimulus online and to provide the option of excluding stimuli after each run. In other words, from one run to the next, N_r can either decrease or remain constant. Typically, this is used to exclude stimuli that fail to elicit a neuronal response.

We applied this method in the following manner. Patients view a set of visual stimuli on a laptop computer screen. Each trial of the screening starts by displaying a white screen jittered between 0 and 100 ms, followed by a fixation cross displayed for 100 ms. Subsequently, the stimulus is presented. After 1 s the stimulus is replaced by a white screen, and the subject has to indicate whether the picture contained a human face or not by pressing the up or down arrow key, respectively. This simple yes/no task is used to ensure that the subject consciously attends each stimulus. The next trial commences immediately after the subject's key press.

In our example, the adaptive screening procedure started with 190 stimuli ($N_1 = N_2 = N_3 = 190$), and the paradigm was configured to remove the 100 least response-eliciting stimuli after the third run ($N_{4,5,6} = 90$) and an additional 80 stimuli after the sixth run, leaving a small set of 10 stimuli that elicited the largest responses to be presented for three additional runs ($N_{7,8,9} = 10$). This procedure replaces a conventional screening procedure in which $N = 145$ stimuli are presented for 6 times in the same amount of time.

2.3. Data analysis

The software we developed to perform this adaptive screening procedure consists of a MATLAB-based presentation script that handles stimulus presentations and a standalone analysis program, which is a multi-threaded application written in C/C++. For each recording channel, we spawn three threads; one for preprocessing data from the acquisition system, one for clustering and template matching, and one for stimulus score calculation. A full and up-to-date documentation as well as the source code are available at http://asp.knieling.org.

Once a data stream between the data acquisition system and the analysis program has been established, the analysis program sends a list of N_1 stimulus identification numbers to the presentation script. These numbers uniquely identify each stimulus to be presented during the first run. The presentation script then starts to present the appropriate stimuli. At distinct times of a trial (e.g. stimulus onset) the presentation script sends event signatures to the data acquisition system that are relayed to the analysis program. The timestamps of these events enable the analysis program to match the recorded data with the presented stimuli and to quantify the neuronal responses. After the last trial of a given run r, the analysis program generates a new list consisting of N_{r+1} stimuli (in pseudorandom order) that elicited the strongest neuronal responses in the previous runs and sends this list to the presentation script. Upon receiving this list, the presentation script continues with the presentation of the new stimulus list.

The data received from the data acquisition system is preprocessed in segments of $t_s = 5$ s or after receiving a stimulus offset event signature, whichever happens first. The preprocessing is done according to Quiroga et al. (2004). The MER raw-data is band-pass filtered between 0.3 kHz and 3.0 kHz. We use an open-source elliptic IIR-filter from the DSPFilters library, developed by Vincent Falco (https://github.com/vinniefalco/DSPFilters). Neuronal action potentials (spikes) are detected (via an automated threshold detection), extracted and aligned to their peaks. Spike sorting is then used to separate spikes generated by different neurons on the same recording channel. A characteristic feature of our adaptive screening procedure is that spike sorting, the most time-consuming part, is performed only once during the paradigm. Any spike recorded after this step is assigned to an existing cluster via template-matching based on Euclidian distance, which can easily be done online and in real time. After spike sorting, a cluster of spikes is more likely to correspond to the activity of a single neuron than the entirety of spikes recorded on a channel. However, some clusters will likely correspond to artifacts due to movement or other confounding factors such as recording noise. An important parameter for the screening procedure is after which run r_c the clustering algorithm is executed. While clustering should not be applied too early in order to ensure a representative sampling of spikes from all neurons present in the data, it should also not be started too late as it is a necessary step in assessing response behavior elicited by a stimulus.

After run r_c the clustering starts. If the number of detected spikes of the respective recording channel exceed a certain limit, only the first M spikes within this limit are fed to the clustering algorithm (in our case $M = 10{,}000$). This limit ensures that the clustering algorithm concludes before the next run commences. As described in Quiroga et al. (2004), 10 wavelet coefficients for each spike are calculated and used as the input to a superparamagnetic clustering algorithm described in Blatt et al. (1996). For the implementation of this algorithm we use the standalone SPC v2.1 program (Cluster.exe) provided by Eytan Domany that comes with the Wave_Clus package. Our software starts one instance of SPC v2.1 per channel.

After the clustering, an automated temperature selection criterion (Quiroga et al., 2004) is used to select an adequate set of clusters from the SPC's results. To determine which cluster responded to which stimulus, we use the statistical criterion described in Mormann et al. (2008, 2011). The idea is to generate a matrix for each cluster responding to each stimulus consisting of overlapping time bins as columns and trials as rows. We divide the time during stimulus presentation into 19 overlapping bins of 100 ms, and for each bin we compare the spike rates for the r presentations of each stimulus to all the baseline intervals of 500 ms before the stimuli onsets ($N_1 + \ldots + N_r$) by means of a two-tailed Mann-Whitney U test, using the Simes procedure to correct for multiple comparisons and applying a conservative threshold of $p = 0.001$ to reduce false positive detections.

Denoting by $p_{s,c}$ the smallest corrected p-value of a given stimulus and cluster across bins, we define $S_{s,c} = 1/p_{s,c}$ as the response score of a stimulus s for the respective cluster c. The overall score S_s of stimulus s is calculated by summing up the m (in our case $m = 3$) highest response scores $S_{c,s}$ of a given stimulus across all clusters from all channels. This slightly biases the selection criterion towards stimuli that elicit responses in more than one cluster. This is favorable since a single cluster could be lost over time, leaving no responsive unit for the selected stimulus. To prevent stimuli that seem to elicit low responses in a larger number of clusters from receiving higher overall scores than a stimulus that elicits a strong response in only one cluster, m is kept low. Overall stimulus scores are updated after each run $r \geq r_c$. After each run $r = r_c + 1, \ldots, R-1$, the N_{r+1}-N_r stimuli with the lowest overall scores are removed from the remainder of the screening. An additional constraint that can be applied for any of the removals is to allow only the best n_s response scores $S_{s,c}$ of each cluster to contribute to the overall stimulus score S_s. If a stimulus is not among the n_s highest scores of any one cluster, its score is set to zero. In other words, only the n_s best stimuli per cluster over all clusters are considered. This selectivity constraint can be applied to prevent indifferent clusters (that respond to many stimuli) from having a disproportionately high

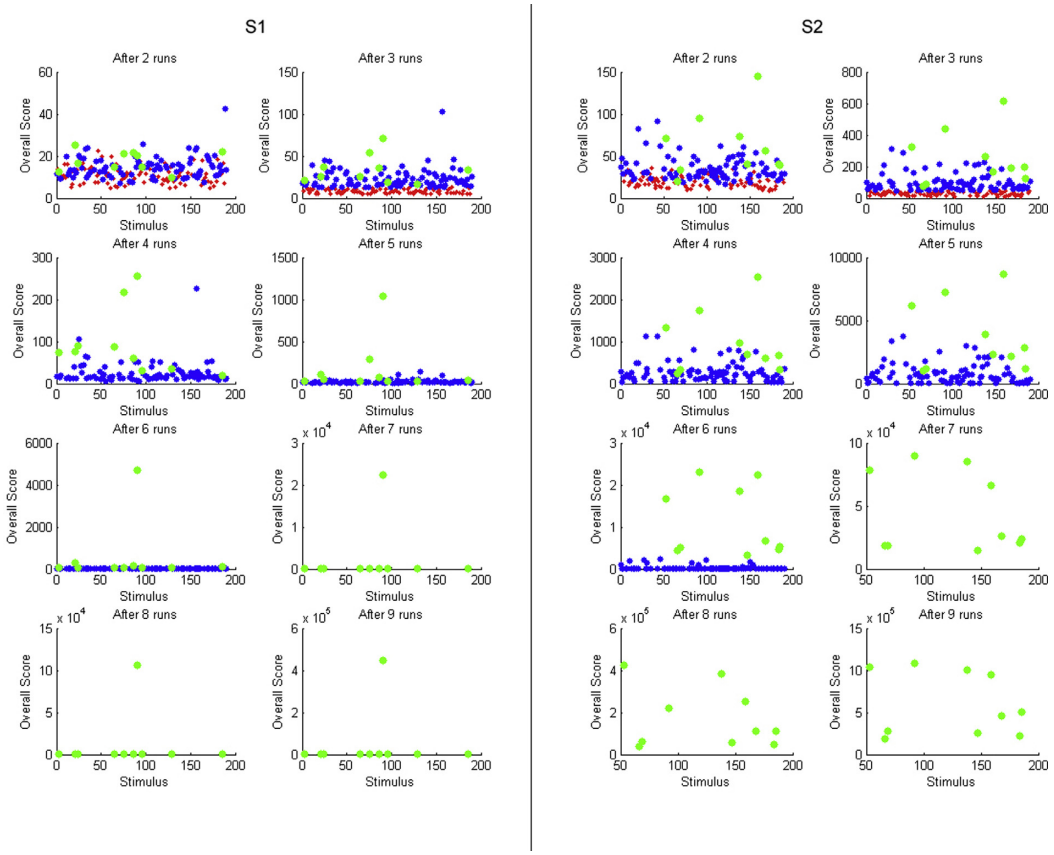

Fig. 2. Overall scores used to exclude stimuli. After three runs, the 100 stimuli with the lowest scores were removed from the remaining experiment (red dots). After six runs, an additional 80 stimuli were removed (blue dots). The ten stimuli with the highest scores after six runs were presented for three more runs (green dots). Left: Screening Session S1. Right: Session S2. (For interpretation of the references to colour in this figure legend, the reader is referred to the web version of this article.)

impact on the stimulus selection. The selectivity constraint is useful if the goal for a screening procedure is to maximize the number of units that respond to only a few of the presented stimuli. We used this constraint with $n_s = 2$ for the removal in run 6 (see Experimental procedure).

3. Results

As an example application of our method, we present two adaptive screening sessions recorded in two different patients. In the following, these sessions will be denoted by S1 and S2, respectively. Each session consisted of R = 9 runs. S1 lasted for 24 min and 20 s and S2 for 25 min and 56 s. The first three runs included 190 stimuli, the next three runs 90 stimuli, and the last three runs 10 stimuli.

Spike sorting was started after the end of the second run, which was at 11 min and 42 s in S1, and at 11 min and 9 s in S2. In S1, the spike sorting procedure took 38 s and was completed 13% into the third run, and in S2, spike sorting took 76 s and was completed 22% into the third run. This spike sorting yielded a total of 75 clusters from 61 recording channels in S1, and 125 clusters from 80 recording channels in S2.

Fig. 2 shows the overall stimulus scores for each stimulus after each run of S1 and S2, starting at run two, which is the first run for which scores could be calculated. Stimuli in red were presented 3 times, stimuli in blue 6 times, and stimuli in green 9 times. Note that some of the stimuli discarded after the sixth run in S2 actually turned out to reflect valid responses as evidenced by our response criterion (Mormann et al., 2011, 2008) and visual inspection.

Next we compared our results to a standard offline analysis. We retrospectively analyzed the data offline using Wave_Clus (Quiroga et al., 2004) in an unsupervised fashion with default parameters. The neuronal response patterns were similar to the ones found by our online procedure. Figure 3 shows the response-eliciting stimuli that were presented 9 times for both algorithms. Apart from minor differences in spike detection, we did not find major differences between an unsupervised Wave_Clus-based offline analysis and the online analysis performed by our adaptive screening software.

To estimate how many responsive units we might lose by discarding 53% of the stimuli after 3 runs, we retrospectively analyzed 14 regular screening sessions from 3 patients, using the replay feature of our software that allows to analyze run-based paradigms post-hoc to see which stimuli would have been discarded. These 14 sessions included 100 stimuli that were shown 6 times each. On average, by discarding 53 stimuli after 3 runs, 5.1 stimuli per sessions that would have been discarded after 3 runs ended up meeting the significance criterion reported in Mormann et al. (2008, 2011). Of these, an average of only 1.4 stimuli were not false positives as confirmed by visual inspection. Since some of the responses to stimuli that would have been discarded after 3 runs were from neurons that also responded to other stimuli that would not have been dis-

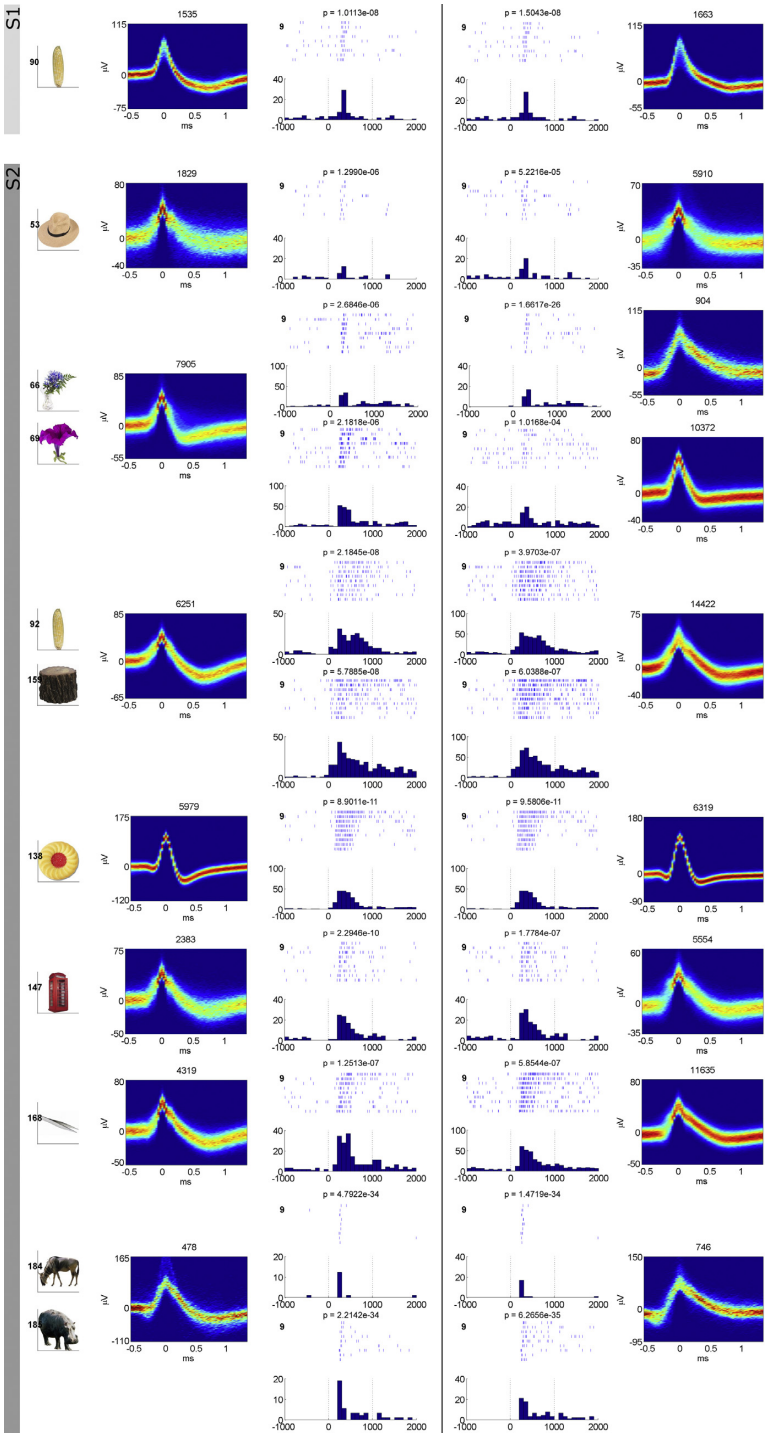

Fig. 3. Neuronal response pattern. Neuronal responses to response-eliciting stimuli that were presented 9 times during screening sessions S1 and S2. Trials are visualized as raster plot and *peri*-stimulus time histogram (PSTH). The dotted lines at 0 and 1000 mark stimulus onset and offset, respectively. The *p*-values above each raster plot show the response score described in Mormann et al. (2008, 2011), with values of $p < 0.001$ typically reflecting valid responses. Next to the response patterns are density plots of the respective units and the number of spikes attributed to them. Left: Neuronal response patterns calculated by our adaptive screening software. Right: Neuronal response patterns calculated by Wave_Clus using default parameters (unsupervised). Differences in spike shapes are mostly due to different filter implementations. Note that the second unit in S2 (responding to stimuli 66 and 69) was separated into two clusters by Wave_Clus.

carded, an average of only 0.3 responsive units per session would have been lost.

4. Discussion

We present an adaptive screening algorithm designed to optimize standard screening procedures for response-eliciting stimuli during MER.

In the presented sessions, we simultaneously analyzed 61 and 80 channels, respectively, in an online fashion. The analysis included filtering, spike detection, spike sorting, template matching and calculation of neuronal response scores. Based on these scores, our screening procedure enabled automated removal of those stimuli that evoked the lowest neuronal responses from the remainder of the screening session.

In other screening sessions (data not shown) we analyzed up to 128 channels without reaching a limit for our online analysis program, i.e., without causing any delays that were noticeable by our patients. The only noteworthy delay generated by the adaptive screening software occured between two consecutive runs. Using a dedicated LAN switch operating at 1 Gbit/s, we measured short delays around 250 ms which were mainly caused by the presentation script receiving the new stimulus order (approx. 200 ms). In one of the screening sessions (S1), we preferred to use the hospital's intranet connection (100 Mbit) so we could keep the analysis PC outside the patient's room, which was already crowded with digital equipment. In this setting, we observed delays of approx. 2 s after each run, depending on the intranet's network load. The execution time needed by the spike sorting program SPC v2.1 ranged from a few seconds to a few minutes, depending on the number of spikes to sort. Therefore we do not recommend performing spike sorting and the first stimulus removal after the same run as this could potentially cause a noticeable delay.

The clustering part of our procedure – using SPC to cluster the first two runs and template matching for subsequent runs – is unlikely to perform quite as well as an offline clustering algorithm fed with the entirety of the spikes, especially if manual care is taken to optimize the clustering outcome. However, we believe that the benefit of being able to present more stimuli to the patients clearly outweighs the possibly lower clustering quality. Especially since conventional (manual) offline analysis can still be performed after the experiment if desired.

The entire data generated by our program is saved and can be plotted and analyzed after the screening. This provides the possibility to track which stimuli were removed at which point, and to compare the neuronal responses to the ones obtained by using conventional post hoc spike sorting. It also allows to manually recluster the response data, at least for stimuli that were presented six times or more. While manually supervised spike sorting is currently regarded as gold standard for microwire (monotrode) recordings, it is not a feasible option if response-eliciting stimuli are to be used in an immediate follow-up paradigm. Future versions of our procedure might include alternative spike sorting packages such as Combinato (Niediek et al., 2016), which allows to better separate response-eliciting units in an automated fashion, but the Combinato package was developed in Python and is not optimized for the computational speed necessary to work in real time.

In comparison with post hoc offline analysis using Wave_Clus, our adaptive screening software yields similar results. Wave_Clus calculates thresholds for large data segments retrospectively based on the data of the same segment, which means it uses information to which an online procedure has no access. Therefore, there are slight differences in the determined thresholds and consequently in the number of spikes detected. By decreasing the influence of new chunks of data on the detection threshold, one could create a more rigid threshold behavior and potentially decrease the detection gap between Wave_Clus and our adaptive screening procedure, but at the same time one would run the risk of increasing the number of false positive or false negative detections in response to a sudden change in background activity (e.g. due to patient movement).

A feature of our software that is useful for verification purposes is the replay mode. Given a run-based paradigm, one can feed the data recorded in a regular screening session into our program to find out how the stimuli would have been scored and which stimuli would have been removed. Using this feature retrospectively on some of our regular screening sessions revealed that we might occasionally lose a responsive unit (on average about 0.3 per session when removing 53 out of 100 stimuli after 3 presentations).

Our screening software can also be used for different animal species and for various types of electrodes (wire bundles, Utah arrays, etc.). Furthermore, it can work with any type of stimulus (visual, auditory, olfactory etc.).

The code for the adaptive screening software can easily be adapted for other online applications as well. The possibility to process large numbers of channels simultaneously with minimal delay renders it a powerful tool for various types of biofeedback studies.

It could also be used to adaptively measure neuronal tuning curves by gradually varying some physical parameter of a visual stimulus such as the angle of an oriented grating. A problem in assessing tuning curves for the visually selective neurons found in humans that exhibit semantic invariance ('concept cells') is how to parameterize the semantic distance between stimuli. Here a conceivable solution would be to determine response-eliciting objects and use an online database such as wordassociation.org, Google Knowledge Graph Search API, LinguaTools DISCO, or the lexical database WordNet (wordnet.princeton.edu) to identify semantically associated objects and download their pictures from the internet for subsequent presentation within the same experimental session. Another conceivable extension to our software would be to automatically execute follow-up paradigms that involve the presentation of response-eliciting stimuli. This would not only save time and effort, but also reduce the risk of 'losing' responsive units due to micro-movement of electrodes over time.

Acknowledgements

This research was supported by the Volkswagen Foundation (Lichtenberg Program), the German Research Council (DFG MO930/4-1 and SFB 1089),and the European Commission (FP7 602102 EPITARGET).

References

Blatt, M., Wiseman, S., Domany, E., 1996. Superparamagnetic clustering of data. Phys. Rev. Lett. 76, 3251–3254, http://dx.doi.org/10.1103/PhysRevLett.76.3251.

Cerf, M., Thiruvengadam, N., Mormann, F., Kraskov, A., Quiroga, R.Q., Koch, C., Fried, I., 2010. On-line, voluntary control of human temporal lobe neurons. Nature 467, 1104–1108, http://dx.doi.org/10.1038/nature09510.

De Falco, E., Ison, M.J., Fried, I., Quian Quiroga, R., 2016. Long-term coding of personal and universal associations underlying the memory web in the human brain. Nat. Commun. 7, 13408, http://dx.doi.org/10.1038/ncomms13408.

Fried, I., MacDonald, K.A., Wilson, C.L., 1997. Single neuron activity in human hippocampus and amygdala during recognition of faces and objects. Neuron 18, 753–765.

Fried, I., Cameron, K.A., Yashar, S., Fong, R., Morrow, J.W., 2002. Inhibitory and excitatory responses of single neurons in the human medial temporal lobe during recognition of faces and objects. Cereb. Cortex 12, 575–584.

Gelbard-Sagiv, H., Mukamel, R., Harel, M., Malach, R., Fried, I., 2008. Internally generated reactivation of single neurons in human hippocampus during free recall. Science 322, 96–101, http://dx.doi.org/10.1126/science.1164685.

Gross, C.G., Bender, D.B., Rocha-Miranda, C.E., 1969. Visual receptive fields of neurons in inferotemporal cortex of the monkey. Science 166, 1303–1306.

Gross, C.G., Rocha-Miranda, C.E., Bender, D.B., 1972. Visual properties of neurons in inferotemporal cortex of the Macaque. J. Neurophysiol. 35, 96–111 (4621506).

Ison, M.J., Mormann, F., Cerf, M., Koch, C., Fried, I., Quiroga, R.Q., 2011. Selectivity of pyramidal cells and interneurons in the human medial temporal lobe. J. Neurophysiol. 106, 1713–1721, http://dx.doi.org/10.1152/jn.00576.2010.
Ison, M.J., Quian Quiroga, R., Fried, I., 2015. Rapid encoding of new memories by individual neurons in the human brain. Neuron 87, 220–230, http://dx.doi.org/10.1016/j.neuron.2015.06.016.
Kamiński, J., Sullivan, S., Chung, J.M., Ross, I.B., Mamelak, A.N., Rutishauser, U., 2017. Persistently active neurons in human medial frontal and medial temporal lobe support working memory. Nat. Neurosci. 20, 590–601, http://dx.doi.org/10.1038/nn.4509.
Kornblith, S., Quian Quiroga, R., Koch, C., Fried, I., Mormann, F., 2017. Persistent single-neuron activity during working memory in the human medial temporal lobe. Curr. Biol. 27, 1026–1032, http://dx.doi.org/10.1016/j.cub.2017.02.013.
Kraskov, A., Quiroga, R.Q., Reddy, L., Fried, I., Koch, C., 2007. Local field potentials and spikes in the human medial temporal lobe are selective to image category. J. Cogn. Neurosci. 19, 479–492.
Kreiman, G., Koch, C., Fried, I., 2000a. Category-specific visual responses of single neurons in the human medial temporal lobe. Nat. Neurosci. 3, 946–953.
Kreiman, G., Koch, C., Fried, I., 2000b. Imagery neurons in the human brain. Nature 408, 357–361.
Kreiman, G., Fried, I., Koch, C., 2002. Single-neuron correlates of subjective vision in the human medial temporal lobe. Proc. Natl. Acad. Sci. U. S. A. 99, 8378–8383.
Mormann, F., Kornblith, S., Quiroga, R.Q., Kraskov, A., Cerf, M., Fried, I., Koch, C., 2008. Latency and selectivity of single neurons indicate hierarchical processing in the human medial temporal lobe. J. Neurosci 28, 8865–8872, http://dx.doi.org/10.1523/JNEUROSCI (1640-08.2008).
Mormann, F., Dubois, J., Kornblith, S., Milosavljevic, M., Cerf, M., Ison, M., Tsuchiya, N., Kraskov, A., Quiroga, R.Q., Adolphs, R., Fried, I., Koch, C., 2011. A category-specific response to animals in the right human amygdala. Nat. Neurosci. 14, 1247–1249, http://dx.doi.org/10.1038/nn.2899.
Mormann, F., Niediek, J., Tudusciuc, O., Quesada, C.M., Coenen, V.A., Elger, C.E., Adolphs, R., 2015. Neurons in the human amygdala encode face identity, but not gaze direction. Nat. Neurosci. 18, 1568–1570, http://dx.doi.org/10.1038/nn.4139.
Mormann, F., Kornblith, S., Cerf, M., Ison, M.J., Kraskov, A., Tran, M., Knieling, S., Quian Quiroga, R., Koch, C., Fried, I., 2017. Scene-selective coding by single neurons in the human parahippocampal cortex. Proc. Natl. Acad. Sci. U.S.A., http://dx.doi.org/10.1073/pnas.1608159113.
Niediek, J., Boström, J., Elger, C.E., Mormann, F., 2016. Reliable analysis of single-unit recordings from the human brain under noisy conditions: tracking neurons over hours. PLoS One 11, e0166598, http://dx.doi.org/10.1371/journal.pone.0166598.
Pedreira, C., Mormann, F., Kraskov, A., Cerf, M., Fried, I., Koch, C., Quiroga, R.Q., 2010. Responses of human medial temporal lobe neurons are modulated by stimulus repetition. J. Neurophysiol. 103, 97–107, http://dx.doi.org/10.1152/jn.91323.2008.
Quian Quiroga, R., Kraskov, A., Mormann, F., Fried, I., Koch, C., 2014. Single-cell responses to face adaptation in the human medial temporal lobe. Neuron 84, 363–369, http://dx.doi.org/10.1016/j.neuron.2014.09.006.
Quiroga, R.Q., Nadasdy, Z., Ben-Shaul, Y., 2004. Unsupervised spike detection and sorting with wavelets and superparamagnetic clustering. Neural Comput. 16, 1661–1687.
Quiroga, R.Q., Reddy, L., Kreiman, G., Koch, C., Fried, I., 2005. Invariant visual representation by single neurons in the human brain. Nature 435, 1102–1107.
Quiroga, R.Q., Reddy, L., Koch, C., Fried, I., 2007. Decoding visual inputs from multiple neurons in the human temporal lobe. J. Neurophysiol. 98, 1997–2007.
Quiroga, R.Q., Kreiman, G., Koch, C., Fried, I., 2008a. Sparse but not grandmother-cell coding in the medial temporal lobe. Trends Cogn. Sci. (Regul. Ed.) 12, 87–91, http://dx.doi.org/10.1016/j.tics.2007.12.003.
Quiroga, R.Q., Mukamel, R., Isham, E.A., Malach, R., Fried, I., 2008b. Human single-neuron responses at the threshold of conscious recognition. Proc. Natl. Acad. Sci. U. S. A. 105, 3599–3604.
Quiroga, R.Q., Kraskov, A., Koch, C., Fried, I., 2009. Explicit encoding of multimodal percepts by single neurons in the human brain. Curr. Biol. 19, 1308–1313, http://dx.doi.org/10.1016/j.cub.2009.06.060.
Quiroga, R.Q., 2012. Concept cells: the building blocks of declarative memory functions. Nat. Rev. Neurosci. 13, 587–597, http://dx.doi.org/10.1038/nrn3251.
Reddy, L., Quiroga, R.Q., Wilken, P., Koch, C., Fried, I., 2006. A single-neuron correlate of change detection and change blindness in the human medial temporal lobe. Curr. Biol. 16, 2066–2072.
Reddy, L., Poncet, M., Self, M.W., Peters, J.C., Douw, L., van Dellen, E., Claus, S., Reijneveld, J.C., Baayen, J.C., Roelfsema, P.R., 2015. Learning of anticipatory responses in single neurons of the human medial temporal lobe. Nat. Commun. 6, 8556, http://dx.doi.org/10.1038/ncomms9556.
Rey, H.G., Fried, I., Quian Quiroga, R., 2014. Timing of single-neuron and local field potential responses in the human medial temporal lobe. Curr. Biol. 24, 299–304, http://dx.doi.org/10.1016/j.cub.2013.12.004.
Rey, H.G., Ison, M.J., Pedreira, C., Valentin, A., Alarcon, G., Selway, R., Richardson, M.P., Quian Quiroga, R., 2015. Single-cell recordings in the human medial temporal lobe. J. Anat. 227, 394–408, http://dx.doi.org/10.1111/joa.12228.
Rutishauser, U., Ye, S., Koroma, M., Tudusciuc, O., Ross, I.B., Chung, J.M., Mamelak, A.N., 2015. Representation of retrieval confidence by single neurons in the human medial temporal lobe. Nat. Neurosci. 18, 1041–1050, http://dx.doi.org/10.1038/nn.4041.
Steinmetz, P.N., Cabrales, E., Wilson, M.S., Baker, C.P., Thorp, C.K., Smith, K.A., Treiman, D.M., 2011. Neurons in the human hippocampus and amygdala respond to both low- and high-level image properties. J. Neurophysiol. 105, 2874–2884, http://dx.doi.org/10.1152/jn.00977.2010.
Suthana, N.A., Parikshak, N.N., Ekstrom, A.D., Ison, M.J., Knowlton, B.J., Bookheimer, S.Y., Fried, I., 2015. Specific responses of human hippocampal neurons are associated with better memory. Proc. Natl. Acad. Sci. U.S.A. 112, 10503–10508, http://dx.doi.org/10.1073/pnas.1423036112.
Valdez, A.B., Papesh, M.H., Treiman, D.M., Smith, K.A., Goldinger, S.D., Steinmetz, P.N., 2015. Distributed representation of visual objects by single neurons in the human brain. J. Neurosci. 35, 5180–5186, http://dx.doi.org/10.1523/JNEUROSCI (1958-14.2015).
Viskontas, I.V., Quiroga, R.Q., Fried, I., 2009. Human medial temporal lobe neurons respond preferentially to personally relevant images. Proc. Natl. Acad. Sci. U.S.A. 106, 21329–21334, http://dx.doi.org/10.1073/pnas.0902319106.
Waydo, S., Kraskov, A., Quian Quiroga, R., Fried, I., Koch, C., 2006. Sparse representation in the human medial temporal lobe. J. Neurosci. 26, 10232–10234.

3. An unsupervised online spike-sorting framework

Author	Contribution (CASRAI Contributor Role Taxonomy)
Simeon Knieling[1,2]	Conceptualization, data curation, formal analysis, investigation (experiments), methodology, software, validation, visualization, writing – original draft, writing – review & editing
Kousik S. Sridharan[1]	Investigation (experiments), writing – review & editing
Paolo Belardinelli[1]	Supervision, writing – review & editing
Georgios Naros[1]	Investigation (surgery), writing – review & editing
Daniel Weiss[3]	Resources, writing – review & editing
Florian Mormann[2]	Project administration, resources, supervision, writing – review & editing
Alireza Gharabaghi[1]	Funding acquisition, investigation (surgery), project administration, resources, supervision, writing – review & editing

[1] Division of Functional and Restorative Neurosurgery & Division of Translational Neurosurgery, Department of Neurosurgery, and Neuroprosthetics Research Group, Werner Reichardt Centre for Integrative Neuroscience, Eberhard Karls University Tuebingen
[2] Cognitive and Clinical Neurophysiology, Department of Epileptology, University of Bonn
[3] Department for Neurodegenerative Diseases and Hertie Institute for Clinical Brain Research, and German Centre of Neurodegenerative Diseases (DZNE), Eberhard Karls University Tuebingen

This work was originally published in the *International Journal of Neural Systems*:

Knieling S, Sridharan KS, Belardinelli P, Naros G, Weiss D, Mormann F, and Gharabaghi A (2016). *An Unsupervised Online Spike-Sorting Framework*. **International Journal of Neural Systems** 26.5:1550042. https://doi.org/10.1142/S0129065715500422

3.1 Introduction

As introduced in Section 1.5, spike sorting offers a means to separate spikes (i.e., action potentials) generated by different neurons that were recorded on the same channel. If spikes are separated sufficiently well, inferences can be made about the activity of individual neurons.

The best way to ensure good separation is to record with a high signal-to-noise ratio (SNR). To increase the signal, multiple micro-electrodes can be linked together to record the same neurons from slightly different locations. Means to reduce noise include shielding the recording setup from external electromagnetic fields, using an active-ground circuit, using a reference in close proximity to the recording electrode, keeping analog cables as short as possible, and fixating electrodes, cables, and possibly subjects. When these options are limited — which is usually the case when recording from patients — a capable spike-sorting algorithm is crucial to achieve adequate sorting results.

Offline algorithms generally produce superior sorting results because they have more information available when the sorting process starts. Their applicability, however, is mostly limited to post-hoc analyses. For example, the adaptive screening described in Chapter 2 switches from offline spike-sorting to online template-matching in order to be able to analyse neuronal responses online. However, responses of concept cells that were silent before the template matching took over could not be evaluated, since no template could have been generated for them. Using an online spike-sorting algorithm would increase the efficacy of the iterative screening proposed in Section 1.8 to map a concept-cell's semantic network, because responses of previously silent cells, responding to concepts presented for the first time later in the experiment, could still be evaluated.

3.2 Summary

In the following manuscript, we describe an unsupervised online spike-sorting framework capable of producing sorting results superior to established online and offline algorithms. We maximize the distinctiveness of different spike shapes by transforming them to wavelet components and weighting each component by its distribution's deviation from normality. This is done using a sliding window to account for gradually changing spike shapes that are frequently encountered in intra-operative recordings. Our framework is highly modular and allows for the replacement of individual components.

International Journal of Neural Systems

AN UNSUPERVISED ONLINE SPIKE-SORTING FRAMEWORK

SIMEON KNIELING[†,§,*], KOUSIK S. SRIDHARAN[†], PAOLO BELARDINELLI[†], GEORGIOS NAROS[†], DANIEL WEISS[‡], FLORIAN MORMANN[§] and ALIREZA GHARABAGHI[†,*]

[†] *Division of Functional and Restorative Neurosurgery & Division of Translational Neurosurgery, Department of Neurosurgery, and Neuroprosthetics Research Group, Werner Reichardt Centre for Integrative Neuroscience, Eberhard Karls University Tuebingen, Otfried-Mueller-Str.45, 72076 Tuebingen, Germany*
alireza.gharabaghi@uni-tuebingen.de

[‡] *Department for Neurodegenerative Diseases and Hertie Institute for Clinical Brain Research, and German Centre of Neurodegenerative Diseases (DZNE), Eberhard Karls University Tuebingen, Germany*

[§] *Cognitive and Clinical Neurophysiology, Department of Epileptology, University of Bonn, Bonn, Germany.*
knieling@uni-bonn.de

Extracellular neuronal microelectrode recordings can include action potentials from multiple neurons. To separate spikes from different neurons, they can be sorted according to their shape, a procedure referred to as spike sorting. Several algorithms have been reported to solve this task. However, when clustering outcomes are unsatisfactory, most of them are difficult to adjust to achieve the desired results. We present an online spike-sorting framework that uses feature normalization and weighting to maximize the distinctiveness between different spike shapes. Furthermore, multiple criteria are applied to either facilitate or prevent cluster fusion, thereby enabling experimenters to fine-tune the sorting process. We compare our method to established unsupervised offline (Wave_Clus) and online (OSort) algorithms by examining their performance in sorting various test datasets using two different scoring systems (AMI and the Adamos metric). Furthermore, we evaluate sorting capabilities on intra-operative recordings using established quality metrics. Compared to Wave_Clus and OSort, our algorithm achieved comparable or higher scores on average and produced more convincing sorting results for intra-operative datasets. Thus, the presented framework is suitable for both online and offline analysis and could substantially improve the quality of microelectrode-based data evaluation for research and clinical application.

Keywords: Online spike sorting; real-time clustering; unsupervised; microelectrode recording; intraoperative mapping; deep brain stimulation.

1. Introduction

Single neurons generate their rhythmic activity through spikes. The interest for the characteristics of neuronal spiking and its implications for computational systems has generated a large number of modeling studies.[1,2,3,4,5,6,7,8,,9,10]

Yet, recording action potentials from a single neuron is not a trivial task since extracellular recordings from a single microelectrode often contain action potentials from more than one neuron. Spike sorting offers a solution to this problem.

Action potentials from different neurons around the electrode produce different spike shapes in the recording. Thus, spikes can be sorted into clusters according to their shape. Depending on the quality of the sorting process, those clusters are either referred to as single units and ideally correspond to single neuron activity or as multi-units in case separation was unsuccessful. Several different approaches to spike sorting have been proposed, both offline[11,12,13] and online.[14,15,16,17,18]

In animal research, under strictly controlled experimental conditions, the electrode position can be

* **Corresponding authors**

optimized for distinctive spike shapes. Depending on experimental settings, it might even be possible to reposition the electrode in response to declining signals. Furthermore, the surrounding conditions are usually controllable and allow reducing external noise. Under such optimized conditions, the signal quality (signal-to-noise ratio as well as the distinctiveness of different spike shapes) is generally very good and thus, many of the previously reported algorithms should produce sufficient results. However, when spiking activity is recorded from a patient, the recording conditions are much less controllable and determined by the clinical setting. This often implies suboptimal settings for electrophysiological measurements.[19,20] The imposed constraints are especially present during intra-operative recordings, e.g. during deep brain stimulation surgery, where microelectrode recordings are often used to localize the target area.[21,22] While there is no need for spike sorting to verify the general target region, e.g. the borders of the subthalamic nucleus (STN), it is of value to address different subregions and physiological biomarkers more specifically.[23,24,25,26,27,28]
The constraints on such recordings include:

- gradually changing spike shapes due to tissue drifts[29] and brain shifts,[30]
- fast changing spike shapes due to abrupt patient movement or accidental movement of high-impedance cables,
- pink noise from adjacent neurons due to the high neuronal density of the STN,[31]
- electromagnetic noise from the surrounding operation room equipment,
- little or no possibility of shielding against external noise,
- very short, sometimes interrupted recording sessions.

In addition to the above-mentioned difficulties caused by environmental factors, a researcher must also deal with obstacles caused by the spike-sorting software itself. In offline sorting, when an investigator encounters under-clustering — i.e. when a spike-sorting software sorted two or more distinct spike shapes into the same cluster — adjusting the sorting parameters for an optimal result can be difficult. Some parameters might refer to abstract concepts of the underlying clustering algorithm, which makes their fine-tuning to obtain the desired clustering output rather complicated.[32] These abstract parameters make it even harder to decide on their values to prepare an online spike-sorting session, when one cannot know the number of single units that will be present in the recording channel and how similar their shapes will be.
Another possible concern for an investigator might be what kind of features to use for the actual clustering. Depending on computation time or personal preferences the investigator might favor e.g. whitened spike shapes,[15] PCA components,[11] ICA components[29] or wavelet features.[12] While these features are different, the basic steps of many spike-sorting algorithms are quite similar.
With the above-mentioned difficulties in mind, our goal was to develop an algorithm that

- is robust to noise,
- can adapt to slowly changing spike shapes,
- increases distinctiveness of different spike shapes,
- has more parameters to fine-tune clustering outcomes,
- avoids abstract parameters,
- can work unsupervised,
- can work online

and to incorporate these features in a modular framework that allows to exchange building blocks like feature extraction, without the need to develop a completely new spike-sorting algorithm from scratch. We expect that the presented approach will help to facilitate the development of even better algorithms in the future.

2. Materials and Methods

2.1. *Framework structure*

Many spike-sorting algorithms share — at least partially — the following processing steps:

- accumulation of sampling points,
- preprocessing of data,
- detecting spikes,
- whitening of spike shapes,
- extracting features from spikes,
- selecting features for sorting,
- sorting spikes based on those features,
- communication of the outcome,

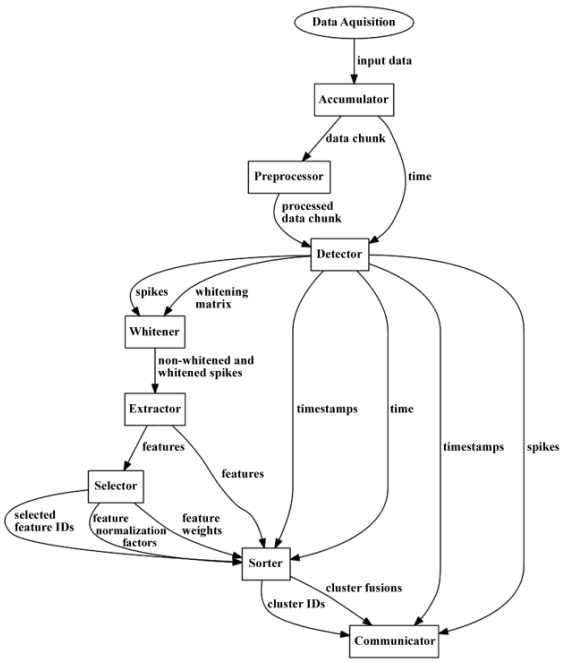

Fig. 1. Structural organization of the proposed spike-sorting framework. Each square represents a module and each arrow represents data sent from one module to the next (see text). Data acquisition can be a recording system (online sorting) or a file (offline sorting).

For each of these steps we designed a module that performs its particular processing task (Fig. 1).

2.1.1. *Accumulator*

Considering an online spike-sorting scenario, the data from the data acquisition system arrive as small packages. Our implementation expects packages of 16bit integer arrays. If the recording is of higher bit-resolution, this can be changed in the code we provide.
The smaller the packages are, the more frequently preprocessing and detection steps have to be performed, especially with high sampling rates. By handling small packages, the time between the occurrence of a spike and the beginning of its sorting is kept minimal. However, if preprocessing or detection includes time consuming operations, this might limit the number of channels that can be analyzed in parallel. If this becomes an issue, the *Accumulator* allows collecting more raw data before it is passed to the *Preprocessor*. This way, preprocessing and detection have to be performed less frequently and more channels can be analyzed in parallel, at the cost of increased delays.

2.1.2. *Preprocessor*

The *Preprocessor* filters each data chunk and passes it to the *Detector*. The filter is a first-order elliptic band-pass filter with 0.8 dB ripple. These settings can be changed in the code if necessary. The pass-band is a parameter. Its default value is 0.3kHz to 3.0kHz. Chunks are overlapping to avoid filter artifacts at the beginning or the end of each chunk. As the number of overlapping data points influences the delay, this number can be set as a parameter as well.

2.1.3. *Detector*

We implemented an online version of the automated threshold detection introduced by Quian Quiroga *et al.*[12]. It is based on the median of the absolute values of the filtered data. Once a data point crosses the threshold, the nearby peak is determined and a variable number of points around the peak are cut out. Furthermore, the *Detector* cuts out noise traces between spikes. These noise traces are used to calculate a whitening matrix. The method we implemented is based on the post hoc whitening used in OSort.[15] The whitening matrix is calculated using the Cholesky decomposition of the inverse Toeplitz matrix of the auto-correlation of the concatenated noise traces. Spike shapes and whitening matrix are passed to the *Whitener*.

2.1.4. *Whitener*

Spike shapes coming out of the *Detector* are contaminated with strongly correlated noise.[33] To remove the auto-correlation introduced by noise, spike shapes are multiplied with the transpose of a whitening matrix (see 2.1.3). Thereby the previously auto-correlated noise is converted to white noise and the Euclidean distance becomes a valid measure of separation.[34] Whitened and non-whitened spike shapes are passed to the *Extractor*.

2.1.5. *Extractor*

The *Extractor* extracts features from spike shapes. We implemented a Haar Wavelet decomposition[12] of the non-whitened spike shapes. All features (whitened spike shapes plus wavelet components of non-whitened spike

shapes) are passed to the *Selector*. The number of all features n_a that are available to the selector is therefore equal to the number of data points per whitened spike shape plus the number of wavelet components per non-whitened spike shape.

2.1.6. *Selector*

If the distribution of a particular feature is close to a normal distribution, that feature does not contain information that can be used to separate different spike shapes. Thus, not all features are helpful to sort spikes into clusters. The *Selector* determines how similar each feature's distribution is to a normal distribution using the Lilliefors modification of the Kolmogorov-Smirnov test. The test returns a value (in the following referred to as KS value) between zero (normally distributed) and one. Out of all available features n_a, a certain number of features n_f with the highest KS values are chosen to be used for spike sorting.[12] By default we use half of n_a as n_f. However, as one of our sorting criteria is based on the Euclidean distance, selecting different features introduces a problem: higher scaled wavelet components usually have larger variances than lower scaled ones or other data points. Differences in a feature with high variance might supersede differences in several other features with lower variance, even if the features with lower variance might be more suitable for sorting. Thus, the *Selector* calculates the standard deviation (SD) of each feature and uses this value to normalize that particular feature. In this way, the influence of each feature on the distance is comparable. However, normally distributed features tend to have a lower SD than non-normally distributed ones. Dividing each feature by its SD would thus decrease the influence of those features which are most suitable for sorting. To compensate for this, each feature is weighted by its KS value. Thereby the ability to differentiate between spike shapes is maximized. Since spike shapes might change over time, standard deviation and KS value are calculated in a moving window fashion. Consequently, subsequent modules only store the original values of each feature and perform normalization and weighting before each operation using the most recent SD and KS values.

2.1.7. *Sorter*

Within the *Sorter*, a cluster is defined as an object that holds all features from its last n_w spikes and their mean, which is referred to as the cluster's representative. Only storing the last n_w spikes of a cluster enables the *Sorter* to adapt to slowly changing spike shapes.

When the *Sorter* starts processing incoming spikes, it creates a new cluster for each new spike. Subsequently, the main sorting loop starts and is repeated until none of the remaining clusters can be fused: The Euclidean distances of the selected, normalized and weighted features of all cluster representatives to all other cluster representatives are determined and cluster pairs are sorted by their distance. From the closest to the most distant pair, clusters are tested for fusion. We implemented three different fusion criteria:

(i) If the Euclidean distance of both representatives is below threshold T_f, clusters are fused without further tests.
(ii) If the largest absolute distance between the auto-correlation of the larger cluster's representative and the cross-correlation of both cluster's representatives is above T_c, clusters are not fused. Heuristically, we determined that this criterion works better if we artificially increase the correlation between the selected features. This is done by sorting the features of the larger cluster by value and the features of the other cluster accordingly (so that the feature indices of both clusters are in the same order). This criterion is more sensitive to the actual shape than a simple distance measure. However, as it is based on correlation, scaled versions of the same shape are considered equal. If scaled versions of the same shape occur within a short time period (without a gradual change) they might not be considered equal by the experimenter and should therefore be separable. In order to achieve this, we implemented a third criterion.
(iii) If the Euclidean distance of the representatives is above T_n, clusters are not fused and all subsequent tests (of more distant pairs) are avoided.

Once two clusters are fused, the clustering loop repeats. As we only consider the last n_w spikes, distance between clusters can fluctuate over time. These fluctuations might lead to spurious crossings of the distance threshold, resulting in erroneous fusion of large (mature) clusters that make up different single-units. To decrease the likelihood of such an incident, the three thresholds T_f, T_c and T_n can be set to stricter (i.e. lower)

values for comparing two mature clusters (i.e. clusters that both contain more than n_m spikes).
The advantage of these fusion techniques lies in the fact that we can handle newly occurring clusters at an advanced stage in the recording. However, spikes which are more corrupted by noise are likely to end up in small clusters of only a few spikes because they are too different from the cluster they belong to and are only fused with similarly corrupted spikes. These small clusters might be fused with the correct cluster later in the recording but until then, their identity is not known.

This can be a problem for closed loop experiments, when every spike of a certain single unit has to trigger an event in very close succession to the occurrence of that spike. To resolve this issue, we also implemented a distance-based template matching. A certain time t_s after the recording started, all clusters containing less than n_t spikes that have not been fused in the last t_f seconds are fused with the closest cluster containing more than n_m spikes, if the distance between those clusters is less than T_u. In this way, it is guaranteed that after the time t_f, the identity of a spike is known.

Table 1. Important parameters. Reasonable ranges are given in square brackets, default values in brackets.

n_f	Number of features that are used for the sorting process. The more features are used, the more likely is it that even small differences in spike shapes can be separated. However, more features will also increase the influence of noise, as features are selected based on their KS value. [10, 64] (n_a / 2)
n_w	Number of spikes to consider when calculating the representative of a cluster. This determines how fast the sorter adapts to changing spike shapes. Lowering this number will result in a faster adaptation. Increasing this number will result in more accurate means and thus in more stable representatives. [150, 300] (150)
T_f	If the Euclidean distance of the selected, normalized and weighted features (in the following simply referred to as Euclidean distance) of two cluster representatives is below T_f, these clusters will be fused. Increasing this threshold will increase sensitivity and even small differences will decrease the likelihood of fusion. This could lead to over-clustering. Decreasing this value will lead to fusion of less similar clusters. Fusing these could potentially decrease the distance to other clusters, thereby increasing the chance of further fusions. This could lead to under-clustering. [0.3, 0.7] (0.36)
T_c	If, after ordering the selected features of two cluster representatives as described in 2.1.7, the largest absolute distance between the auto-correlation of the larger cluster's features and the cross-correlation of both cluster's features is above T_c, cluster fusion is prevented. Unlike the distance metric, this metric is influenced only by the shapes themselves and not by the amplitude of those shapes. This metric is only used if the distance of the clusters in question is between T_f and T_n. Increasing it will increase the likelihood that these clusters are fused, depending on how similar their shapes are. [0.04, 0.12] (0.08)
T_n	If the Euclidean distance of two cluster representatives is above T_n, clusters will not be fused. Increasing this threshold will decrease the influence of the distance metric of our sorter, and clusters that are further apart but still pass the T_c metric will be fused. Decreasing this threshold will increase the influence of the distance metric and, even if clusters pass the T_c metric, fusion will be prevented if the distance surpasses T_n. [0.5, 1.0] (0.55)
n_m	If a cluster has more than n_m spikes we refer to it as a mature cluster. The thresholds T_f, T_c and T_n can be set to stricter values for assessing the fusion of two mature clusters. This will decrease the likelihood of under-clustering without preventing single spikes or small clusters to be absorbed by the correct single unit's cluster. [20, 50] (50)
Mature T_f, T_c, T_n	Multipliers for T_f, T_c and T_n when the fusion of two mature clusters is assessed. [0.2, 1.0] (T_f, T_n: 0.2, T_c: 0.5)
t_s	Time after which template forcing is activated.
n_t	If template forcing is active, only clusters with less than or equal to n_t spikes will be forced to fuse with their nearest mature clusters. [1, n_m - 1] (n_m - 1)
t_f	If template forcing is active, only clusters that were not fused within the last t_f seconds are forced to fuse with their nearest mature clusters.
T_u	If template forcing is active, only clusters for which the Euclidean distances between them and their nearest mature clusters are below T_u are forced to fuse. [1.0, 2.5] (1.5)

However, investigators should take care when using this feature. If T_u is set too high, it can make the detection of newly occurring single units difficult after the onset of template forcing.

2.1.8. *Communicator*

The *Communicator* supplies the output of the spike-sorting algorithm in real time. It sends the following information to the user via a callback function:

- raw spike shapes,
- spike timestamps,
- spike IDs,
- pairs of cluster IDs that were fused (the ID of a cluster is equal to the ID of its first spike).

This information can be used to construct the current clustering status online (e.g. to visualize clusters in a GUI) or to write the clustering outcome to file.

2.2. *Implementation*

We implemented our online spike-sorting framework as an open-source multi-threaded C/C++ library. While a complete and up-to-date documentation as well as the source code are available online at http://cl.knieling.org, we summarized the most important parameters in Table 1. Reasonable ranges for those parameters where found heuristically.

2.3. *Test datasets*

To evaluate sorting capabilities we used several sets of artificial data for which the time of each spike as well as the neuron to which it belongs is known. We used 45 test datasets published by Wild *et al.*[32] (M10). These datasets contain 1 to 9 neurons at 5 different noise levels. Their spike shapes were taken from human STN recordings.

To prevent a bias towards STN in our analysis, we generated similar test datasets from spikes recorded *in vivo* from the human hippocampus and neocortex (parahippocampal cortex). For each of these regions, we chose 9 single units that differed substantially in their mean waveforms, to cover a wide variety of possible signals. We generated datasets including n neurons by using the mean waveforms of the first n of these selected single units as spike-shape templates for our artificial neurons. We superimposed spike-shape templates on 30min of a micro-wire recording of local field potentials (LFP) (band-pass filtered between 0.3kHz and 3.0kHz) that did not contain any spikes originally. However, we ensured that the signal exhibited the typical frequency spectrum of human LFP[35] to prevent us from accidentally choosing a recording from a faulty micro-wire as background activity. By superimposing the spike shapes on an actual recording we intended to generate datasets that were close to the properties of real data.

To generate different noise levels, similarly to Wild *et al.*[32], we divided the background activity by its standard deviation and multiplied it by 0.05, 0.10, 0.15, 0.20 or 0.30 respectively. The n selected spike-shape templates were scaled to a maximum between 1.0 and 0.4 before superimposing them on the scaled background activity.

For each neuron present, we chose an independent Poisson model with an absolute refractory period of 1ms and a relative refractory period of 2ms to determine the time of each spike in the artificial recording. Firing rates for the 9 neurons ranged from 0.1Hz to 0.9Hz.

In real recordings, due to discrete sampling, it is unlikely to sample the exact peak of a spike. To account for this type of variability, we up-sampled the spike-shape templates by a factor of 9 using cubic spline interpolation, and for each fired spike, we randomly cut off the first 0 to 8 data points before down-sampling it again.

This procedure yielded another 45 test datasets (from 1 to 9 neurons at 5 different noise levels) for each of the aforementioned regions.

To test sorting capabilities of non-Gaussian spike distributions in feature space we used test datasets published by Quian Quiroga *et al.*[12]. They simulated electrode movement during recording, bursting neurons as well as correlation between spikes and the LFP.

2.4. *Evaluation and comparison*

In order to assess the sorting quality, we compared our framework (ClusterLizard) to OSort and Wave_Clus, which are established unsupervised online and offline algorithms, respectively. Since we wanted to compare the quality of spike sorting rather than spike detection, we modified each respective spike-sorting software to work with pre-supplied spike-timestamps instead of using their inherent spike detection capabilities.

To assess the sorting quality we used two different scoring systems — the Adjusted Mutual Information (AMI)[36,37] and an error metric described by Adamos *et*

al.[38]. AMI is an information-theoretic measure for clustering comparison. It is a variation of mutual information that has been adjusted for agreement by chance. For calculation we used the MATLAB code provided by the author Nguyen Xuan Vinh.[39] In rare cases, the algorithm returned negative scores which were set to zero.

The error metric introduced by Adamos *et al.*[38] is based on the following two equations:

$$\mathrm{error}_c = \frac{\mathrm{Fn}_c + \mathrm{Fp}_c}{\sum_{c=1}^{c_{\max}} S_c} \,. \qquad (1)$$

$$\mathrm{error}_{\mathrm{spiketrain}} = \sum_{c=1}^{c_{\max}} \mathrm{error}_c \,. \qquad (2)$$

where the index c is a particular known cluster. Fn_c is the number of false negative spikes, Fp_c the number of false positive spikes and S_c is the total number of spikes in that cluster. A detailed description is given in Adamos *et al.*[38]. For a better comparison to the AMI scores we changed the error metric in the following way:

$$\mathrm{AdamosScore} = 1 - \min(1, \mathrm{error}_{\mathrm{spiketrain}}) \,. \qquad (3)$$

Both scores (AMI and the Adamos Score) can be calculated from a contingency table. Our contingency tables had one row for each known cluster, one column for each detected cluster and one column for spikes classified as noise. A row for noise that was classified as spikes was not necessary, as spike-timestamps were pre-supplied (see Appendix B for an example).

Clustering the same dataset multiple times using Wave_Clus, does not yield the same results. This behavior persists even when the SPC program included in Wave_Clus is initialized with the same seed. These small changes can cause Wave_Clus's automated temperature selection to select a different temperature for the same dataset. This can lead to over- or under-clustering. We, therefore, worked with median sorting results in order to get a reliable estimate. We used Wave_Clus's batch mode to cluster 45 datasets in a row and we repeated this 100 times. For comparison, we chose the batch that was — in both scoring systems — closest to (and still above), the median score.

In the test datasets of Wild *et al.*,[32] spike shapes are composed of about 37 data points. However, at a sampling rate of 24kHz, OSort cuts out 64 data points around the spike peak. As OSort is based on Euclidean distance of the (whitened) spike shapes, we changed the cut-out region to 37 data points, to avoid unnecessary noise in the spike waveforms. The same was done for the test datasets published by Quian Quiroga *et al.*[12] Additionally, we used OSorts *exact* threshold method.

Except for the mentioned modifications, each software's default parameters were used (a list of parameters and values we used is provided in Appendix A).

Performance differences between algorithms were assessed for both scoring systems using the two-sided Wilcoxon signed rank test with Bonferroni-Holm as a correction for multiple (n=3) comparisons.

2.5. *Extracellular recordings*

We tested our algorithm on intra-operative extracellular recordings obtained during the implantation of deep brain stimulation electrodes in the subthalamic nucleus (STN) of a patient suffering from Parkinson's disease. These recordings were acquired to determine the exact target region for implantation and are part of the standard surgical procedure at the Department of Neurosurgery of the University of Tuebingen.

Extracellular potential differences were measured using NeuroProbe microelectrodes (Alpha Omega). The differential signal was amplified, filtered between 0.075Hz and 10kHz and sampled at approximately 44.6kHz using the NeuroOmega system (Alpha Omega). Impedances were generally around 600kOhm.

3. Results

We evaluated the performance of Wave_Clus, OSort and our algorithm (ClusterLizard) on test datasets containing 1 to 9 different spike shapes at 5 different noise levels. These datasets were generated from real spike shapes of human STN, hippocampus and neocortex (see 2.3). To measure performance, we used two different scoring systems — Adjusted Mutual Information (AMI)[37] and a score based on the error metric described by Adamos *et al.*[38]. The smallest contingency table that can be evaluated using AMI is 2 by 2.

Thus, datasets that contain just one spike-shape could only be evaluated by the Adamos metric, not by AMI.

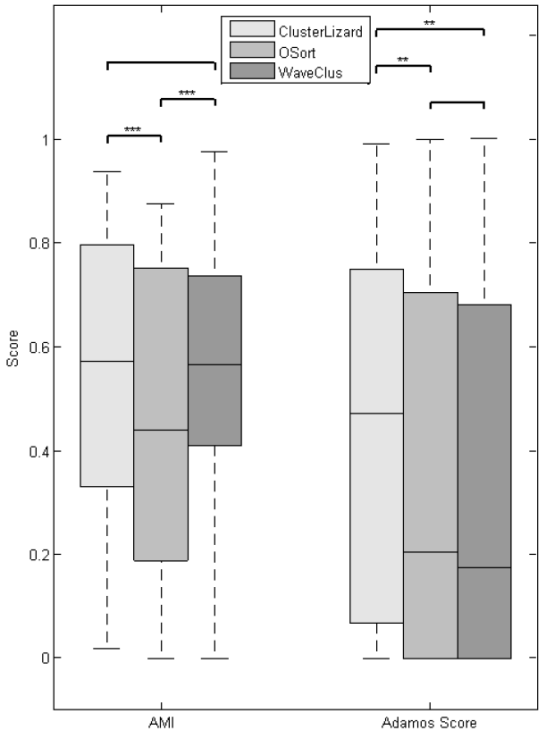

Fig. 2. Box-plots of AMI and Adamos scores from our algorithm (ClusterLizard), OSort and Wave_Clus. Each AMI box-plot was generated from the scores of each sorting algorithm on 120 test datasets. Each Adamos box-plot was generated from the scores of each sorting algorithm on 135 test datasets. **, p<0.01; ***, p<0.001.

Fig. 2 shows two box-plots for each algorithm, generated from 120 AMI and 135 Adamos scores, respectively. Our algorithm shows significantly higher AMI scores than OSort and significantly higher Adamos scores than OSort and Wave_Clus. Futhermore, Wave_Clus shows significantly higher AMI scores than OSort.

Scores for the non-Gaussian datasets published by Quian Quiroga et al.[12] are shown in Table 2.

Another goal was to overcome the difficulties that intra-operative recordings pose on spike sorting. Those include short recording times, changing spike shapes due to tissue drifts and brain shifts as well as noise from surrounding OR equipment. Fig. 3 shows a typical extracellular recording from the human STN and the sorting outcome of our algorithm.

Table 2. AMI and Adamos scores (AS) from ClusterLizard (CL), OSort (OS) and Wave_Clus (WC) for non-Gaussian datasets. CL* shows scores obtained by ClusterLizard when using more liberal (higher) threshold values (T_f = 0.65, T_n = 1.0, T_c = 0.12, T_u = 2.5, mature T_f, T_n and T_c = 1.0). The other CL scores as well as the scores of the other algorithms were obtained using the parameters in Appendix A.

	Burst		Drift		LFP corr.	
	AMI	AS	AMI	AS	AMI	AS
CL*	0.83	0.93	0.88	0.95	0.86	0.94
CL	0.55	0.47	0.44	0.32	0.44	0.29
OS	0.57	0.65	0.67	0.74	0.44	0.51
WC	0.52	0.56	0.61	0.67	0.53	0.64

Table 3. Estimation of false positives and false negatives for the three units in Fig. 3 using the quality metrics of Hill *et al.* [40]

	False positives					
	Single cluster error	**Multiple cluster errors**				**Composite**
		Overlap of clusters				
No. of spikes	**ISI violations f^p_1**	**1-2**	**1-3**	**2-3**	**Sum f^p_2**	**max(f^p_1,f^p_2)**
Cluster 1 (794)	0.26	0.031	0.00007		0.031	0.26
Cluster 2 (254)	0.28	0.27		0.045	0.31	0.31
Cluster 3 (204)	0.54		0.000008	0.058	0.058	0.54

	False negatives						
	Single cluster error	**Multiple cluster errors**					**Composite**
		Overlap of clusters				**Censored**	
No. of spikes	**Undetected spikes f^n_1**	**1-2**	**1-3**	**2-3**	**Sum f^n_2**	**spikes f^n_3**	**[1-(1-f^n_1)*(1-f^n_3)] + f^n_2**
Cluster 1 (794)	0.40	0.086	0.000002		0.086	0.010	0.49
Cluster 2 (254)	0.0196	0.098		0.047	0.14	0.022	0.19
Cluster 3 (204)	0.00006		0.0003	0.056	0.056	0.023	0.08

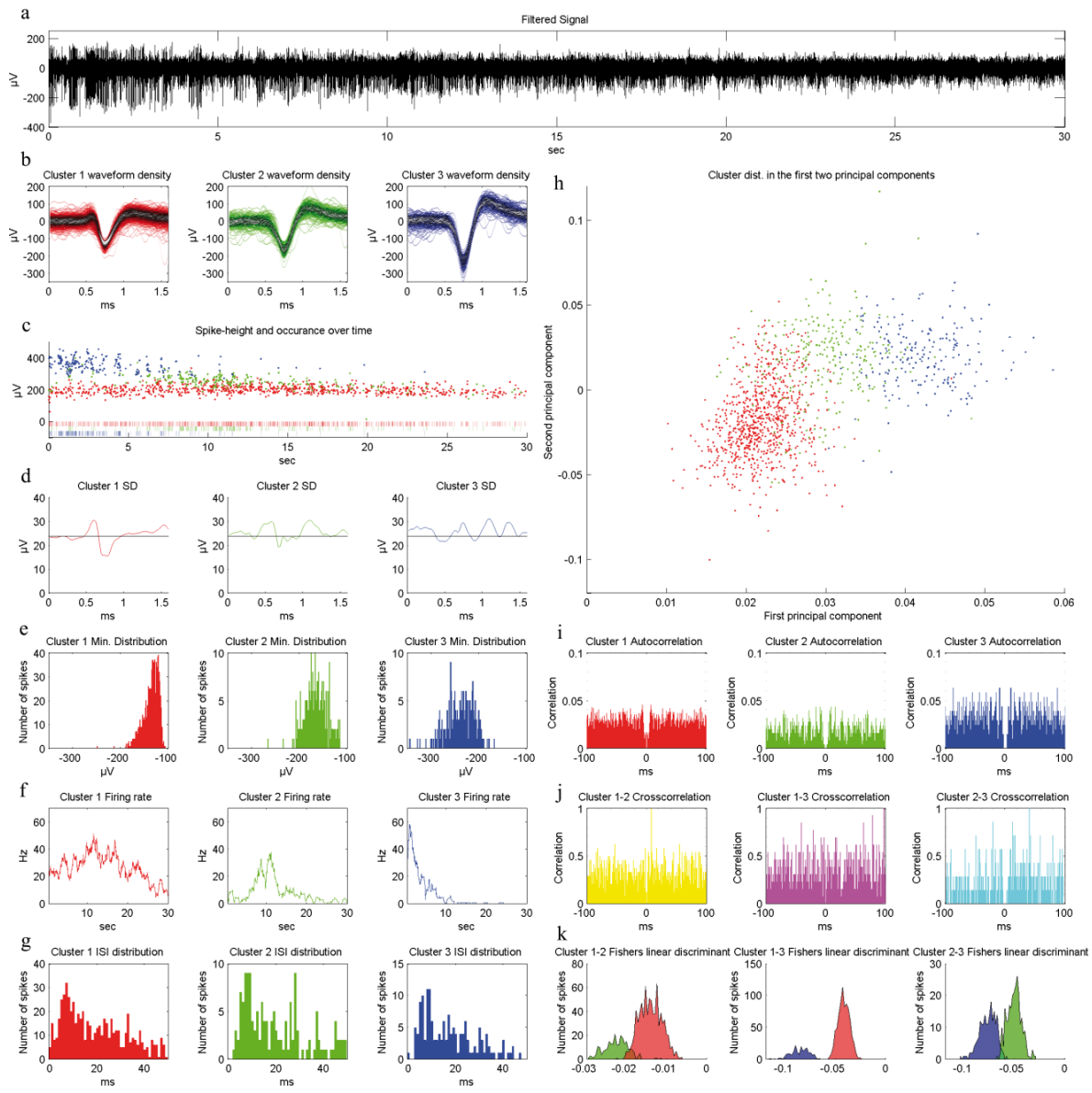

Fig. 3: Sorting results obtained by using ClusterLizard on the signal shown in a. (a) Typical intra-operative recording filtered between 300 and 3000 Hz. (b) Density plot of the three resulting clusters. With increasing overlap the color first changes to black and then to white. (c) Spike height (top) and occurrence (bottom) of all three clusters over time. (d) Standard deviation of each cluster. The black line indicates the SD of the background noise. (e) Minimum distribution of each cluster. (f) Firing rate of each cluster over time. The size of the moving window is 1sec. (g) ISI distribution from 0 to 50 ms of each cluster. (h) Scatter plot of all 3 clusters in the plane of the first two principal components. (i) Autocorrelation of each cluster. The autocorrelation at a time lag of exactly 0.0ms is 1.0 and was omitted from the plot. (j) Cross-correlation of all cluster pairs. Gaps or small values around a time lag of 0.0ms are caused by the censor-period of the detector module. (k) Histograms of all cluster pairs projected onto Fisher's linear discriminant.

Table 4. Estimation of false positives and false negatives for the two units in Fig. 4 using the quality metrics of Hill *et al.* [40]

	False positives			
	Single cluster error	**Multiple cluster errors**		**Composite**
		Overlap of clusters		
No. of spikes	**ISI violations f^p_1**	**1-2**	**Sum f^p_2**	**max(f^p_1,f^p_2)**
Cluster 1 (414)	0.55	0.063	0.063	0.55
Cluster 2 (287)	0.27	0.083	0.083	0.27

	False negatives				
	Single cluster error	**Multiple cluster errors**			**Composite**
		Overlap of clusters		**Censored**	
No. of spikes	**Undetected spikes f^n_1**	**1-2**	**Sum f^n_2**	**spikes f^n_3**	**[1-(1-f^n_1)*(1-f^n_3)] + f^n_2**
Cluster 1 (414)	0.38	0.057	0.057	0.0064	0.44
Cluster 2 (287)	0.19	0.092	0.092	0.0093	0.29

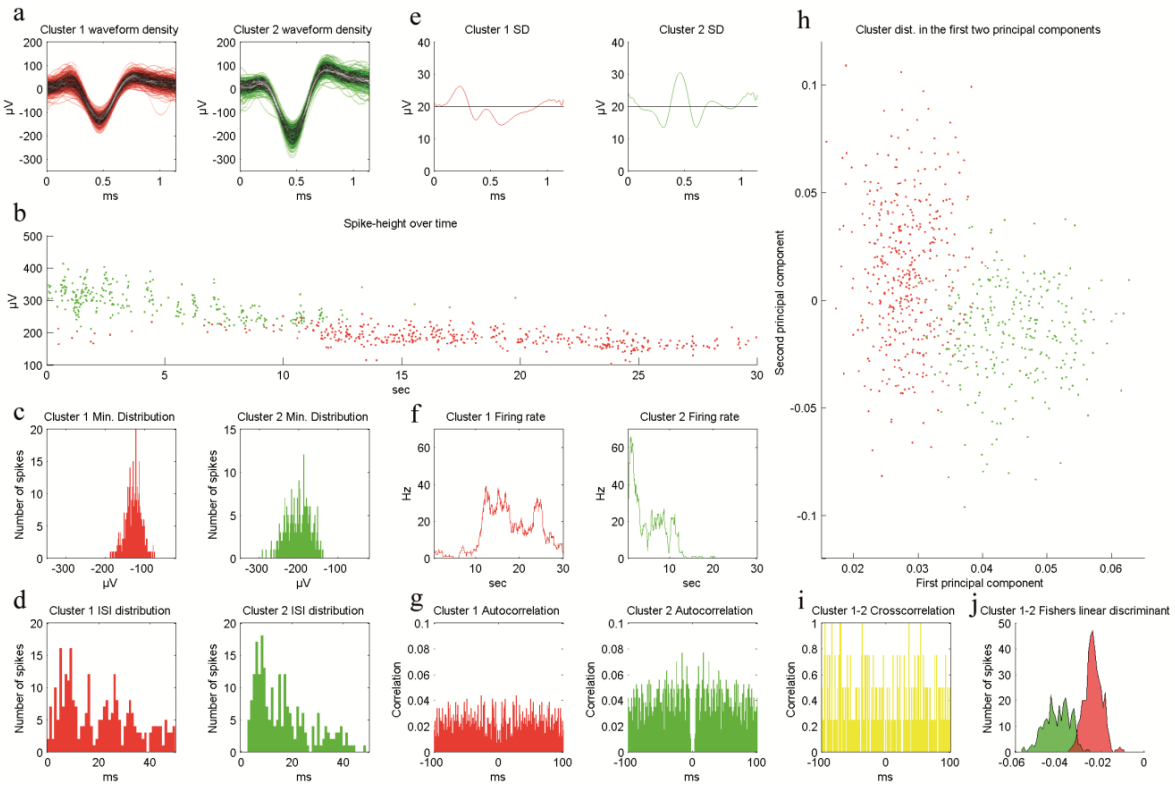

Fig. 4 Sorting results obtained by using OSort on the signal shown in Fig. 3a. (a) Density plot of the two resulting clusters. With increasing overlap the color first changes to black and then to white. (b) Spike height of both clusters over time. (c) Minimum distribution of each cluster. (d) ISI distribution from 0 to 50 ms of each cluster. (e) Standard deviation of each cluster. The black line indicates the SD of the background noise. (f) Firing rate of each cluster over time. The size of the moving window is 1sec. (g) Autocorrelation of each cluster. The autocorrelation at a time lag of exactly 0.0ms is 1.0 and was omitted from the plot. (h) Scatter plot of both clusters in the plane of the first two principal components. (i) Cross-correlation of both clusters. Gaps or small values around a time lag of 0.0ms are caused by the censor-period of the detector module. (j) Histograms of both clusters projected onto Fisher's linear discriminant.

Table 5. Estimation of false positives and false negatives for the two units in Fig. 5 using the quality metrics of Hill *et al.* [40]

		False positives		
	Single cluster error	**Multiple cluster errors**		**Composite**
		Overlap of clusters		
No. of spikes	**ISI violations f^p_1**	**1-2**	**Sum f^p_2**	**max(f^p_1,f^p_2)**
Cluster 1 (1422)	0.41	0.095	0.095	0.41
Cluster 2 (228)	0.58	0.0097	0.0097	0.58

		False negatives			
	Single cluster error	**Multiple cluster errors**			**Composite**
		Overlap of clusters		**Censored**	
No. of spikes	**Undetected spikes f^n_1**	**1-2**	**Sum f^n_2**	**spikes f^n_3**	**[1-(1-f^n_1)*(1-f^n_3)] + f^n_2**
Cluster 1 (1422)	0.41	0.0015	0.0015	0.011	0.42
Cluster 2 (228)	0.00015	0.595	0.595	0.071	0.67

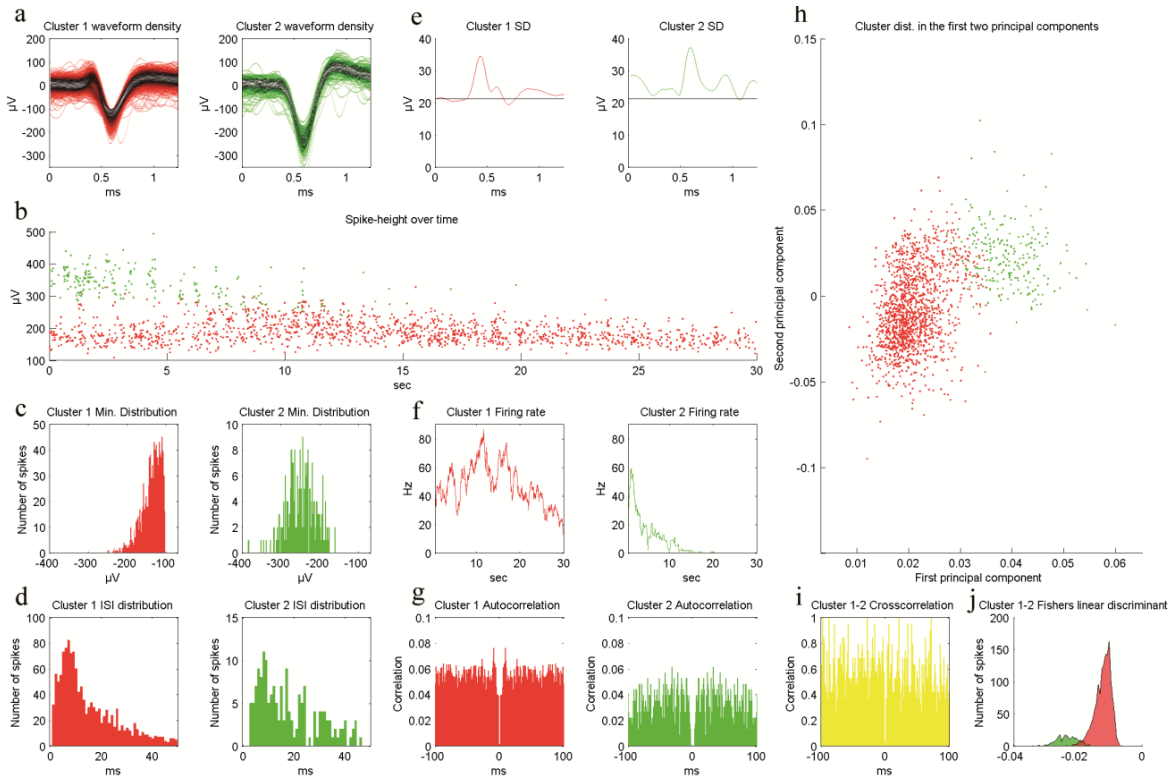

Fig. 5 Sorting results obtained by using Wave_Clus on the signal shown in Fig. 3a. (a) Density plot of the two resulting clusters. With increasing overlap the color first changes to black and then to white. (b) Spike height of both clusters over time. (c) Minimum distribution of each cluster. (d) ISI distribution from 0 to 50 ms of each cluster. (e) Standard deviation of each cluster. The black line indicates the SD of the background noise. (f) Firing rate of each cluster over time. The size of the moving window is 1sec. (g) Autocorrelation of each cluster. The autocorrelation at a time lag of exactly 0.0ms is 1.0 and was omitted from the plot. (h) Scatter plot of both clusters in the plane of the first two principal components. (i) Cross-correlation of both clusters. Gaps or small values around a time lag of 0.0ms are caused by the censor-period of the detector module. (j) Histograms of both clusters projected onto Fisher's linear discriminant.

As the ground truth in extracellular recordings is not known, we assessed the detection and sorting quality by estimating the following parameters using the quality metrics of Hill *et al.*[40] :

- false positive spike detections based on refractory period violations,
- false negative spike detections based on detection thresholds,
- false negative spike detections based on censored data,
- false positive and false negative spikes in the sorting process based on overlaps between pairs of clusters in a projection onto Fisher's linear discriminant.

Censored data is a result of the detector's censor-period. For a very short amount of time (usually 0.6 to 1.5ms) after the spike's peak, no spike will be detected to prevent one spike-waveform from being detected as multiple spikes. Instead of originating from a separate spike, local maxima within this period could result from noise superimposed on the already detected spike-waveform.
For estimations of false-positively detected spikes, we used a refractory period of 4ms, which is a typical value for the STN.[41] Results are shown in Table 3, 4 and 5.

4. Discussion

4.1. *Test datasets*

We here propose a modular spike-sorting framework that is able to match and outperform OSort and Wave_Clus at sorting a diverse pool of test datasets.
For the three sets of data containing 1 to 9 different spike shapes at 5 different noise levels (Fig. 2) the AMI scores seem to suggest that our algorithm rather matched Wave_Clus' performance while the Adamos scores suggests that we outperformed Wave_Clus. We used two different scoring systems to ensure that our results are not dependent on one single approach to assess sorting quality. While the Adamos Score penalizes under-clustering severely, AMI scores can still be rather high (above 0.5) even when the algorithm under-clustered heavily, as long as at least one cluster is rather clean (low false-positives) and complete (low false-negatives). Due to these differences, AMI and Adamos scores seem to complement each other reasonably well.
We noticed in our contingency tables that for recordings containing more than five neurons, Wave_Clus has difficulties extracting all of them. In those cases it seems to focus on some distinct clusters that it manages to extract rather completely and with a low number of false-positives, while the rest is under-clustered (see Appendix B for an example). This behavior explains the pronounced differences between Wave_Clus's AMI and Adamos scores. AMI is able to reward even small numbers of clean clusters with a rather high score compared to the Adamos Score which will be zero in response to severe under-clustering. However, this reduces AMI's resolution to reward nearly perfect solutions. For these, the Adamos Score seems to be more accurate; also, the cut between acceptable and unacceptable sorting results appears to be sharper and thus more intuitive to interpret. Finally, N. X. Vinh[39] warns that his AMI script might deviate from the actual AMI score due to insufficient floating-point precision of Matlab.
To assess sorting capabilities of non-Gaussian spike distributions in feature space we used test datasets simulating electrode movement during recording, bursting neurons as well as correlation between spikes and the LFP.[12] Using our default parameters, ClusterLizard performed slightly worse on these datasets than OSort and Wave_Clus. However, using more liberal thresholds, ClusterLizard achieved a remarkable separation (see Table 2).

4.2. *Computation*

Similar to OSort, our spike sorting algorithm works online and unsupervised. Sorting one test dataset at a time and using default parameters, ClusterLizard sorted with an average speed of 1495 spikes/s on our test station (personal computer running on an Intel Core i7-4820K [3.7 GHz] using 16GB of DDR3 RAM). On the same machine, OSort sorted the same datasets with an average speed of 465 spikes/s.
While OSort likely needs to perform less calculations than ClusterLizard, its Matlab implementation is not optimized for computation speed as discussed in Rutishauser *et al.*[15]. We implemented our algorithm in a fast, compilable programming language (C++) and used multi-threading and a custom-made memory manager to optimize the computation speed of our open-source

framework. We hope this will encourage other experimenters to build upon our work and to use it to quickly prototype new and fast spike sorting algorithms.

4.3. *Intra-operative recording*

ClusterLizard's sorting results of a representative intra-operative recording are shown in Fig. 3. These findings appear to be convincing, though the estimated false-positives and -negatives based on the quality metrics of Hill *et al.*[40] would suggest suboptimal results. False-negative spikes due to censored data, based on the censor-period of the detection algorithm, are rather low. However, the false-negative spikes based on the detection threshold are rather high, suggesting that our detection algorithm could be improved. False-positive and false-negative spikes due to cluster overlaps are rather low except for some contamination of cluster two in cluster one. Increased false-positives due to ISI violations might indicate miss-classifications. However, those high values could also be due to a refractory period that is set too high. Bar-Gad *et al.*[41] stated that 4ms is a typical value for STN neurons. However, the rapidly declining amplitude of the signal could suggest a tissue drift. During tissue drift, the electrode could have mechanically excited the neurons to fire more rapidly during the relative refractory period, while the absolute refractory period of these neurons might be lower than 4ms. Assuming for example a refractory period of 3ms would change the false-positive rate due to ISI violations to 28% for cluster one, 10% for cluster two and 0% for cluster three.

Looking at the result of OSort and the median result of Wave_Clus (see Fig. 4 and 5), the density plots suggest a high contamination in both OSort's and Wave_Clus's first cluster. Furthermore, there are even higher estimates of false-positives due to ISI violations. False-negative rates due to cluster overlap are rather large in Wave_Clus while in OSort they are slightly lower than in our algorithm. False-negatives due to undetected spikes are large in all three algorithms. While Wave_Clus detected more spikes than our algorithm, OSort detected less spikes. The reason that our algorithm detected less spikes than Wave_Clus, even though we use basically the same detection technique is that we frequently update the threshold with the median of the absolute data of each new data-chunk. We weighted this new median with 0.02 in comparison to the previous threshold. This way the threshold can react quickly to changes in signal amplitude. However, this also leads to increasing thresholds in response to high firing rates and, therefore, spikes might be missed. A quick solution would be to further decrease the influence of the new data chunk on the threshold, at the cost of decreasing reaction time to abruptly changing signal amplitudes.

5. Conclusion

On average, the presented sorting algorithm performed equally well or better than Wave_Clus and OSort in a diverse pool of test datasets. However, previous studies have shown that the sorting quality depends highly on the parameter settings of the respective algorithms[32] offering the possibility to improve the performance of the algorithms we compared, with some ad-hoc parameter settings. The advantage of the newly developed approach is that it provides several parameters that affect the sorting process in an understandable manner, while avoiding abstract parameters, which would be unpredictable for the experimenter. In this way, experimenters can easily adjust the algorithm to compensate for unsatisfactory sorting outcomes. Moreover, we were able to achieve convincing results for intra-operative recordings which are known to be difficult to sort. Finally, the clear, modular architecture of our framework allows for easy replacement of individual components such as the *Detector*. We hope that this will facilitate the development of novel algorithms to further improve the detection of neuronal signatures related to healthy or pathological conditions.

Acknowledgements

We thank J. Niediek for his valuable comments during the drafting of this manuscript. FM acknowledges support from the German Research Council (DFG MO 930/4-1, DFG SFB 1089), the Volkswagen Foundation, and the European Commission (FP7 Epitarget). AG was supported by grants from the German Research Council [DFG GH 94/2-1, DFG EC 307], and from the Federal Ministry for Education and Research [BFNT 01GQ0761, BMBF 16SV3783, BMBF 03160064B, BMBF V4UKF014].

Appendix A. Sorting parameters

Sorting parameters for test-datasets. Parameters in the first column were used for the datasets of Wild et al.[32] and the non-Gaussian datasets of Quian Quiroga et al.[12]. Parameters in the second column were used for our datasets (see section 2.3).

ClusterLizard			**OSort**			**Wave_Clus**		
samplingFrequency:	24000	32000	SamplingFreq:	24000	32000	w_pre:	12	20
T_f:	0.36	0.36	minNrSpikes:	50	50	w_post:	25	44
T_n:	0.55	0.55	thresholdMethod:	2	2	detection:	'pos'	'pos'
T_c:	0.08	0.08	prewhiten:	0	0	stdmin:	5.00	5.00
Mature T_f:	0.2	0.2	defaultAlignMethod:	1	1	stdmax:	50	50
Mature T_n:	0.2	0.2	peakAlignMethod:	1	1	interpolation:	'y'	'y'
Mature T_c:	0.5	0.5	detectionMethod:	1	1	int_factor:	10	10
T_u:	1.4	1.4	kernelSize:	18	18	detect_fmin:	300	300
n_t:	49	49	extractionThreshold:	5	5	detect_fmax:	3000	3000
n_m:	50	50	rawTraceLength:	37	64	sort_fmin:	300	300
n_w:	150	150	beforePeak:	11	20	sort_fmax:	3000	3000
t_s:	55	1500	afterPeak:	25	43	segments:	1	1
t_f:	0.05	2.0				sr:	24000	32000
n_f:	37	64				min_ref_per:	1.5	1.5
detection:	1	1				int_factor:	10	10
prePeak:	11	20				max_spk:	20000	20000
postPeak:	25	43				template_type:	center	center
f_high_pass:	300	300				template_sdnum:	11	11
f_low_pass:	3000	3000				features:	wav	wav
						inputs:	10	10
						scales:	4	4
						mintemp:	0	0
						maxtemp:	0.301	0.301
						tempstep:	0.01	0.01
						stab:	0.8	0.8
						SWCycles:	100	100
						KNearNeighb:	11	11
						randomseed:	15485	15485
						min_clus_abs:	20	20
						min_clus_rel:	0.005	0.005
						force_auto:	y	y
						max_spikes:	5000	5000

Sorting parameters for intra-op datasets

ClusterLizard		**OSort**		**Wave_Clus**	
samplingFrequency:	44642	SamplingFreq:	44642	w_pre:	25
T_f:	0.36	minNrSpikes:	50	w_post:	30
T_n:	0.55	thresholdMethod:	1	detection:	'neg'
T_c:	0.08	prewhiten:	0	stdmin:	5.00
Mature T_f:	0.2	defaultAlignMethod:	2	stdmax:	50
Mature T_n:	0.2	peakAlignMethod:	1	interpolation:	'y'
Mature T_c:	0.5	detectionMethod:	1	int_factor:	10
T_u:	2.0	kernelSize:	18	detect_fmin:	300
n_t:	19	extractionThreshold:	5	detect_fmax:	3000
n_m:	20	rawTraceLength:	55	sort_fmin:	300
n_w:	300	beforePeak:	24	sort_fmax:	3000
t_s:	15	afterPeak:	30	segments:	1
t_f:	0.05			sr:	44642
n_f:	55			min_ref_per:	1.5
detection:	2			int_factor:	10
prePeak:	24			max_spk:	20000
postPeak:	30			template_type:	center
f_high_pass:	300			template_sdnum:	11
f_low_pass:	3000			features:	wav
				inputs:	10
				scales:	4
				mintemp:	0
				maxtemp:	0.301
				tempstep:	0.01
				stab:	0.8
				SWCycles:	100
				KNearNeighb:	11
				randomseed:	15485
				min_clus_abs:	20
				min_clus_rel:	0.005
				force_auto:	y
				max_spikes:	5000

Appendix B. Exemplary contingency table

Exemplary contingency table produced by Wave_Clus. Nine distinct spike shapes where present in the recording. Wave_Clus generated 3 clusters. The first one is heavily under-clustered but the remaining two are well separated. The Adamos Score for this sorting outcome is 0 but the AMI score is 0.56. The contingency table has one row for each known cluster, one column for each detected cluster and one column for spikes classified as noise.

48	1	1120	0
1540	0	2	0
581	0	3	0
726	1	3	0
27	1274	2	0
174	0	28	0
1682	2	4	0
338	1	50	0
912	0	3	0

References

1. Friedrich J, Urbancziky R, and Senn W. Code-specific learning rules improve action selection by populations of spiking neurons. Int J Neural Syst 2014 24(5)
2. Strack B., Jacobs KM, Cios KJ. Simulating vertical and horizontal inhibition with short term dynamics in a multi-column, multi-layer model of neocortex Int J Neural Syst. 2014 24(5)
3. Shapero S, Zhu M, Hasler P, Rozell C. Optimal sparse approximation with integrate and fire neurons. Int J Neural Syst. 2014; 24(5)
4. Rosselló JL, Canals V, Oliver A, Morro A Studying the role of synchronized and chaotic spiking neural ensembles in neural information processing Int J Neural Syst. 2014 24(5)
5. Wang Z, Guo L Adjouadi M. A generalized leaky Integrate-and-Fire neuron model with fast implementation method. Int J Neural Syst. 2014 24(5)
6. Zhang G, Rong H, Neri F, Perez-Jimenez MJ. An optimization spiking neural P system for approximately solving combinatorial optimization problems. Int J Neural Syst. 2014 24(5)
7. Ghosh-Dastidar Z, Adeli H. Spiking neural networks. Int J Neural Syst 2009 19(4): 295-308.
8. Rossello JL, Canals V, Morro A, Verd J. Chaos-based mixed signal implementation of spiking neurons. Int J Neural Syst. 2009 19(6): 465-71.
9. Ghosh-Dastidar S Adeli H. A new supervised learning algorithm for multiple spiking neural networks with application in Epilepsy and seizure detection. Neural Netw. 2009 22(10): 1419-31.
10. Ghosh-Dastidar S, Adeli H. Improved spiking neural networks for EEG classification and Epilepsy seizure detection. Integr Comput-Aid Eng. 2007 14(3): 187-212.
11. Harris KD, Henze DA, Csicsvari J, Hirase H, Buzsáki G. Accuracy of tetrode spike separation as determined by simultaneous intracellular and extracellular measurements. J Neurophysiol. 2000 Jul;84(1):401-14.
12. Quiroga RQ, Nadasdy Z, Ben-Shaul Y. Unsupervised spike detection and sorting with wavelets and superparamagnetic clustering. Neural Comput. 2004 Aug;16(8):1661-87.
13. Wood F, Goldwater S, Black MJ. A non-parametric Bayesian approach to spike sorting. Conf Proc IEEE Eng Med Biol Soc. 2006;1:1165-8.
14. Aksenova TI, Chibirova OK, Dryga OA, Tetko IV, Benabid AL, Villa AE. An unsupervised automatic method for sorting neuronal spike waveforms in awake and freely moving animals. Methods. 2003 Jun;30(2):178-87.
15. Rutishauser U, Schuman EM, Mamelak AN. Online detection and sorting of extracellularly recorded action potentials in human medial temporal lobe recordings, in vivo. J Neurosci Methods. 2006 Jun 30;154(1-2):204-24.
16. Franke F, Natora M, Boucsein C, Munk MH, Obermayer K. An online spike detection and spike classification algorithm capable of instantaneous resolution of overlapping spikes. J Comput Neurosci. 2010 Aug;29(1-2):127-48.
17. Oliynyk A, Bonifazzi C, Montani F, Fadiga L. Automatic online spike sorting with singular value decomposition and fuzzy C-mean clustering. BMC Neurosci. 2012 Aug 8;13:96.
18. Gibson S, Judy JW, Markovic D. Comparison of spike-sorting algorithms for future hardware implementation 30th Annual International IEEE EMBS Conference Vancouver, Canada, 2008 August 20.
19. Vedala K, Yaylali I, Cabrerizo M, Goryawala M, Adjouadi M. Peak detection of somatosensory evoked potentials using an integrated principal component analysis-walsh method. J Clin Neurophysiol. 2012 Apr;29(2):165-73.
20. Goryawala M, Yaylali I, Cabrerizo M, Vedala K, Adjouadi M. An effective intra-operative neurophysiological monitoring scheme for aneurysm clipping and spinal fusion surgeries J Neural En. 2012 Mar 15; 9 (2)
21. Hutchison WD, Allan RJ, Opitz H, Levy R, Dostrovsky JO, Lang AE, Lozano AM. Neurophysiological identification of the subthalamic nucleus in surgery for Parkinson's disease. Ann Neurol. 1998 Oct;44(4):622-8.
22. Novak P, Przybyszewski AW, Barborica A, Ravin P, Margolin L, Pilitsis JG. Localization of the subthalamic nucleus in Parkinson disease using multiunit activity. J Neurol Sci. 2011 Nov 15;310(1-2):44-9.
23. Abosch A, Hutchison WD, Saint-Cyr JA, Dostrovsky JO, Lozano AM. Movement-related neurons of the

subthalamic nucleus in patients with Parkinson disease. J Neurosurg. 2002 Nov;97(5):1167-72.
24. Theodosopoulos PV, Marks WJ Jr, Christine C, Starr PA. Locations of movement-related cells in the human subthalamic nucleus in Parkinson's disease. Mov Disord. 2003 Jul;18(7):791-8.
25. Romanelli P, Heit G, Hill BC, Kraus A, Hastie T, Brontë-Stewart HM. Microelectrode recording revealing a somatotopic body map in the subthalamic nucleus in humans with Parkinson disease. J Neurosurg. 2004 Apr;100(4):611-8.
26. Brodkey JA, Tasker RR, Hamani C, McAndrews MP, Dostrovsky JO, Lozano AM. Tremor cells in the human thalamus: differences among neurological disorders. J Neurosurg. 2004 Jul;101(1):43-7.
27. Shimamoto SA, Ryapolova-Webb ES, Ostrem JL, Galifianakis NB, Miller KJ, Starr PA. Subthalamic nucleus neurons are synchronized to primary motor cortex local field potentials in Parkinson's disease. J Neurosci. 2013 Apr 24;33(17):7220-33.
28. Sharott A, Gulberti A, Zittel S, Tudor Jones AA, Fickel U, Münchau A, Köppen JA, Gerloff C, Westphal M, Buhmann C, Hamel W, Engel AK, Moll CK. Activity parameters of subthalamic nucleus neurons selectively predict motor symptom severity in Parkinson's disease. J Neurosci. 2014 Apr 30;34(18):6273-85.
29. Lewicki MS. A review of methods for spike sorting: the detection and classification of neural action potentials. Network. 1998 Nov;9(4):R53-78.
30. Halpern CH, Danish SF, Baltuch GH, Jaggi JL. Brain shift during deep brain stimulation surgery for Parkinson's disease. Stereotact Funct Neurosurg. 2008;86(1):37-43.
31. Hardman CD, Henderson JM, Finkelstein DI, Horne MK, Paxinos G, Halliday GM. Comparison of the basal ganglia in rats, marmosets, macaques, baboons, and humans: volume and neuronal number for the output, internal relay, and striatal modulating nuclei. J Comp Neurol. 2002 Apr 8;445 (3):238-55.
32. Wild J, Prekopcsak Z, Sieger T, Novak D, Jech R. Performance comparison of extracellular spike sorting algorithms for single-channel recordings. J Neurosci Methods. 2012 Jan 30;203(2):369-76.
33. Pouzat C, Mazor O, Laurent G. Using noise signature to optimize spike-sorting and to assess neuronal classification quality. J Neurosci Methods. 2002 Dec 31;122(1):43-57.
34. Bankman IN, Johnson KO, Schneider W. Optimal detection, classification, and superposition resolution in neural waveform recordings. IEEE Trans Biomed Eng. 1993 Aug;40(8):836-41.
35. Milstein J, Mormann F, Fried I, Koch C. Neuronal shot noise and Brownian 1/f2 behavior in the local field potential. PLoS One. 2009;4(2):e4338.
36. Vinh N, Epps J, Bailey J. Information theoretic measures for clusterings comparison: is a correction for chance necessary? In: Proceedings of the 26th annual international conference on machine learning. ACM; 2009. p. 1073–80.
37. Vinh N, Epps J, Bailey J. Information theoretic measures for clusterings comparison: variants, properties, normalization and correction for chance. JMLR 2010;11:2837–54.
38. Adamos DA, Kosmidis EK, Theophilidis G. Performance evaluation of PCA-based spike sorting algorithms. Comput Methods Programs Biomed. 2008 Sep;91(3):232-44.
39. Vinh N. The Adjusted Mutual Information. Matlab Central. 2011 Oct; http://www.mathworks.com/matlabcentral/fileexchange/33144-the-adjusted-mutual-information
40. Hill DN, Mehta SB, Kleinfeld D. Quality metrics to accompany spike sorting of extracellular signals. J Neurosci. 2011 Jun 15;31(24):8699-705.
41. Bar-Gad I, Ritov Y, Bergman H. The neuronal refractory period causes a short-term peak in the autocorrelation function. J Neurosci Methods. 2001 Jan 15;104(2):155-63.

4. Comparison of intracranial electrical stimulation parameters

Author	Contribution (CASRAI Contributor Role Taxonomy)
Simeon Knieling[1]	Conceptualization, data curation, formal analysis, investigation (experiments), methodology, software, validation, visualization, writing – original draft, writing – review & editing
Jan Bostroem[2]	Investigation (surgery)
Christian E. Elger[1]	Resources
Florian Mormann[1]	Conceptualization, funding acquisition, investigation (surgery, experiments), project administration, resources, supervision

[1] Department of Epileptology, University of Bonn
[2] Department of Neurosurgery, University of Bonn

4.1 Introduction

Electrical stimulation of the human brain has been utilized for clinical application and research for decades (Penfield and Boldrey 1937). One of the earliest clinical applications of invasive brain stimulation is the identification of brain tissue associated with a patient's pathophysiology for subsequent ablation (removal or destruction). During awake surgery, surgeons stimulate regions of interest and assess the patient's responses. Based on indicative effects after stimulating certain brain areas, including the induction or reduction of symptoms, surgeons are able to delineate healthy tissue from tissue involved in a patient's pathology. For example, before invasive presurgical monitoring (see Section 1.2) was introduced, surgeons often relied on electrical stimulation to localize the epileptic focus in epilepsy patients (Penfield 1936). The stereotactic apparatus (Spiegel et al. 1947) drastically increased targeting accuracy (especially for areas deep inside the brain) and ablative neurosurgery became available as a treatment option for various other conditions including movement disorders, chronic pain, and psychological disorders.

Electrical stimulation used as a localization tool in various conditions enabled surgeons to explore the effects of stimulation in numerous areas of the brain. One prominent finding in patients with movement disorders is that low frequency stimulation of certain areas can exacerbate symptoms, while high-frequency stimulation can reduce symptoms (Hassler et al. 1960). This insight eventually led to the development of chronically implantable deep brain stimulators as an alternative for ablation in movement disorders (Bekhtereva et al. 1975; Benabid et al. 1987).

The next improvement over ablation and constant stimulation is to adapt stimulation to selectively disrupt pathological activity when it occurs. Activity in the local field potential (LFP) is monitored for changes associated with the patient's pathophysiology. Upon detection, the application of an electrical pulse train is triggered. The effectiveness of such an adaptive deep brain stimulation (also called closed-loop stimulation) has already been shown for movement disorders, chronic pain, and epilepsy (Rosin et al. 2011; Little et al. 2013; Sun and Morrell 2014), and further improvements are anticipated (Widge et al. 2018). Compared to constant stimulation, optimally timed stimulation can increase efficacy and battery life, and decrease side effects.

Besides timing, there are other stimulation parameters that can be optimized, including amplitude, phase width, frequency and pulse-train duration (see Fig. 1.4). For example, Mark and Gallistel (1993) found that in rats the subjective reward magnitude resulting from medial forebrain stimulation increases with increasing frequency and duration. A similar relationship between these parameters was found by Schmidt et al. (1996) who reported that increasing frequency, duration, or phase width will decrease the amplitude threshold needed to evoke phosphenes in a patient's visual cortex. Yet, increasing parameter values does not necessarily mean increasing the desired effects, as Rajdev et al. (2011) reported that compared to higher frequencies, low frequency stimulation is more effective in stopping seizure activity. A better understanding of how stimulation parameters compare and interact in affecting neuronal firing rates, the LFP, and possibly behavior would be of great value to further improve stimulation protocols.

During our investigation of parahippocampal cortex (PHC) stimulation we came across such an opportunity. Out of 17 patients who participated in stimulation studies, three reported that right-hemisphere PHC stimulation evoked a percept. In all three patients the evoked percept was a visual artifact (phosphene) in their left field of view. They described the percept as a "red flickering", a "colorless flickering", and "scattering splashes of paint", respectively. For detailed descriptions see the transcripts in Appendix A.1. Further investigation revealed that varying amplitude, phase width, frequency, or pulse-train duration affected the likelihood of evoking a percept.

Table 4.1: Stimulation parameters and their values compared in this study.

Parameter	**Values**
Amplitude	0.5, 1.0, 1.5 mA
Phase width	100, 200 µs
Frequency	25, 50, 100, 200, 300 Hz
Train duration	100, 400 ms

Given these favorable circumstances, we ran a parameter screening in which we applied a pulse train of a pseudo-randomly chosen parameter-value combination every 2 to 3 seconds. All combinations listed in Table 4.1 were tested, covering a wide range of what is commonly used in the macro-stimulation literature. Patients were asked to report a percept by pushing a key while looking at a static screen. Trials were not cued.

Here, we compare the effects of amplitude, phase width, frequency, and duration on perception, the LFP, and individual neurons (single units) by means of a stimulation-parameter screening.

4.2 Materials and Methods

4.2.1 Subjects

The study described in this chapter was conducted on three patients with pharmacologically intractable medial temporal lobe epilepsy. They were implanted with Behnke–Fried depth electrodes (Ad-Tech, Racine, WI) to localize the epileptic focus for possible resection (see Section 1.2).

Every depth electrode was equipped with 8 macro-contacts, 1.28 mm in diameter and 1.57 mm in length. The centers of the two most distal contacts were 3 mm apart. Nine micro-wires (eight recording channels plus one reference) with a diameter of 40 µm protruded from the tip of the electrode by approximately 3 to 5 mm (see Fig. 1.3).

Patients provided written informed consent for implantation of micro-electrodes and participation in cognitive paradigms involving electrical stimulation delivered though macro-contacts. All studies and procedures were approved by the internal review board of the University of Bonn.

4.2.2 Experimental setup

Macro-electrodes were connected to an ATLAS HC Headbox (Neuralynx, Bozeman, MT), which in turn was connected to the amplifier (Neuralynx ATLAS system). The

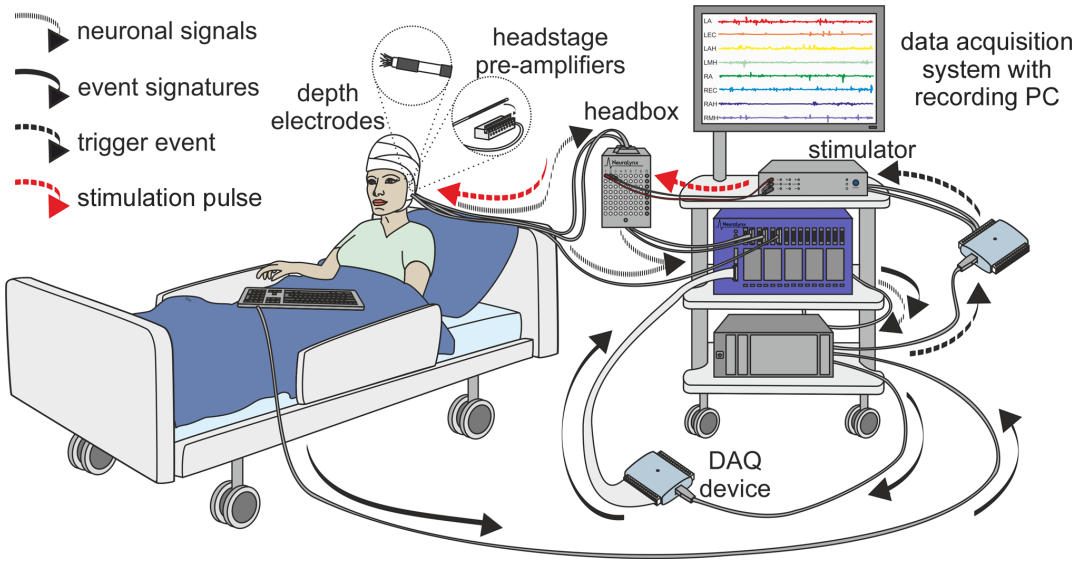

Figure 4.1: **Experimental setup for a stimulation-parameter screening**. See Section 4.2 for details. Figure adapted from Knieling et al. (2017). Permission for publication in this thesis was granted.

headbox allowed for a continuous recording during stimulation. The amplifier was connected to a recording PC running Neuralynx's data acquisition software Cheetah ATLAS (version 1.1.0). A constant current stimulator (STG 4004, Multi Channel Systems, Germany) was connected to the contacts of the headbox that corresponded to the two most distal (i.e., medial) macro-contacts of the patient's right PHC depth-electrode.

The experiment's computer program (described in Section 4.2.3) ran on the recording PC which was connected to the stimulator directly via USB as well as to its trigger input via a USB DAQ device (Measurement Computing's USB-1208FS). The direct USB connection was used to program the stimulator while the DAQ device was used to trigger stimulation. A second DAQ device connected the recording PC to the TTL input of the ATLAS system to send event signatures (such as stimulation onset) to the recording system.

The micro-wires protruding from the depth electrodes were connected to headstage pre-amplifiers (CHET-10, Neuralynx, Bozeman, MT), which in turn were connected to the ATLAS system. A schematic of the experimental setup is depicted in Fig. 4.1.

4.2.3 Experimental protocol

The experimental protocol started with an exploratory session in which we applied electrical stimulation to the patient's PHC macro-contacts. This session was used to gauge if stimulation within the reported parameter space (see Table 4.1) would evoke a percept.

The exploratory session took approximately 5 to 10 minutes.

If the patient reported a percept in response to the stimulation, we asked them to describe the percept, and proceeded with the main experiment. The patient was given a keyboard and was instructed to push the left arrow key whenever they perceive something similar to what they had described earlier during the exploratory session. During the experiment the patient either looked at a static screen on a laptop computer (not connected to the rest of the setup) or at the wall of their room, depending on how they found it easiest to perceive the visual disturbance.

The experiment was operated by a Matlab (Mathworks) script running on the recording PC that pseudo-randomly chose a combination of the parameter values in Table 4.1, and triggered stimulation. Stimulation was applied every 2 to 3 seconds (jittered). There were 22 applications of each of the 60 parameter combinations, 22 applications of single pulses at different current amplitudes (0.5, 1.0, and 1.5 mA) and 44 trials in which no stimulation was applied. In total, 64 conditions that amount to 1430 trials (60 * 22 + 3 * 22 + 44). The experiment took 60 minutes. We recorded two sessions with each patient. One patient aborted the experiment after 519 trials due to fatigue. Hence, the total number of trials per parameter combination across patients differs slightly (see Fig. 4.2).

4.2.4 Signal processing

The micro-electrode signals were acquired at a sampling frequency of 32,768 Hz. The acquisition software band-pass filtered the signal between 0.1 and 9,000 Hz. Before data were saved to file for further processing and analysis, the signal was inverted. Hence positive deflections appear negative and vice versa. This inversion concerns spikes as well as LFP data.

Spikes

Combinato (Niediek et al. 2016) was used for spike detection and sorting, due to its artifact-rejection capabilities.[1] After Combinato's automatic spike sorting concluded, we used its user interface to manually reject remaining artifacts and to correct for over- and under-clustering.

To calculate instantaneous neuronal firing rates after stimulation for a particular com-

[1]The following parameters were changed to improve the separation of stimulation artifacts and spikes. In *mask_artifacts.py*, *binlength* was set to 100, *max_spk_per_bin* was set to 150, and *min_dist* was set to 0.75. In *concurrent.py*, *BIN_MS* was set to 1. In *options.py*, *RecursiveDepth* was set to 2 and *MinInputSizeRecluster* was set to 500. In *filters.py*, *DETECT_HIGH* was set to 3000.

bination of stimulation parameters, the timestamps of a unit's spike occurrences (relative to the end of the pulse train) in all trials of the respective parameter combination were combined. Next, a histogram (bin size = 1 ms) of the combined trials was calculated, and its weighted moving average was determined using a Gaussian kernel ($\sigma = 0.1$ s). The result was divided by the number of trials, and multiplied by the histogram's sampling rate (1000 Hz) to determine instantaneous firing rates. The mean firing rate over all units was bootstrapped using 10,000 repetitions to estimate the standard error of the mean (SEM).

To evaluate differences in firing rate during trials that either elicited a percept (P) or elicited no percept (NP) in the same condition (i.e., parameter combination), three mean instantaneous neuronal firing rates were determined: the mean firing rates across P-trials, the mean firing rates across NP-trials and the overall mean firing rates during the condition. This was done for each unit in each condition that included at least 5 P- and 5 NP-trials. The relative change in the area under the curve (AUC) between firing rates during P- and NP-trials was determined according to the formula $\frac{\sum_i y_p - y_u}{\sum_i y_0}$, where y_p is the instantaneous firing rate during P-trials, y_u the instantaneous firing rate during NP-trials, y_0 the overall firing rate during the respective condition, and i the index over the first 1.6 s of samples after the end of the pulse train.

Local field potentials

To determine whether an LFP response (i.e., an event-related potential) was evoked during a trial, micro-electrode signals were segmented into trials: the first 1.6 s after stimulation (i.e., after the end of the pulse train). Each segment was smoothed using a Gaussian kernel ($\sigma = 0.2$ ms) and downsampled to 1 kHz. Smoothing prior to downsampling decreases noise in the downsampled segment caused by high-frequency components. Subsequently, the downsampled segment was smoothed using a Gaussian kernel ($\sigma =$ 4.0 ms) and low-pass-filtered at 4 Hz.

To detect event-related potentials (ERPs), we converted segments from µV to z-scores by dividing each segment by the standard deviation (SD) across all segments of the *'No stimulation'* condition. Subtracting the mean prior to dividing by the SD was unnecessary as our signal was band-pass filtered. Hence, the mean was approaching zero. Since there were no auditory or visual cues that could have introduced a systematic offset to the baseline, minimal deviations from zero in the mean of the signal of the *'No stimulation'* condition were likely caused by the limited number of trials and should not be considered in a z-score transformation. An ERP was defined as a local maximum

greater than 2.58 (the 99% confidence interval for z-scores) in the first 50 to 500 ms after stimulation. Since every trial was recorded on 8 channels, the boolean variable of whether or not an ERP was evoked during a particular trial was exclusively determined by the channel that recorded the most ERPs over the entire session.

To evaluate differences in ERPs during trials that either elicited a percept (P) or elicited no percept (NP) in the same condition (i.e., parameter combination), three median signals were determined: the median signal during P-trials, the median signal during NP-trials and the overall median signal of the condition. Median signals were downsampled, smoothed, and filtered as described above. This was done for each condition of each session that included at least 5 P- and 5 NP-trials. The relative change in the absolute area under the curve (AUC) between the median LFP during P- and NP-trials was determined according to the formula $\frac{\sum_i |y_p - y_u|}{\sum_i |y_0|}$, where y_p is the median signal of the P-trials, y_u the median signal of the NP-trials, y_0 the overall median signal of the respective condition, and i the index over the first 1.6 s of samples after the end of the pulse train.

4.2.5 Statistical analysis

We computed a logistic regression analysis of the behavioral response-probability using a generalized linear model (GLM) of the binomial family (link = logit) with the help of the *R* command *glm()* of the *stats* package. In a first step, frequency, amplitude, phase width, pulse-train duration, repetition, patient ID (effect coding), and session (dummy coding) were declared as independent variables (predictors). In a second step, the interactions frequency × duration (i.e., pulses) and amplitude × phase width (i.e., charge per phase) were added. All non-categorical predictors were rescaled to a maximum of 1.0 prior to model estimation. Bias-corrected and accelerated (BCa) confidence intervals for odds ratios were obtained using the *boot.ci()* command. The same analysis was used to model the probability of evoking an ERP.

The behavioral response latency was modeled using a GLM of the gamma family (link = inverse), with the same independent variables as above.

4.2.6 Electrode localization

We calculated projections of the electrodes' contacts in MNI space using *spm12*. First, a post-implantation CT was coregistered with a pre-implantation MRI. The MRI was normalized, and the deformations were saved to file. The deformations file was used to transfer the CT from subject space into MNI space. Subsequently, all voxels other than

those representing the two most distal contacts of the right PHC electrode were removed from the CT. The combined center of mass of the three patients' PHC macro-contacts was computed to determine the slices on which to project the macro-contacts. Finally, MRIcroN was used to render the projections of the patients' electrodes onto the MNI brain (ICBM 152 linear).

4.3 Results

4.3.1 Effects of stimulation on behavioral measures

The proportion of behavioral responses to every parameter combination as well as to scaled single pulses and no stimulation are presented in Fig. 4.2. Based on these data, a two-step logistic regression model was generated to compare the effects of different stimulation parameters on evoking a percept (phosphenes). The model is summarized in Table 4.2. The first step shows that all four stimulation parameters had a positive effect on evoking a percept while the number of repetitions of a parameter combination had a negative effect. However, the effects of the four stimulation parameters could still have been mediated by interdependent parameters. A higher frequency also means a higher number of pulses. Similarly, applying a higher amplitude also means applying a higher charge. To be able to differentiate between these interdependent parameters, we included the interactions frequency $\times$ duration (pulses) as well as amplitude $\times$ phase width (charge) in a second step of the model. The second step reveals that charge per phase had a positive effect on evoking a percept, and its inclusion in the model

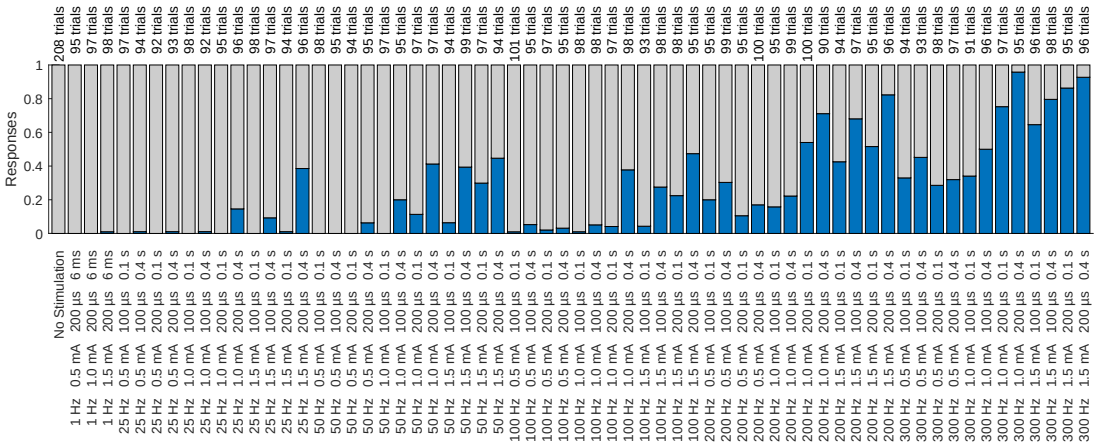

Figure 4.2: **The proportion of evoked percepts reported in each condition across patients**.

decreased the significance of amplitude and phase width. Compared to frequency and duration, the number of pulses had a negative effect. Since the predictors were rescaled to a maximum of 1.0 prior to estimating the model, the regression coefficients provide a rank order for the stimulation parameters within the given parameter space. Frequency had the largest positive effect on evoking a percept, followed by amplitude, phase width, and pulse-train duration. Table 4.2 also contains the odds ratio of a predictor, i.e., the exponential of the predictor's regression coefficient. The odds ratio expresses by how much the odds of evoking a percept change as a result of a unit change in the predictor. Since the predictors were rescaled, a unit change is the difference between zero and the maximum value of that predictor. The model's predictions of the probability of evoking a percept as a function of a predictor's untransformed value are depicted in Fig. 4.4A. Adding whether or not an event-related potential (ERP) was evoked as an additional predictor to the model in Table 4.2 did not result in an improvement of step 1 ($p = 0.96$) and only explained approximately 0.2% more variance (Δ Pseudo R^2 of HL) when added to step 2 ($p < 0.01$).

A histogram of the patients' response times is shown in Fig. 4.3. The histogram's mode is 650 ms. The median response time was 689 ms. A GLM to estimate the effects of stimulation parameters on the response time is summarized in Table 4.3. Frequency, phase width, amplitude, and the number of repetitions had a negative effect on response time. Again, frequency had the greatest effect magnitude, followed by phase width, amplitude, and repetition. Pulse-train duration had no significant effect on response time. Adding pulses or charge per phase as predictors did not improve the model significantly and was hence omitted. The model's predictions of the response time as a function of a predictor's untransformed value are depicted in Fig. 4.4B.

4.3.2 Effects of stimulation on event-related potentials

Some stimulation parameters caused ERPs in the LFP recorded from nearby micro-electrodes. Figure 4.5 shows the median LFP of each of the eight micro-electrodes protruding from the stimulated PHC macro-electrode during all 64 conditions of a stimulation-parameter screening session from one of the patients. For each session, the micro-electrode on which the most ERPs were detected was used to decide whether an ERP was evoked during a given trial. The proportion of ERPs in each condition is presented in Fig. 4.6. Based on these data, we estimated another two-step logistic regression model (analogous to the previously described model for evoking a percept) to compare the effects of stimulation parameters on evoking an ERP. The model is

Table 4.2: GLM (family: binomial, link: logit) of the effects of stimulation parameters on phosphene detection.

			95% CI for odds ratio			
Fixed effects	**b**	**SE(b)**	**lower**	**odds ratio**	**upper**	**p**
Step 1: Pseudo R^2 = .47 ^{HL} / .41 ^{CS} / .61 ^{N}				Model χ^2 (8) = 3307.68 ***		
Intercept	10.19	0.32				***
Frequency	4.96	0.15	105.20	142.97	189.80	***
Amplitude	4.41	0.18	57.08	82.36	115.89	***
Phase width	2.45	0.18	8.12	11.61	16.27	***
Train duration	1.95	0.12	5.57	7.02	8.89	***
Repetition	−1.02	0.14	0.27	0.36	0.48	***
Step 2: Δ Pseudo R^2 = .023 ^{HL} / .013 ^{CS} / .030 ^{N}				Δ Model χ^2 (2) = 84.06 ***		
Intercept	9.19	0.48				***
Frequency	6.70	0.29	461.20	815.14	1419.00	***
Charge / phase †	3.80	0.65	12.79	44.61	147.61	***
Train duration	3.39	0.24	19.50	29.60	45.32	***
Amplitude	1.52	0.52	1.70	4.58	13.06	**
Phase width	−0.26	0.50	0.32	0.77	1.93	0.59
Repetition	−1.04	0.15	0.27	0.35	0.48	***
Pulses ‡	−2.45	0.34	0.047	0.086	0.16	***

Independent variables were rescaled to [0,1] prior to model estimation. The model further includes the fixed effects patient ID (effect coding) and session (dummy coding) that are omitted in this table.

Patients = 3, observations = 6256. ** $p < 0.01$, *** $p < 0.001$.

^{HL} Hosmer–Lemeshow

^{CS} Cox–Snell

^{N} Nagelkerke

† Charge per phase was modelled as the interaction amplitude × phase width.

‡ Pulses were modelled as the interaction frequency × train duration.

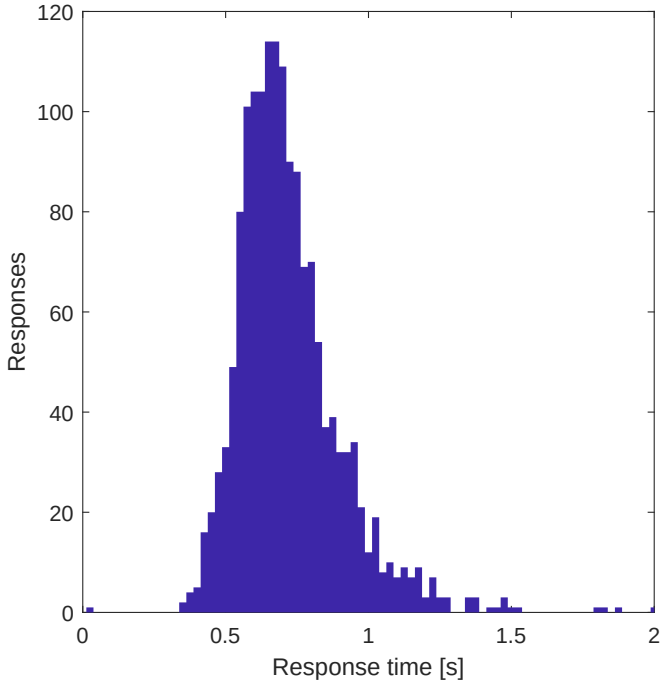

Figure 4.3: **Histogram of response times to evoked percepts across patients**.

Table 4.3: GLM (family: gamma, link: inverse) of the effects of stimulation parameters on response time in a phosphene detection task.

Fixed effects	**b**	**SE(b)**	**p**
Model: Multiple $R^2 = .180$ Adjusted $R^2 = .176$ Model χ^2 (8) = 18.12 *			
Intercept	0.74	0.058	***
Frequency	0.27	0.028	***
Phase width	0.14	0.033	***
Amplitude	0.12	0.036	***
Repetition	0.090	0.027	***
Train duration	−0.011	0.023	0.63

Independent variables were rescaled to [0,1] prior to model estimation. The model further includes the fixed effects patient ID (effect coding) and session (dummy coding) that are omitted in this table. Adding the fixed effects pulses and charge per phase did not improve the model.
Patients = 3, observations = 1564. * $p < 0.05$, *** $p < 0.001$.

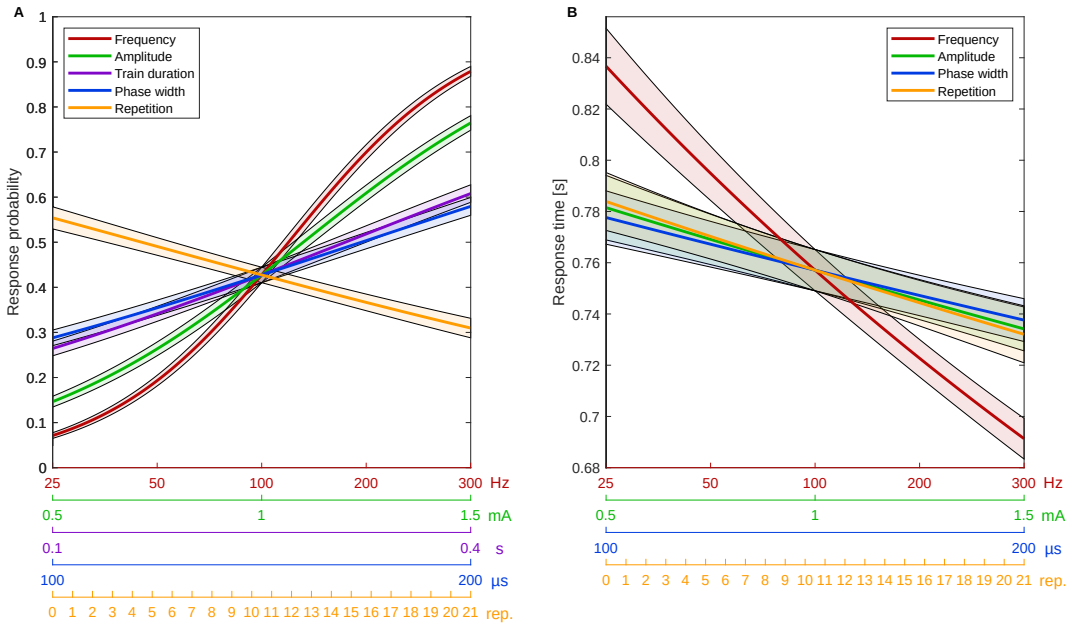

Figure 4.4: **Predictions of the evoked percepts model in Table 4.2**. **A**: Predictions of the probability of evoking a percept as a function of a predictor's untransformed value. **B**: Predictions of the response time as a function of a predictor's untransformed value. Shadows represent the standard error of the mean (SEM).

summarized in Table 4.4. The first step shows that amplitude had the largest positive effect, followed by phase width and frequency while pulse-train duration had a negative effect. The number of repetitions had no significant effect. The second step reveals that charge per phase had the largest positive effect while the number of pulses (compared to frequency and duration) had no significant effect. Adding whether or not an evoked percept was reported as a predictor to the model in Table 4.4 did not result in a significant improvement of either step 1 ($p = 0.40$) or step 2 ($p = 0.19$).

Stimulation parameters also affected the shape of the ERP; in particular the ERP's peak latency, height, and width. Quantifying these effects in a GLM violated the assumptions of homoscedasticity and normally distributed errors. Hence, we present qualitative differences in a density plot of the median ERP recorded on each of the eight micro-electrodes during each condition in each session of the three reported patients. Figure 4.7 shows that increasing the stimulation frequency increased the ERP's peak latency, height, and possibly width. These effects seem to have saturated between 100 and 200 Hz. Increasing the stimulation's amplitude increased the ERPs' height, width, and possibly peak latency. Increasing the stimulation's phase width had a similar effect. Both amplitude and phase width determine the charge per phase, which seems to have been the most effective parameter in evoking an ERP. This is indicated by the model in

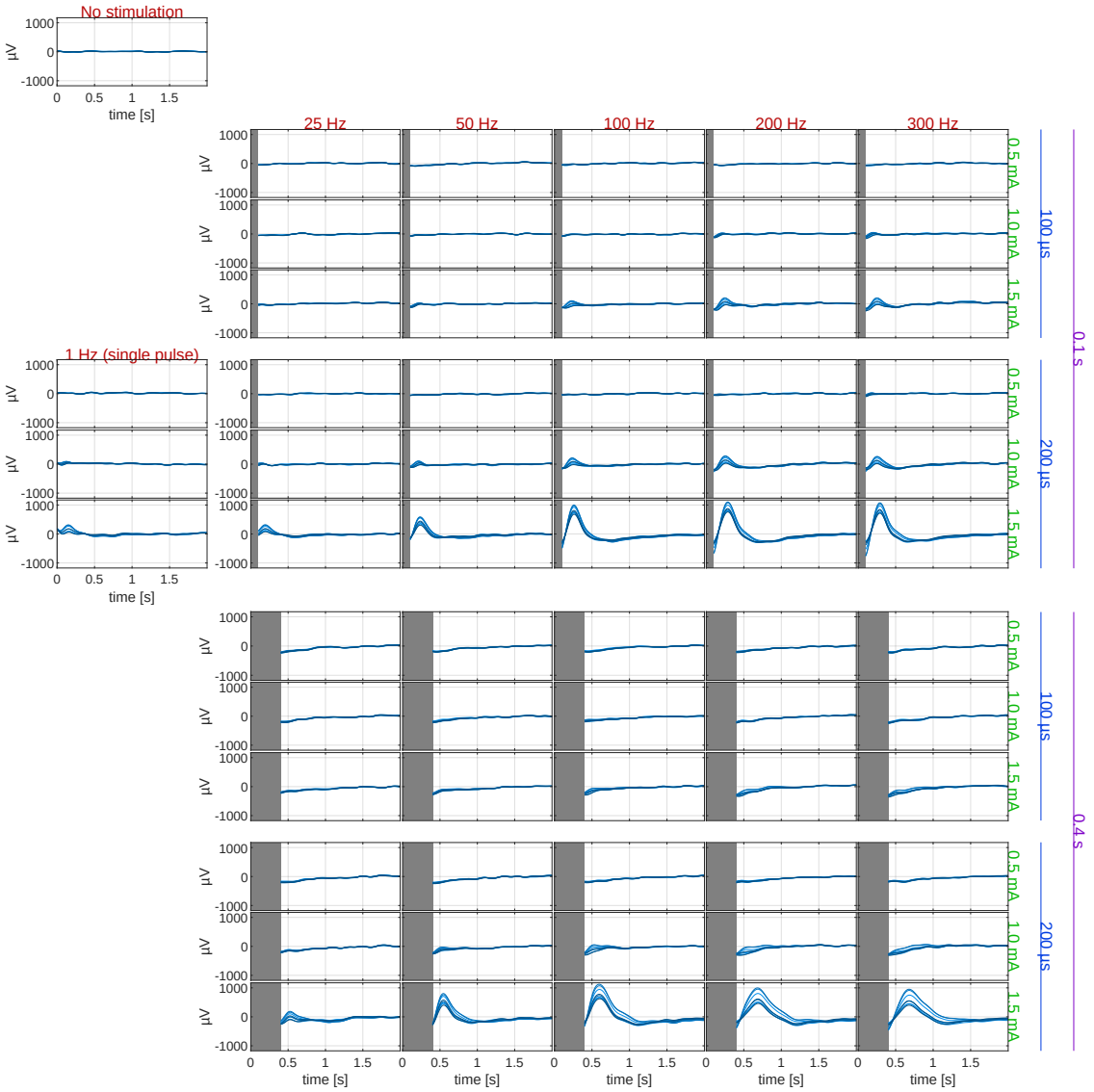

Figure 4.5: **Example of event-related potentials during a stimulation-parameter screening session**. Blue lines represent the median LFP of each of the eight micro-electrodes in one session.

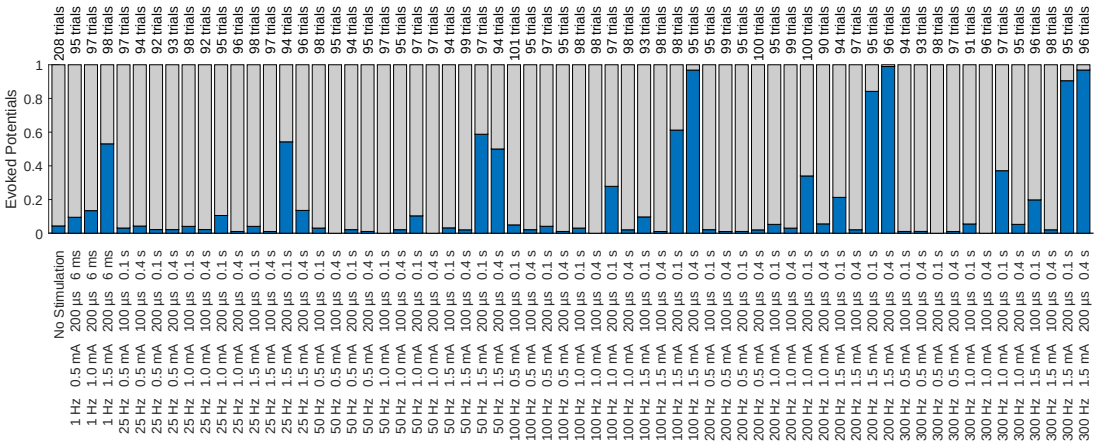

Figure 4.6: **The proportion of event-related potentials detected in each condition**.

Table 4.4: GLM (family: binomial, link: logit) of the effects of stimulation parameters on the generation of ERPs.

			95% CI for odds ratio			
Fixed effects	**b**	**SE(b)**	**lower**	**odds ratio**	**upper**	**p**
Step 1: Pseudo R^2 = .43 ^{HL} / .32 ^{CS} / .54 ^{N}				Model χ^2 (8) = 2389.35 ***		
Intercept	−12.82	0.40				***
Amplitude	6.74	0.24	419.00	842.96	1738.80	***
Phase width	5.95	0.24	195.20	383.70	760.80	***
Frequency	1.70	0.13	4.17	5.50	7.27	***
Repetition	0.15	0.15	0.89	1.17	1.53	0.32
Train duration	−1.02	0.12	0.29	0.36	0.44	***
Step 2: Δ Pseudo R^2 = .098 ^{HL} / .048 ^{CS} / .12 ^{N}				Δ Model χ^2 (2) =	309.10 ***	
Intercept	−3.90	0.32				***
Charge / ph. †	13.54	0.62	1.94×10^5	7.59×10^5	3.09×10^6	***
Frequency	2.05	0.23	4.84	7.75	12.23	***
Repetition	0.18	0.17	0.89	1.20	1.62	0.28
Pulses ‡	0.11	0.34	0.61	1.12	2.03	0.74
Train duration	−1.16	0.20	0.22	0.31	0.47	***
Amplitude	−4.53	0.46	0.0044	0.011	0.027	***
Phase width	−5.05	0.44	0.0023	0.0064	0.017	***

Independent variables were rescaled to [0,1] prior to model estimation. The model further includes the fixed effects patient-ID (effect coding) and session (dummy coding) that are omitted in this table.

Patients = 3, observations = 6256. *** $p < 0.001$.

^{HL} Hosmer–Lemeshow

^{CS} Cox–Snell

^{N} Nagelkerke

† Charge per phase was modelled as the interaction amplitude × phase width.

‡ Pulses were modelled as the interaction frequency × train duration.

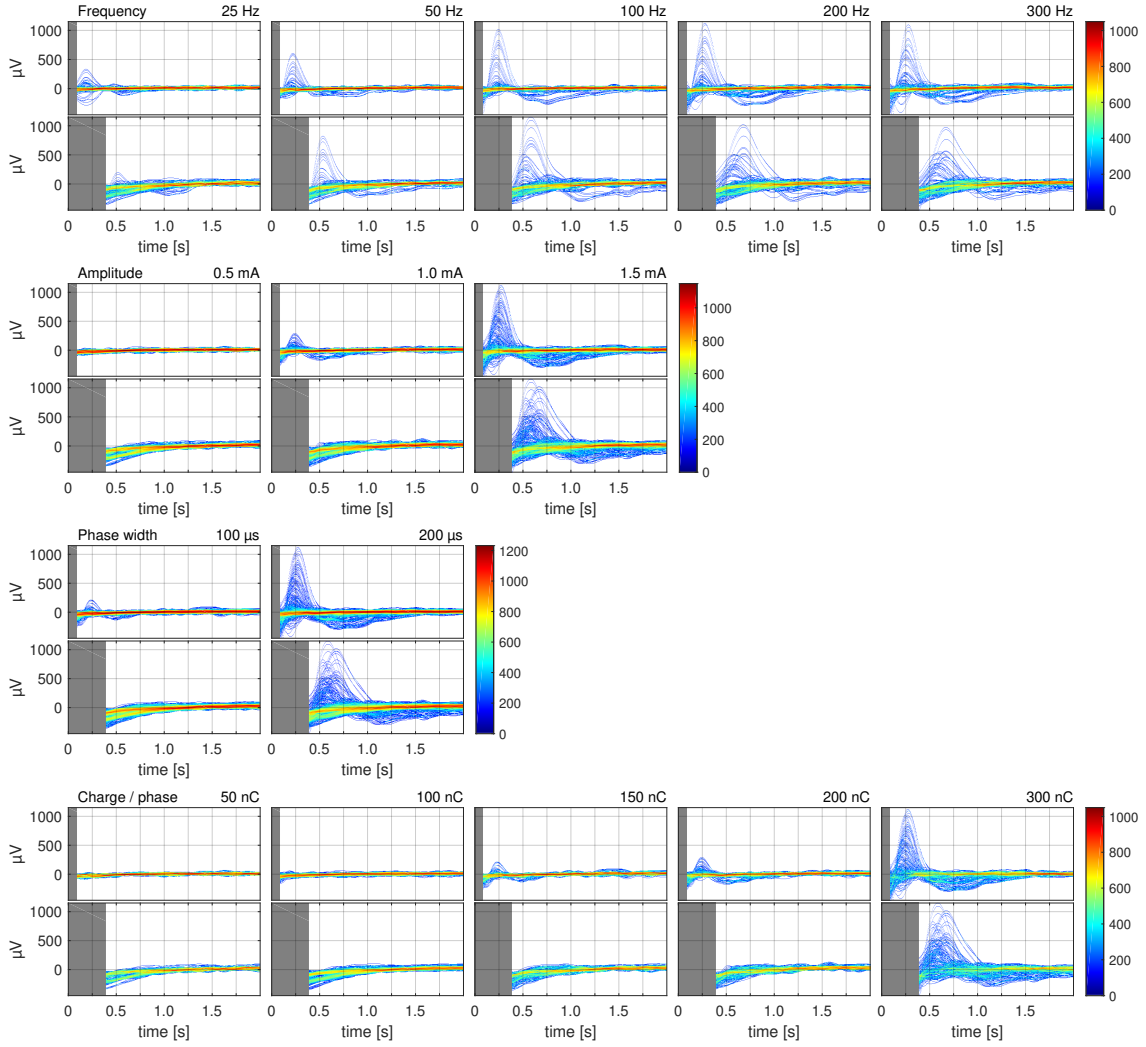

Figure 4.7: **Density plot of event-related potentials**. Each row of graphs includes one median ERP for each of the eight micro-electrodes during each condition in each session of each of the three reported patients. There are twice as many conditions that use 100 nC per phase (0.5 mA for 200 µs and 1.0 mA for 100 µs) as there are conditions that use one of the other values of charge per phase. Hence, for better visualization, density values in the two 100 nC graphs were scaled so that their 99th percentile matches that of the 50 nC plots.

Table 4.4 and also by Fig. 4.7, especially when comparing conditions that used a charge per phase of 300 nC with conditions that used a lower charge per phase. Increasing the stimulation duration increased the threshold of other parameters required for evoking an ERP (which is also reflected by the model in Table 4.4). Increasing the stimulation duration also increased the ERP's width.

In some conditions, some trials evoked a percept (P) while other trials did not (NP). Differences in local field potentials between P- and NP-trials of the same condition were compared by the relative change in the absolute area under the curve (AUC) of the median LFP in each condition of each session that included at least 5 P- and 5 NP-

trials. Only the median LFP of the micro-electrode that recorded the most ERPs during a session was used for this comparison. A Wilcoxon signed-rank test shows that the absolute AUC was greater (median relative change $= 13.34\%$, $p < 0.01$) when a percept was evoked compared to when no percept was evoked.

4.3.3 Effects of stimulation on neuronal firing rates

We also investigated instantaneous firing rates after stimulation. While single units were present in all three patients, the total number of single units found in the PHC of these patients was only six. Their mean instantaneous firing rates after stimulation are presented in Fig. 4.8. A cumulative raster plot presenting all spike times of all single units in all trials is presented in Fig. 4.9. Neuronal firing was inhibited for a short duration after stimulation. The degree of inhibition depended on the stimulation's parameter values. Frequency had the largest effect, followed by charge, amplitude, phase width, and duration. Curiously, 300 Hz was mostly ineffective in inhibiting neuronal firing.

Similarly to differences in local field potentials, differences in instantaneous firing rates between trials that evoked a percept (P) and trials that did not (NP) were compared by the relative change in the AUC of the instantaneous firing rates of each PHC unit in each condition of each session that included at least 5 P- and 5 NP-trials. While the AUC was greater when a percept was evoked compared to when no percept was evoked (median relative change $= 13.03\%$), this effect did not quite reach statistical significance ($p = 0.073$, Wilcoxon signed-rank test)

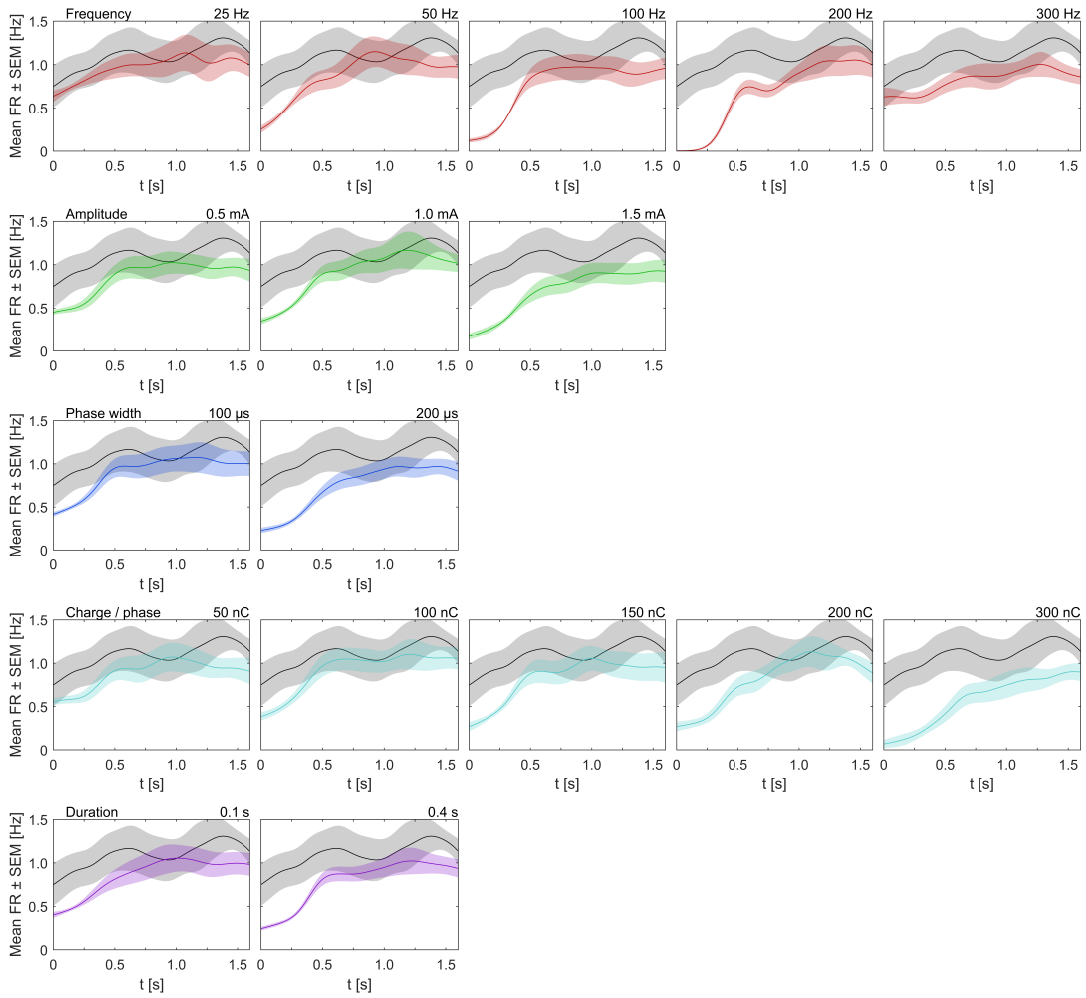

Figure 4.8: **Neuronal firing rates for different conditions (i.e., stimulation parameters)**. The gray line shows the baseline activity (during which no stimulation was applied). Shadows represent the standard error of the mean (SEM), determined by bootstrapping. Firing rates were aligned to the end of the pulse train (t = 0 s).

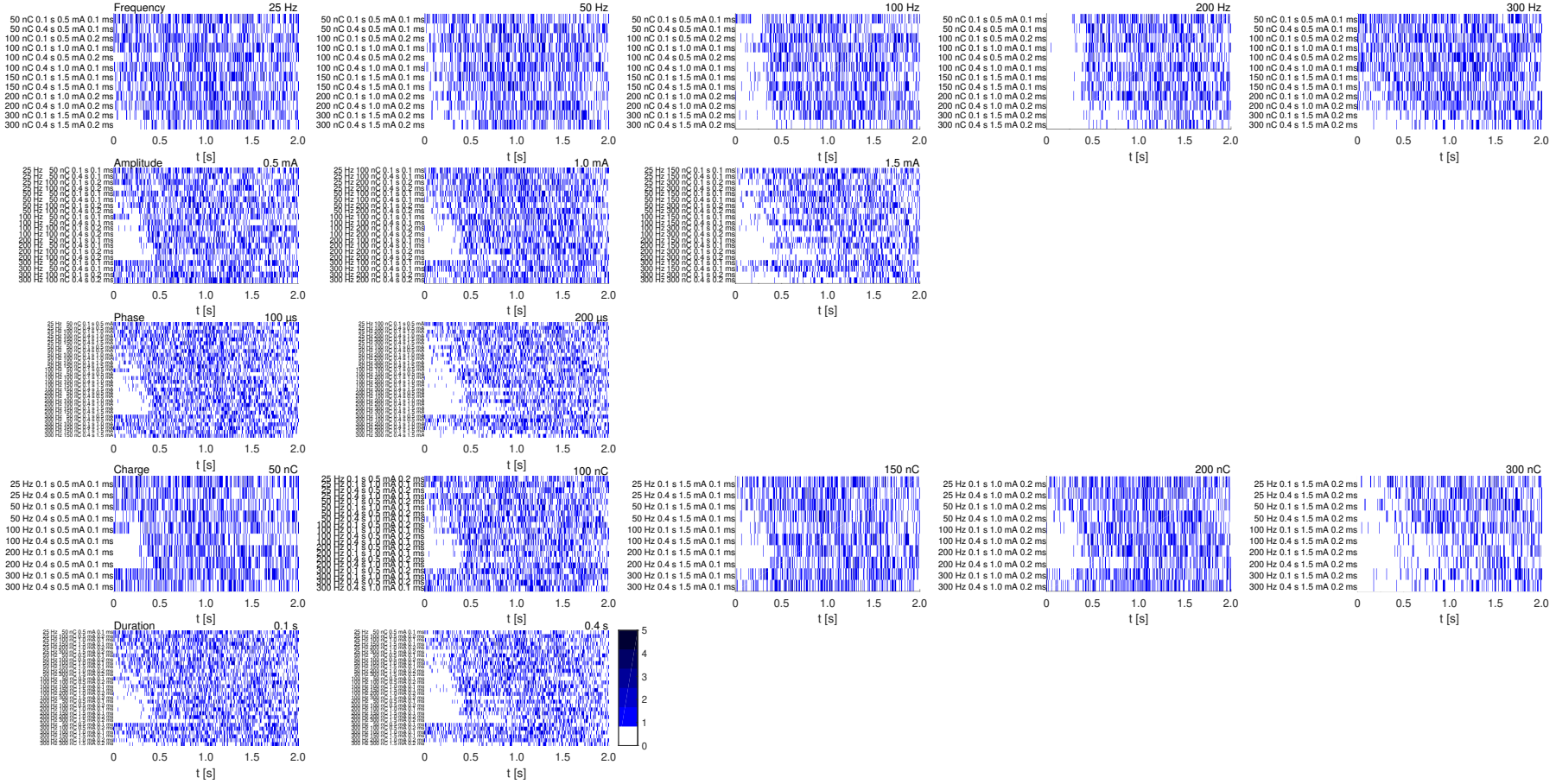

Figure 4.9: **Cumulative raster plots**. Each row represents one stimulation condition and encompasses all trials within this condition. Hence, considering the bin size of 1 ms, there could be two or more spikes in the same bin. Bins with more than one spike were colored according to the depicted colormap.

4.4 Discussion

4.4.1 Phosphene perception

We found a small subset of patients in whom brief stimulation delivered though electrodes residing in the right PHC led to the perception of phosphenes in the left field of view. Murphey et al. (2009) reported similarly simple percepts evoked by brief stimulation of the PHC (in particular the parahippocampal place area). Their report of "little (visual) explosions" might describe a percept similar to what one of our patients described as "scattering splashes of paint". However, given the sparse number of patients (3 out of 17) in whom stimulation of PHC electrodes caused a percept, activation of the PHC might not have been the cause. Small splashes of dots or flickering lights are more consistent with percepts described after stimulation of the primary visual cortex (Brindley and Lewin 1968; Dobelle and Mladejovsky 1974; Kim et al. 2013), which is innervated by the optic radiation. Figure 4.10 shows projections of the PHC electrodes of the three reported patients in red and projections of the PHC electrodes of patients who reported no percept in green. In addition, a probabilistic reconstruction of the optic radiation (based on 35 healthy subjects) is shown in blue (the volumetric dataset was taken from the supplementary material of Wang et al. 2018). The more lateral of the two stimulated contacts of the reported patients' PHC electrodes seem to have been directly adjacent to the optic radiation. Considering the patients' descriptions of the evoked percepts, their electrodes' positions, the high excitability of axons (Rattay 1999), current spread (Tehovnik et al. 2006), and interindividual differences in the optic radiation's exact path (Wang et al. 2018), excitation of fibers of the optic radiation seems plausible. Hence, we hypothesize that incidental stimulation of the optic radiation was causing the reported phosphenes, and we will discuss our results in the context of this hypothesis.

4.4.2 Effects on evoked percepts

Increasing any stimulation parameter (within the reported parameter space) increased the likelihood of evoking a phosphene. Yet, some parameters had a stronger effect than others. Frequency was the most influential parameter, followed by amplitude, phase width, and pulse-train duration. The underlying charge per phase seems to have been responsible for most of the effect of amplitude and phase width while the number of pulses in a pulse train does not seem to have been responsible for the effect of frequency. In addition, we learned from initial exploratory stimulation sessions that frequency, charge

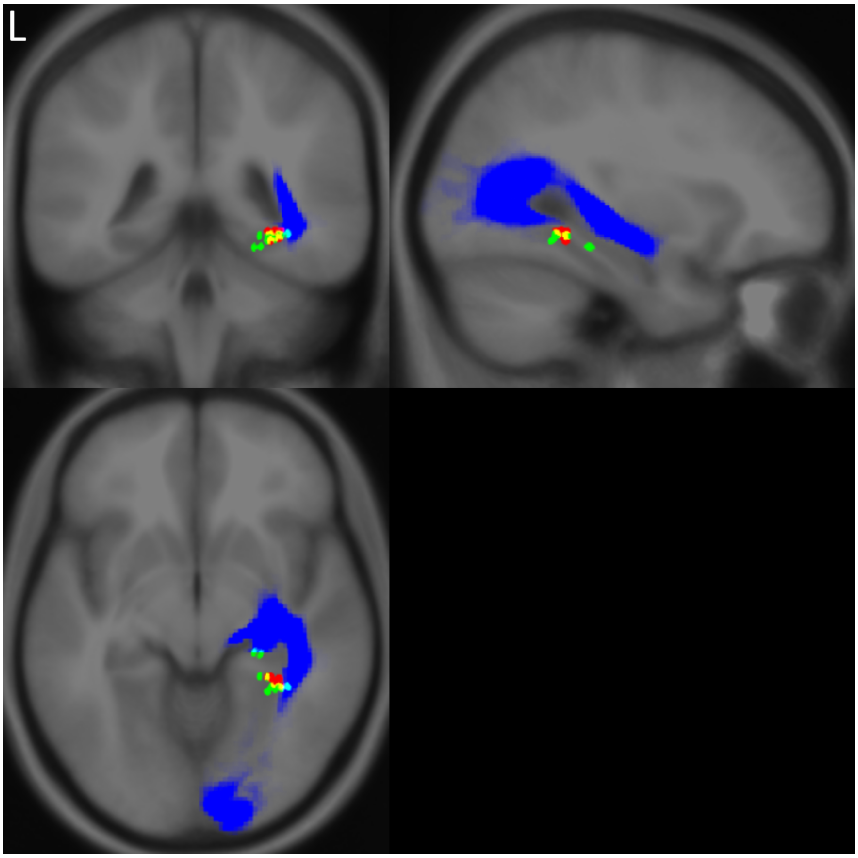

Figure 4.10: **Electrode positions**. Projections of the stimulated macro-contacts of the three patients who perceived phosphenes (in red) and multiple patients who reported no percepts (in green) onto the MNI brain (ICBM 152 linear). A probabilistic reconstruction of the optic radiation is shown in blue (the volumetric dataset was published in Wang et al. 2018). Other colors show overlaps of projections. Yellow areas are overlaps of electrodes in patients who perceived phosphenes with electrodes in patients who did not. Cyan areas are overlaps of electrodes from patients who did not perceive phosphenes with the probabilistic reconstruction of the optic radiation.

per phase, and duration had thresholds (varying across patients) below which no percept could be evoked. These findings are consistent with the previously mentioned case study by Schmidt et al. (1996), who found that increasing frequency, pulse-train duration, or phase width would decrease the amplitude threshold needed to evoke phosphenes via micro-stimulation in a patient's primary visual cortex.

Including the repetition number of the respective parameter combination as a predictor, we found that with increasing repetition, the number of responses decreased. Still, due to strong multicollinearity, this effect could be attributed to various causes, including the passing of time (the patients might lose focus and increase their lapse rate), the repetition of any kind of stimulation, or the repetition of stimulation of a specific parameter combination. The response latency also declined with repetition. Both of these effects (repetition suppression and repetition-dependent decrease in latencies) have also been reported in single neurons responding to repeated visual stimulation (Pedreira et al. 2010; Rey et al. 2015).

4.4.3 Effects on neuronal firing rates

Stimulation parameters also influenced instantaneous firing rates. Firing rates immediately following the pulse train were drastically decreased. In most cases, firing rates seemed to recover back to baseline within the first second. However, the reduced baseline firing rate at $t = 0$ s compared to $t = 1.6$ s indicates that occasionally a full recovery might have taken slightly longer than one trial (which was 2 to 3 s).

Frequency had the largest effect, followed by charge per phase. The effects of amplitude, phase width, and pulse-train duration seem to have been of similar magnitude. Note that we recorded from 6 units only. However, given that these 6 units came from 3 different patients, their instantaneous neuronal firing rates showed surprisingly low standard errors of the mean, indicating that the effects on instantaneous firing rates were rather consistent. In fact, inhibition of neuronal firing after short pulse trains has previously been reported for *micro*-stimulation of neurons in various regions of the basal ganglia, including the globus pallidus, subthalamic nucleus, and substantia nigra (Filali et al. 2004; Lafreniere-Roula et al. 2010).

A neuron's fast action potential will cause a spike in the signal of a micro-electrode located close to the neuron's soma (Buzsáki et al. 2012). The axon is more excitable by electric stimulation than the soma (Rattay 1999; Tehovnik et al. 2006) but excitation of an axon will not produce such a pronounced spike in the micro-electrode's signal. For the absence of spikes after short electrical stimulation, there could be various possible

explanations. Lafreniere-Roula et al. (2010) make a case for excitation of inhibitory axons as a probable cause. They hypothesize that inhibitory postsynaptic potentials (IPSP) mediated by $GABA_A$ receptors may cause a short-term inhibition (less than 50 ms) after each pulse (described in Dostrovsky et al. 2000), while the longer-lasting inhibition after the pulse train may be caused by longer-lasting IPSP mediated by $GABA_B$ receptors (Mott et al. 1999). In our data, we found that a stimulation pulse can have an excitatory effect on a neuron's soma but still cause subsequent inhibition. An example is presented in Fig. 4.11, which shows various trials of the same channel at multiple stimulation frequencies. This finding suggests an involvement of causes other than inhibitory neurotransmitters that could inhibit action potentials for a prolonged period of time.

Judging from the cumulative raster plots in Fig. 4.9, there seem to be two different mechanisms of inhibition. One mediated by charge and one mediated by frequency. Charge-dependent inhibition could be mediated by a neuron's dominant neurotransmitter input. The higher the charge, the more axons are excited and release their neurotransmitter to the postsynaptic neuron (Borchers et al. 2012). Frequency-dependent inhibition could be mediated by a combination of the following three mechanisms. First, repetitive excitation of axons can lead to an increased neurotransmitter concentration at the synapse, causing desensitization of ligand-gated ion channels in the postsynaptic neuron due to continued agonist exposure (Keramidas and Lynch 2013). Second, high-frequency excitation of a neuron increases extracellular K^+ ($[K^+]_e$) around the neuron's membrane. Elevated $[K^+]_e$ may prevent the generation of action potentials (referred to as depolarization block, see Bikson et al. 2001, 2003; Shin et al. 2007), as well as the propagation of action potentials along the axon (referred to as axonal block or functional disconnection, see Bellinger et al. 2008; Feng et al. 2013). Third, repetitive stimulation can lead to increased neuronal activity — and with it an increased influx of Na^+ — that can cause a prolonged afterhyperpolarization mediated by sodium pumps (Gulledge et al. 2013).

Curiously, 200 Hz stimulation shows consistent effects, almost independent of the other stimulation parameters, while the frequency-mediated inhibition at 300 Hz stimulation seems to have mostly been absent. One explanation for this observation might be the relative refractory period of voltage-gated Na^+ channels. While axons might be able to conduct at 200 Hz for a brief period of time, 300 Hz might fall into the relative refractory period. The relative refractory period might often block the generation of action potentials by low-charge pulses, resulting in desynchronization of axonal firing and thereby diminishing the frequency-mediated inhibitory effects at the postsynaptic

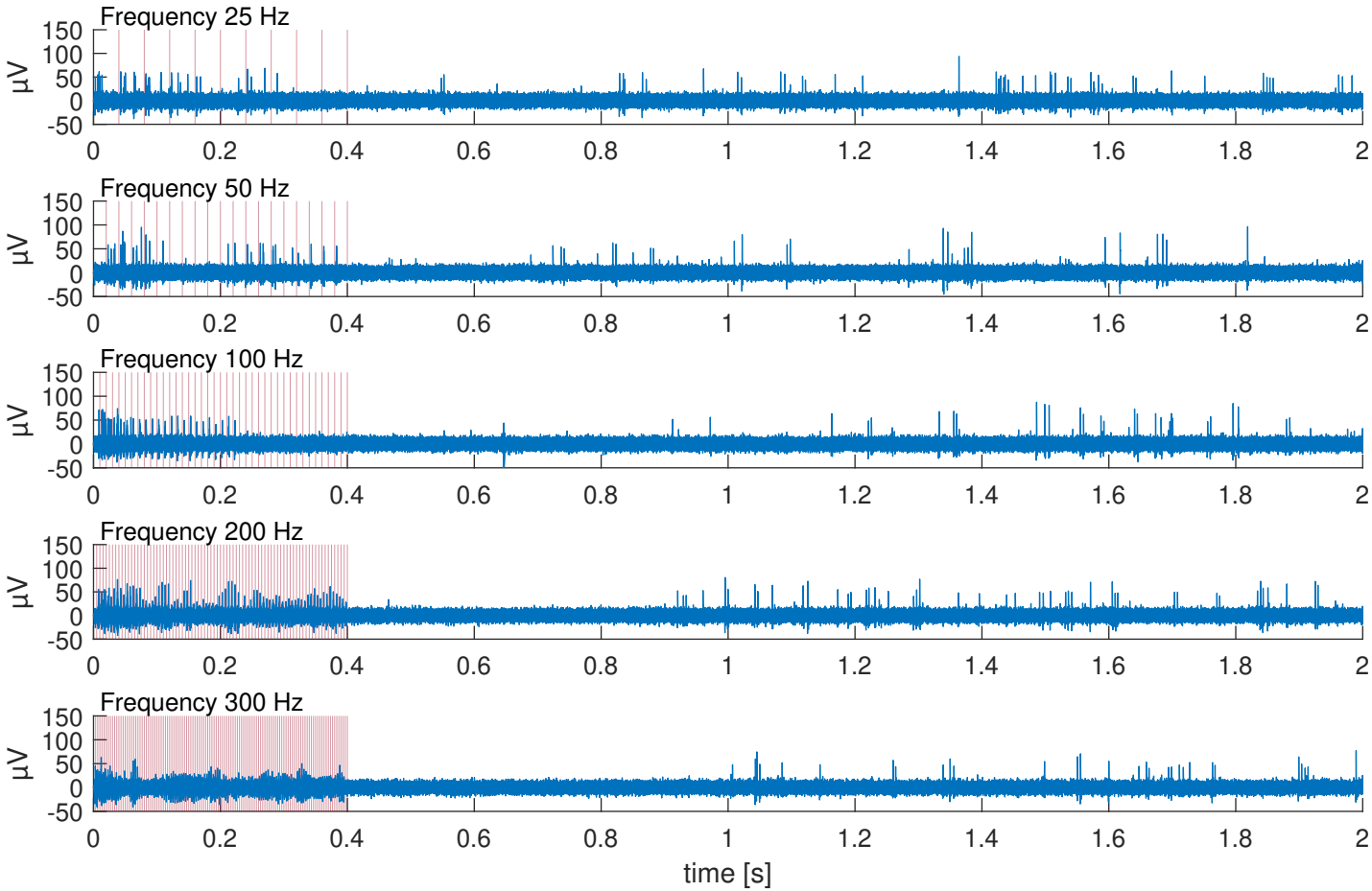

Figure 4.11: **Example of neuronal firing on a single recording channel during stimulation**. Each graph shows a superimposition of multiple trials of the same channel after band-pass filtering (300 to 3,000 Hz) and removal of stimulation artifacts. Stimulation parameters are 1.5 mA, 200 µs, and 0.4 s. Even though a pulse was only 0.4 ms in duration, additional signal distortions required the removal of 2.3 ms per pulse. Hence, artifact removal eliminated more than two thirds of the data during 300 Hz stimulation, considerably impairing spike detection.

neuron.

4.4.4 Effects on event-related potentials

Another effect of electrical stimulation we observed in the PHC is the generation of LFP responses (i.e., ERP) in the delta band. This is not unexpected, as prolonged inhibition of pyramidal neurons has been reported to generate deflections in the delta band (Steriade et al. 1990; Güntekin and Başar 2016). Given this relationship we expected the stimulation parameters' effect size to be in the same order observed for inhibiting unit activity. Interestingly, the effect sizes are in a different order. Amplitude and phase width had a much greater effect than frequency. Pulse-train duration had a negative effect. Repetition of stimulation had no effect and neither had the number of pulses (compared to frequency and duration). The effect of amplitude and phase width seems to have been mediated by the underlying charge per phase. The larger effect size of charge per phase might be explained by the necessity to affect a larger volume (and thereby number) of neurons in order to cause a significant deflection in the LFP. Increasing charge per phase increases the volume of activation. A correlation between charge per phase and the amplitude of the ERP has been shown by Donos et al. (2016). Our data corroborate those findings and further show the effects of frequency and pulse-train duration on the shape of the ERP. Frequency increases the peak latency while pulse-train duration increases the width. However, pulse-train duration also increases the threshold of other stimulation parameters necessary to cause an ERP.

4.4.5 Conclusion

In conclusion, macro-stimulation of the PHC, close to the optic radiation, produced evoked percepts similar to those described in response to stimulation of the primary visual cortex. The likelihood of evoking a percept depended on the stimulation parameters. Frequency was the most effective parameter. Increasing frequency also caused incresingly effective inhibition of local neuronal activity following the pulse train. At 300 Hz, however, frequency-mediated inhibition was largely absent. Increasing charge per phase also incresingly inhibited local neuronal activity following the pulse train. Besides lower firing rates, pulse trains were also followed by ERPs in the delta band. A high charge per phase was most effective in eliciting an ERP; the effect of frequency was comparably small. Taken together, these effects suggest that by stimulating the optic radiation we indirectly stimulated the primary visual cortex. Increased stimulation frequencies likely resulted in increased neurotransmitter release in the visual cortex, leading

to a greater signal distortion and hence to a more salient visual percept. The large effect size of charge per phase in evoking an ERP is likely owed to the stimulation's spread required to inhibit a sufficiently large volume to cause a detectable deflection in the LFP.

Our systematic investigation of different stimulation parameters provides a sound basis to inform numerous applications of brain stimulation in various fields, especially in the development of smart stimulation devices. Particularly interesting is the abrupt cessation of frequency-mediated neuronal inhibition observed when pulses with lower charge per phase were administered at a repetition frequency of 300 Hz versus 200 Hz. In order to investigate this phenomenon further, follow-up studies should focus on frequencies between 200 and 300 Hz. A finer frequency resolution within this range would allow for an estimation of the slope of the effect's cessation on the frequency axis (i.e., how quickly the effect size of the inhibition drops from its maximum at approximately 200 Hz to almost zero at 300 Hz), as well as for the characterization of the slope's interaction with charge per phase.

4.5 References

Bekhtereva NP, Bondartchuk AN, Smirnov VM, Meliutcheva LA, and Shandurina AN (1975). *Method of Electrostimulation of the Deep Brain Structures in Treatment of Some Chronic Diseases*. Stereotactic and Functional Neurosurgery 37.1:136–140.

Bellinger SC, Miyazawa G, and Steinmetz PN (2008). *Submyelin potassium accumulation may functionally block subsets of local axons during deep brain stimulation: a modeling study*. Journal of Neural Engineering 5.3:263–274.

Benabid AL, Pollak P, Louveau A, Henry S, and de Rougemont J (1987). *Combined (thalamotomy and stimulation) stereotactic surgery of the VIM thalamic nucleus for bilateral Parkinson disease*. Applied Neurophysiology 50.1:344–346.

Bikson M, Hahn PJ, Fox JE, and Jefferys JG (2003). *Depolarization Block of Neurons During Maintenance of Electrographic Seizures*. Journal of Neurophysiology 90.4:2402–2408.

Bikson M, Lian J, Hahn PJ, Stacey WC, Sciortino C, and Durand DM (2001). *Suppression of epileptiform activity by high frequency sinusoidal fields in rat hippocampal slices*. The Journal of Physiology 531 (Pt 1):181–191.

Borchers S, Himmelbach M, Logothetis N, and Karnath H.-O (2012). *Direct electrical stimulation of human cortex — the gold standard for mapping brain functions?* Nature Reviews Neuroscience 13.1:63–70.

Brindley GS and Lewin WS (1968). *The sensations produced by electrical stimulation of the visual cortex*. The Journal of Physiology 196.2:479–493.

Buzsáki G, Anastassiou CA, and Koch C (2012). *The origin of extracellular fields and currents — EEG, ECoG, LFP and spikes*. Nature reviews. Neuroscience 13.6:407–420.

Dobelle WH and Mladejovsky MG (1974). *Phosphenes produced by electrical stimulation of human occipital cortex, and their application to the development of a prosthesis for the blind*. The Journal of Physiology 243.2:553–576.1.

Donos C, Mîndruță I, Ciurea J, Mălîia MD, and Barborica A (2016). *A comparative study of the effects of pulse parameters for intracranial direct electrical stimulation in epilepsy*. Clinical Neurophysiology 127.1:91–101.

Dostrovsky JO, Levy R, Wu JP, Hutchison WD, Tasker RR, and Lozano AM (2000). *Microstimulation-induced inhibition of neuronal firing in human globus pallidus*. Journal of Neurophysiology 84.1:570–574.

Feng Z, Zheng X, Yu Y, and Durand DM (2013). *Functional disconnection of axonal fibers generated by high frequency stimulation in the hippocampal CA1 region in-vivo*. Brain Research 1509:32–42.

Filali M, Hutchison WD, Palter VN, Lozano AM, and Dostrovsky JO (2004). *Stimulation-induced inhibition of neuronal firing in human subthalamic nucleus*. Experimental Brain Research 156.3:274–281.

Gulledge AT, Dasari S, Onoue K, Stephens EK, Hasse JM, and Avesar D (2013). *A Sodium-Pump-Mediated Afterhyperpolarization in Pyramidal Neurons*. Journal of Neuroscience 33.32:13025–13041.

Güntekin B and Başar E (2016). *Review of evoked and event-related delta responses in the human brain*. International Journal of Psychophysiology. Research on Brain Oscillations and Connectivity in A New Take-Off State 103:43–52.

Hassler R, Riechert T, Mundinger F, Umbach W, and Ganglberger JA (1960). *Physiological observations in stereotaxic operations in extrapyramidal motor disturbances*. Brain: A Journal of Neurology 83:337–350.

Keramidas A and Lynch JW (2013). *An outline of desensitization in pentameric ligand-gated ion channel receptors*. Cellular and Molecular Life Sciences 70.7:1241–1253.

Kim SE, Kim WS, Kim BG, Chung D, Jeong J, Lee JS, Tae WS, Hong SB, and Lee HW (2013). *Spatiotemporal dynamics and functional correlates of evoked neural oscillations with different spectral powers in human visual cortex*. Clinical Neurophysiology 124.11:2248–2256.

Knieling S, Niediek J, Kutter E, Bostroem J, Elger CE, and Mormann F (2017). *An online adaptive screening procedure for selective neuronal responses*. Journal of Neuroscience Methods 291:36–42.

Lafreniere-Roula M, Kim E, Hutchison WD, Lozano AM, Hodaie M, and Dostrovsky JO (2010). *High-frequency microstimulation in human globus pallidus and substantia nigra*. Experimental Brain Research 205.2:251–261.

Little S, Pogosyan A, Neal S, Zavala B, Zrinzo L, Hariz M, Foltynie T, Limousin P, Ashkan K, FitzGerald J, Green AL, Aziz TZ, and Brown P (2013). *Adaptive deep brain stimulation in advanced Parkinson disease*. Annals of Neurology 74.3:449–457.

Mark TA and Gallistel CR (1993). *Subjective reward magnitude of medial forebrain stimulation as a function of train duration and pulse frequency*. Behavioral Neuroscience 107.2:389–401.

Mott DD, Li Q, Okazaki MM, Turner DA, and Lewis DV (1999). *GABAB-Receptor-mediated currents in interneurons of the dentate-hilus border*. Journal of Neurophysiology 82.3:1438–1450.

Murphey DK, Maunsell JHR, Beauchamp MS, and Yoshor D (2009). *Perceiving electrical stimulation of identified human visual areas*. Proceedings of the National Academy of Sciences of the United States of America 106.13:5389–5393.

Niediek J, Boström J, Elger CE, and Mormann F (2016). *Reliable Analysis of Single-Unit Recordings from the Human Brain under Noisy Conditions: Tracking Neurons over Hours*. PloS One 11.12:e0166598.

Pedreira C, Mormann F, Kraskov A, Cerf M, Fried I, Koch C, and Quian Quiroga R (2010). *Responses of human medial temporal lobe neurons are modulated by stimulus repetition*. Journal of Neurophysiology 103.1:97–107.

Penfield W (1936). *Epilepsy and Surgical Therapy*. Archives of Neurology & Psychiatry 36.3:449–484.

Penfield W and Boldrey E (1937). *Somatic Motor and Sensory Representation in the Cerebral Cortex of Man as Studied by Electrical Stimulation*. Brain 60.4:389–443.

Rajdev P, Ward M, and Irazoqui P (2011). *Effect of stimulus parameters in the treatment of seizures by electrical stimulation in the kainate animal model*. International Journal of Neural Systems 21.2:151–162.

Rattay F (1999). *The basic mechanism for the electrical stimulation of the nervous system*. Neuroscience 89.2:335–346.

Rey HG, Ison MJ, Pedreira C, Valentin A, Alarcon G, Selway R, Richardson MP, and Quian Quiroga R (2015). *Single-cell recordings in the human medial temporal lobe*. Journal of Anatomy 227.4:394–408.

Rosin B, Slovik M, Mitelman R, Rivlin-Etzion M, Haber SN, Israel Z, Vaadia E, and Bergman H (2011). *Closed-loop deep brain stimulation is superior in ameliorating parkinsonism*. Neuron 72.2:370–384.

Schmidt EM, Bak MJ, Hambrecht FT, Kufta CV, O'Rourke DK, and Vallabhanath P (1996). *Feasibility of a visual prosthesis for the blind based on intracortical microstimulation of the visual cortex*. Brain: A Journal of Neurology 119 (Pt 2):507–522.

Shin DS, Samoilova M, Cotic M, Zhang L, Brotchie JM, and Carlen PL (2007). *High frequency stimulation or elevated K+ depresses neuronal activity in the rat entopeduncular nucleus*. Neuroscience 149.1:68–86.

Spiegel EA, Wycis HT, Marks M, and Lee AJ (1947). *Stereotaxic Apparatus for Operations on the Human Brain*. Science (New York, N.Y.) 106.2754:349–350.

Steriade M, Gloor P, Llinás RR, Lopes da Silva FH, and Mesulam M.-.-M (1990). *Basic mechanisms of cerebral rhythmic activities*. Electroencephalography and Clinical Neurophysiology 76.6:481–508.

Sun FT and Morrell MJ (2014). *Closed-loop Neurostimulation: The Clinical Experience*. Neurotherapeutics 11.3:553–563.

Tehovnik EJ, Tolias AS, Sultan F, Slocum WM, and Logothetis NK (2006). *Direct and Indirect Activation of Cortical Neurons by Electrical Microstimulation*. Journal of Neurophysiology 96.2:512–521.

Wang C, Klistorner A, Ly L, and Barnett MH (2018). *White matter tract-specific quantitative analysis in multiple sclerosis: Comparison of optic radiation reconstruction techniques*. PLOS ONE 13.1:e0191131.

Widge AS, Malone DA, and Dougherty DD (2018). *Closing the Loop on Deep Brain Stimulation for Treatment-Resistant Depression*. Frontiers in Neuroscience 12:175.

5. Hearing voices during electrical stimulation of Heschl's gyrus

Author	Contribution (CASRAI Contributor Role Taxonomy)
Simeon Knieling[1]	Conceptualization, data curation, formal analysis, investigation (experiments), methodology, software, validation, visualization, writing – original draft, writing – review & editing
Jan Bostroem[2]	Investigation (surgery)
Christian E. Elger[1]	Resources
Florian Mormann[1]	Conceptualization, funding acquisition, investigation (surgery, experiments), project administration, resources, supervision

[1] Department of Epileptology, University of Bonn
[2] Department of Neurosurgery, University of Bonn

5.1 Introduction

In the literature, *hearing voices* is referred to as acoustic verbal hallucination (AVH). A formal definition for hallucination is provided by David (2004):

> "A sensory experience which occurs in the absence of a corresponding external stimulation of the relevant sensory organ, has a sufficient sense of reality to resemble a veridical perception, over which the subject does not feel s/he has direct and voluntary control, and which occurs in the awake state."

In case of AVH, speech is perceived in the absence of an external acoustic stimulus. Yet, compared to subvocalization (internal speech), imagined speech, or remembered speech, an AVH is perceived as a sensory stimulus (Hugdahl 2015), which often comprises whole sentences of a commenting or commanding nature (David 2004).

AVH are associated with a variety of disorders, including schizophrenia and epilepsy. Characteristics of AVH between schizophrenia and epilepsy are similar in some aspects but differ in others. For example, during dichotic listening tasks, both patient groups

(schizophrenic patients and a heterogeneous group of epilepsy patients) showed reduced activation in the left superior temporal gyrus and left inferior frontal gyrus as well as an absence of the right ear advantage observed in healthy controls (Korsnes et al. 2010). AVH in epilepsy often comprise a single voice localized in the external space contralateral to the epileptic focus. The voice usually speaks in the second person, using a neutral tone. The voice is typically of the same gender and speaks the same language as the patient. In contrast, AVH in schizophrenia often comprise multiple voices of either gender that usually lack specific spatial characteristics. These voices are mostly negative and speak in either the second or third person (Serino et al. 2014).

The mechanisms underlying AVH generation are not yet clear. Functional magnetic resonance imaging (fMRI) studies have shown that Heschl's gyrus (i.e., the transverse temporal gyri) is active during AVH, predominantly in the left (dominant) hemisphere (Dierks et al. 1999; Hauf et al. 2013). Furthermore, schizophrenic patients with AVH show abnormal functional connectivity of Heschl's gyrus with regions involved in self-monitoring and speech (Shinn et al. 2013). Heschl's gyrus largely overlaps with primary auditory cortex or the *core* of the auditory cortex (Sweet et al. 2005), depending on the nomenclature. There is much speculation about AVH generation and the regions that are involved; current hypotheses include unstable memories, insufficient self-monitoring, interhemispheric miscommunication, imbalances in top-down and bottom-up processing, as well as hybrid models involving several of the above (Ćurčić-Blake et al. 2017).

Given the involvement of Heschl's gyrus in AVH as demonstrated by fMRI studies, it is peculiar that electrical stimulation of Heschl's gyrus (in patients suffering from AVH) is reported to induce more basic auditory hallucinations like a tone, buzzing, whistling, or knocking (Penfield and Rasmussen 1950; Penfield and Perot 1963). Yet, AVH can be induced by electrical stimulation in regions anterior and posterior to Heschl's gyrus, e.g., in the planum temporale or the superior temporal gyrus (Penfield and Rasmussen 1950; Penfield and Perot 1963; Serino et al. 2014).

Here, we present a stimulation-parameter screening of Heschl's gyrus in a patient suffering from AVH in the form of recurrent auras as part of her medically intractable medial temporal lobe epilepsy. Using similar stimulation parameters as Penfield and colleagues, we were likewise unable to induce AVH. However, after adjusting parameters, stimulation of Heschl's gyrus reliably induced AVH in this patient. We discuss the mechanisms by which these adjustments could induce AVH and how the effects of stimulation in Heschl's gyrus compare to what we observed in the parahippocampal cortex in Chapter 4.

5.2 Materials and Methods

5.2.1 Subject

We describe a case study of a right-handed female patient (age 31) with pharmacologically intractable medial temporal lobe epilepsy. An fMRI localizer showed left-sided language dominance with some co-activation of the right hemisphere. Non-invasive evaluation was insufficient to localize the epileptic focus with the required diagnostic certainty. Hence, she was implanted with Behnke–Fried depth electrodes (Ad-Tech, Racine, WI) as part of an invasive presurgical evaluation (see Section 1.2).

Depth electrodes comprised 8 cylindrical macro-contacts with a diameter of 1.28 mm and a length of 1.57 mm. The distance between the centers of the two most distal (i.e., most medial after implantation) contacts was 3 mm. Nine micro-wires, 40 µm in diameter, were inserted through the lumen of the hollow depth electrode; eight recording channels and one reference. Micro-wires protruded from the depth electrode's tip by approximately 3 to 5 mm (see Fig. 1.3).

The patient gave written informed consent for all performed procedures, including the implantation of micro-electrodes, the participation in cognitive paradigms, and electrical stimulation delivered though the depth electrodes' macro-contacts. The internal review board of the University of Bonn Medical Center approved all conducted studies and procedures.

5.2.2 Experimental setup

To allow for a continuous recording during electrical stimulation, macro-electrodes were connected to the amplifier (Neuralynx ATLAS system) via an ATLAS HC Headbox (Neuralynx, Bozeman, MT). Data was recorded via Neuralynx's data acquisition software Cheetah ATLAS (version 1.1.0), running on a recording PC connected to the amplifier. To stimulate the left Heschl's gyrus, a constant current stimulator (STG 4004, Multi Channel Systems, Germany) was connected to the corresponding contacts in the headbox.

The computer program that scheduled the electrical stimulation pulses (described in Section 5.2.3) was executed on the recording PC. The recording PC had two connections to the stimulator; one direct USB connection and one indirect connection via a USB DAQ device (Measurement Computing's USB-1208FS). The stimulation parameters were set via the direct USB connection. Stimulation was triggered via the DAQ device connected

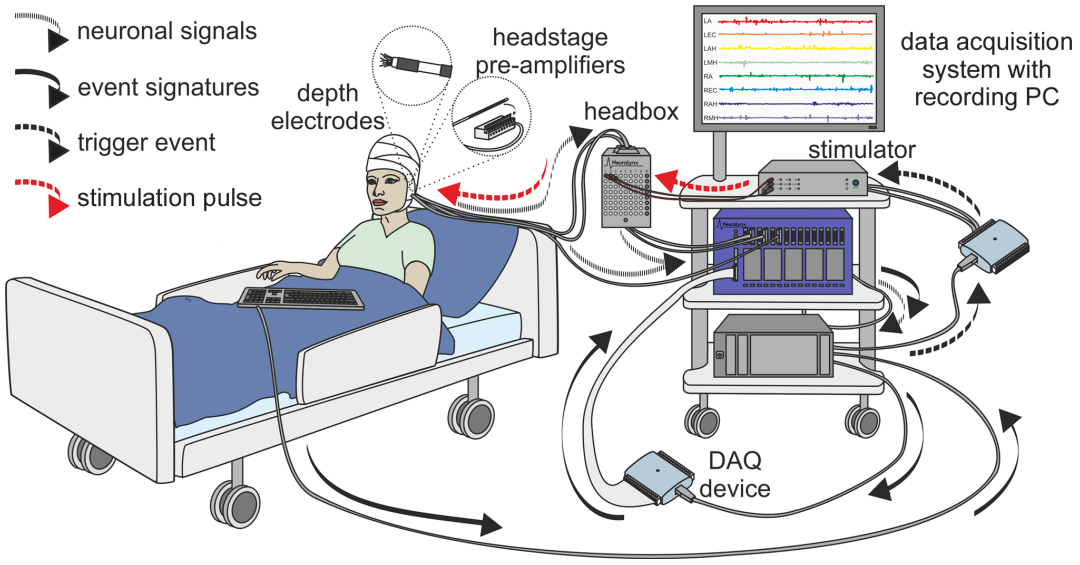

Figure 5.1: **Experimental setup for a stimulation-parameter screening of Heschl's gyrus**. See Section 5.2 for details. Figure adapted from Knieling et al. (2017). Permission for publication in this thesis was granted.

to the stimulator's trigger input. In order to send event signatures (such as stimulation onset) to the recording system, the recording PC was connected to the TTL input of the ATLAS system via a second DAQ device.

Micro-electrode signals were recorded from the eight micro-wires protruding from the depth electrode. Headstage pre-amplifiers (CHET-10, Neuralynx, Bozeman, MT) connected the micro-wires to the ATLAS system. Figure 5.1 depicts a schematic of the experimental setup.

5.2.3 Experimental protocol

In an exploratory session, the left Heschl's gyrus was stimulated using a variety of different parameter values. The purpose of this session was to manually gauge an approximate parameter space capable of evoking an auditory percept without making the patient feel uncomfortable (see Table 5.1). The duration of the exploratory session was approximately 10 minutes.

After the exploratory session, before the main experiment started, the patient was handed a keyboard and was instructed to push the left arrow key whenever she perceived an auditory hallucination. Doors and windows were closed to reduce the noise of the hospital environment.

A Matlab (Mathworks) script applied stimulation of a pseudo-randomly chosen parameter combination every 3 to 4 seconds (jittered). All combinations of the parameter val-

ues in Table 5.1 were applied 10 times each. Additionally, there were 20 trials without stimulation. This amounts to 49 conditions and a total of 500 trials. The experiment lasted for approximately 30 minutes. The patient participated in two sessions.

5.2.4 Signal processing

The sampling frequency of the micro-electrode signal was 32,768 Hz. Signals were inverted and band-pass filtered between 0.1 and 9,000 Hz by the acquisition software before the data were saved to file. Hence, spikes as well as local field potentials (LFPs) presented here are inverted.

Spikes

Spikes (i.e., action potentials) were detected and sorted using the Combinato software by Niediek et al. (2016). It provides several criteria to detect and remove artifacts.[1] Combinato's graphical user interface (GUI) was used to make manual adjustments to the sorting solutions derived by automated clustering, including rejecting remaining artifacts as well as correcting over- and under-clustering.

The effect size of electrical stimulation on instantaneous neuronal firing was determined by creating a histogram of the timestamps of the unit's spike occurrences for each trial (to convert the spike timestamps into one time series per trial). A gaussian kernel ($\sigma = 0.1$ s) was used to calculate each histogram's weighted moving average. The moving average was multiplied by the histogram's sampling rate (1000 Hz), resulting in instantaneous neuronal firing rates for each trial of the unit. For each time point, the bias-corrected Hedge's g* was calculated according to the formula:

$$\text{Hedges's } g^* = \frac{\bar{x_1} - \bar{x_2}}{s^*}\left(1 - \frac{3}{4(n_1 + n_2) - 9}\right) \tag{5.1}$$

where n_1 is the number of trials without stimulation, n_2 the number of trials with a given parameter value, $\bar{x_1}$ the mean firing rate in trials without stimulation, $\bar{x_2}$ the mean firing rate in trials with a given parameter value, and s^* the pooled standard deviation according to the formula:

$$s^* = \sqrt{\frac{(n_1 - 1)s_1^2 + (n_2 - 1)s_2^2}{n_1 + n_2 - 2}} \tag{5.2}$$

[1] To further improve the ability to separate stimulation artifacts from spikes, the following parameters were changed. In *filters.py*, *DETECT_HIGH* was set to 3000. In *mask_artifacts.py*, *binlength* was set to 100, *max_spk_per_bin* was set to 150, and *min_dist* was set to 0.75. In *concurrent.py*, *BIN_MS* was set to 1. In *options.py*, *RecursiveDepth* was set to 2 and *MinInputSizeRecluster* was set to 500.

Local field potentials

To investigate if stimulation was followed by an event-related potential (ERP), the median LFP for each stimulation condition was determined across trials. The signal from each micro-electrode in the left Heschl's gyrus was segmented into the first 2.0 s after stimulation (or after trial onset for the *'No stimulation'* condition). The median of the signal across trials in each stimulation condition was smoothed with a gaussian kernel (σ = 0.2 ms) and downsampled to 1 kHz. The reason for smoothing before downsampling was to decrease the impact of high-frequency noise present in the data. After downsampling, the signal was smoothed again using a wider gaussian kernel (σ = 4.0 ms). Finally, the signal was low-pass-filtered at 4 Hz.

5.2.5 Statistical analysis

To model the probability of evoking an AVH, a generalized linear model (GLM) was estimated using *R* (*glm()* of the *stats* package). The declared predictors were amplitude, phase width, frequency, pulse-train duration, repetition, and session (dummy coding). All predictors except for *session* were rescaled to the range [0,1] prior to estimating the model. The confidence intervals of the odds ratios were calculated via bootstrapping (using the *boot.ci(type = "bca")* command).

A GLM of the gamma family (link = inverse) was used to model the response latency. Again, amplitude, phase width, frequency, pulse-train duration, repetition, and session (dummy coding) were used as predictors.

5.2.6 Electrode localization

To identify the location of the depth electrode's macro-contacts, we used *spm12* to coregister a post-implantation computed tomography (CT) scan with a pre-implantation structural T1 magnetic resonance imaging (MRI) scan. All voxels of the coregistered CT that did not belong to the stimulated macro-contacts were set to a value of zero. The result was used as an overlay in MRIcroN to visualize the location of the stimulated electrodes.

5.3 Results

The patient was diagnosed with epilepsy when she was a child. In the first few years after she started experiencing seizures, she also experienced AVH; often immediately

Table 5.1: Stimulation parameters and their values compared in this study.

Parameter	**Values**
Amplitude	1.0, 1.5, 2.0 mA
Phase width	100, 200 µs
Frequency	50, 100, 200, 300 Hz
Train duration	0.5, 1.0 s

prior to a seizure — a phenomenon referred to as *epileptic aura*. Three months prior to the implantation of depth electrodes (during non-invasive evaluation at our institution), AVH had reoccurred. She had repeatedly reported "hearing voices". After implantation of depth electrodes, stimulation of Heschl's gyrus was also able to evoke AVH. She reported hearing whole sentences (e.g., "turn right at the next light") as well as names ("Ms. so and so"). See Appendix A.2 for a full transcript of her report.

For the stimulation-parameter screening presented here, we used slightly higher parameter values than in Chapter 4. The values used in this chapter are summarized in Table 5.1. Lower values were rarely able to induce AVH in this patient. Electrical stimulation was delivered through two macro-contacts residing in her left Heschl's gyrus. The exact placement in subject space is shown in Fig. 5.2.

5.3.1 Effects of stimulation on behavioral measures

Several stimulation-parameter combinations evoked AVH. A summary of AVH-reports in both sessions is depicted in Fig. 5.3. Based on these reports we estimated a logistic regression model to compare the effects of the stimulation parameters in Table 5.1 on evoking AVH. The results are summarized in Table 5.2. The model shows that all tested stimulation parameters (except for repetition) had a positive effect on evoking AVH. Repetition of stimulation had a negative effect. Including the interactions frequency $\times$ train duration (i.e., pulses) and amplitude $\times$ phase width (i.e., charge per phase) did not improve the model according to a log-likelihood ratio test or the Akaike information criterion (AIC). Hence, these interactions were omitted.

Prior to estimating the model, predictors were rescaled to a maximum of 1.0. Hence the regression coefficients specify a ranking for the stimulation parameters within the tested parameter space. Amplitude had the largest effect on evoking an AVH, followed by phase width, frequency, and pulse-train duration. Rescaling the predictors affects the interpretation of the odds ratio. In Table 5.2, the odds ratio shows by how much the odds of evoking an AVH change when a stimulation parameter is changed from zero to

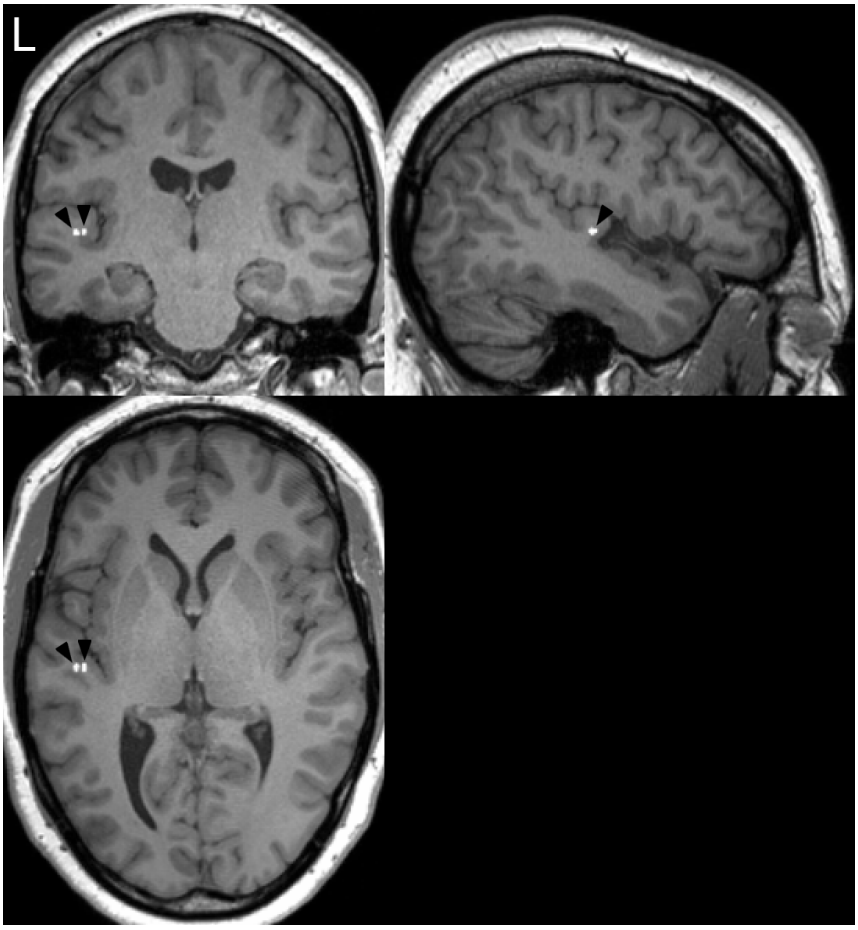

Figure 5.2: **Electrode position**. Black arrow heads point to the position of the stimulated macro-contacts.

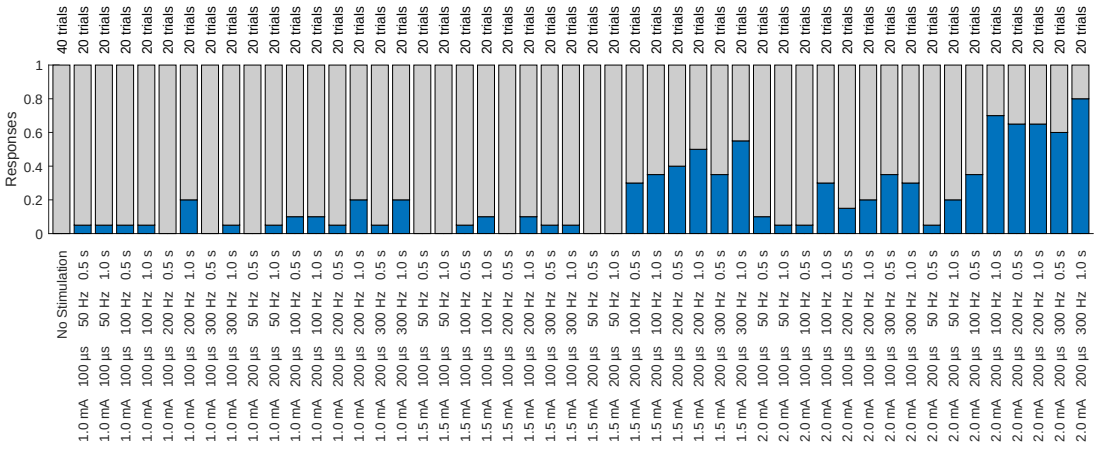

Figure 5.3: **The proportion of evoked AVH reported in each condition**.

Table 5.2: GLM (family: binomial, link: logit) of the effects of stimulation parameters on the induction of AVH.

			95% CI for odds ratio			
Fixed effects	**b**	**SE(b)**	**lower**	**odds ratio**	**upper**	**p**
Step 1: Pseudo R^2 = .24 ^{HL} / .21 ^{CS} / .33 ^{N}			Model χ^2 (6) = 231.10 ***			
Intercept	−9.24	0.75				***
Amplitude	4.39	0.51	27.91	80.45	230.01	***
Phase width	3.33	0.41	12.12	28.02	65.18	***
Frequency	1.92	0.30	3.85	6.80	12.00	***
Train duration	1.36	0.38	1.88	3.92	8.12	***
Repetition	−0.75	0.29	0.26	0.47	0.81	**

Independent variables were rescaled to [0,1] prior to model estimation. The model further includes the fixed effect session (dummy coding) that is omitted in this table. Adding the fixed effects pulses and charge per phase does not improve the model.
Patients = 1, observations = 1000. ** $p < 0.01$, *** $p < 0.001$.
^{HL} Hosmer–Lemeshow
^{CS} Cox–Snell
^{N} Nagelkerke

its maximum value.

The patient's response times (RT) exhibited large variance. A histogram of the RT is depicted in Fig. 5.4. In 13 trials (7% of perceived trials), RT were below 0.5 s after stimulation onset. These responses did not fit the rest of the histogram's distribution and were interpreted as delayed responses to the preceding trial. Hence, Fig. 5.4 shows some RT above the maximum trial duration of 4.0 s. The median response time was 2.21 s.

To investigate the effects of stimulation parameters on RT, we used a GLM. A summary is presented in Table 5.3. Train duration had a positive effect on RT (longer train durations increase RT), while phase width had a negative effect. Significant effects of amplitude, frequency, or repetition could not be identified.

5.3.2 Effects of stimulation on event-related potentials

Compared with our observations in the PHC (see Section 4.3.2), event-related potentials (ERPs) in this patient's Heschl's gyrus were of much lower amplitude and varied in shape. Besides an early component within the first 500 ms, there was a subsequent negative deflection in the low delta band (approximately 0.3 Hz) that arose after stimulation with 200 nC and above. ERP amplitudes were too close to the noise level to reliably detect ERPs in individual trials. Figure 5.5 depicts the median LFP of each of the eight

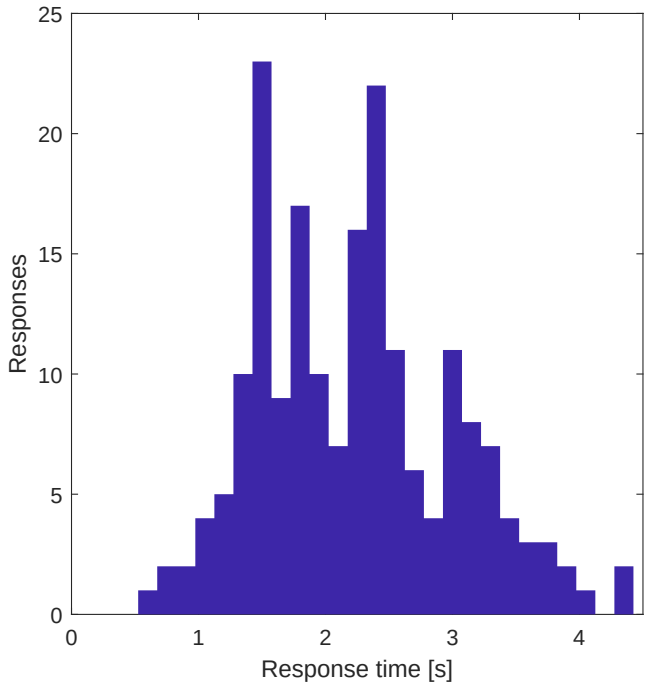

Figure 5.4: **Histogram of response times to evoked AVH**.

Table 5.3: GLM (family: gamma, link: inverse) of the effects of stimulation parameters on response time to induced AVH.

Fixed effects	**b**	**SE(b)**	**p**
Model: Multiple $R^2 = .083$ Adjusted $R^2 = .053$ Model χ^2 (6) = 1.94			
Intercept	0.45	0.086	***
Phase width	0.12	0.048	*
Amplitude	0.02	0.060	0.75
Repetition	−0.009	0.035	0.80
Frequency	−0.026	0.038	0.50
Train duration	−0.14	0.047	**

Independent variables were rescaled to [0,1] prior to model estimation. The model further includes the fixed effect session (dummy coding) that is omitted in this table. Adding the fixed effects pulses and charge per phase does not improve the model.
Patients = 1, observations = 190. * $p < 0.05$, ** $p < 0.01$, *** $p < 0.001$.

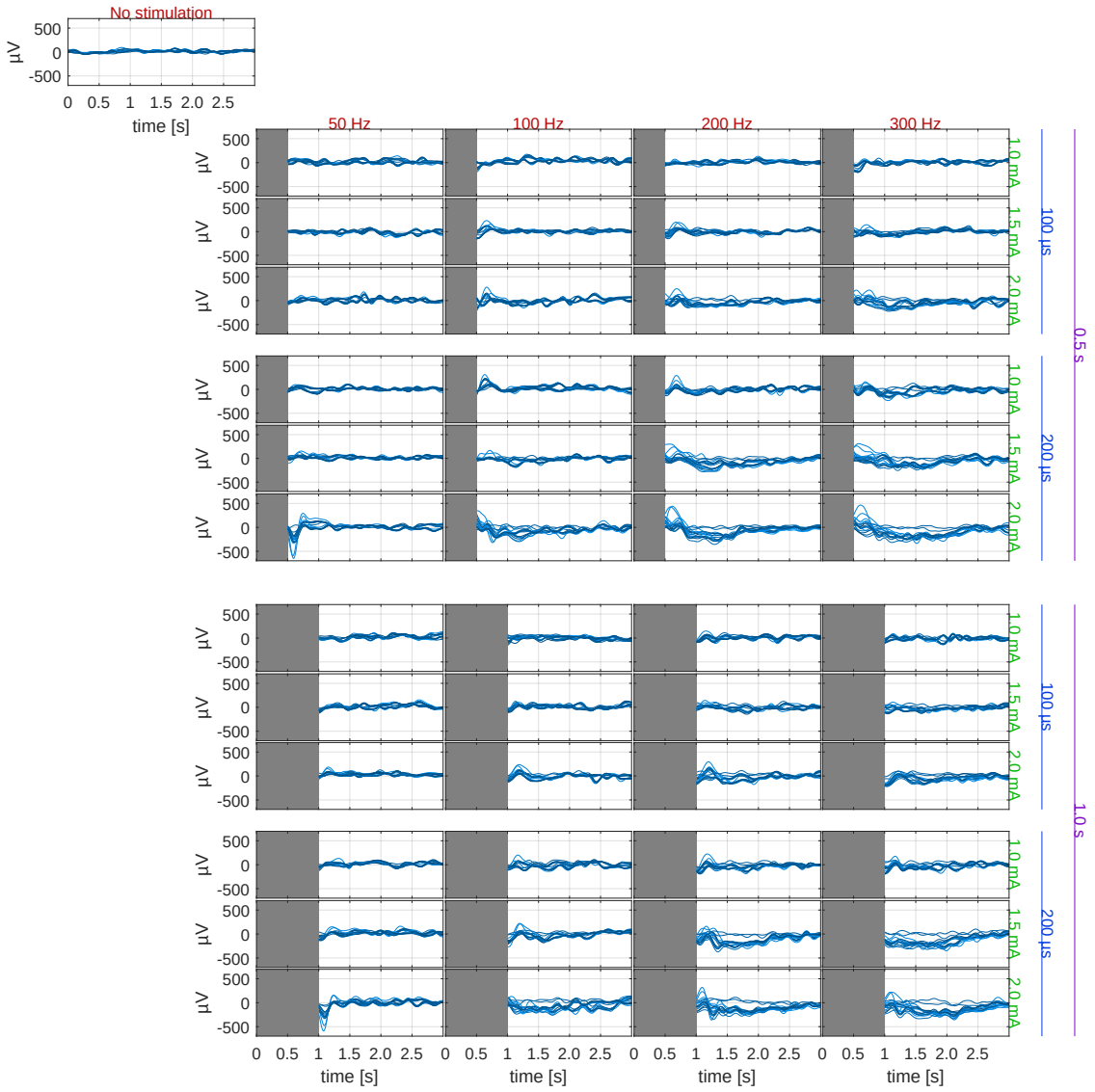

Figure 5.5: **Event-related potentials during different stimulation conditions**. Blue lines represent the median filtered LFP of each of the eight micro-electrodes in Heschl's gyrus in each of the two sessions.

micro-electrodes in Heschl's gyrus in both sessions during all 49 stimulation conditions. In Fig. 5.6 the same median LFPs are grouped according to the parameter values of their stimulation condition. The amplitude of the early component in the median ERP was lower after 1.0 s stimulation than after 0.5 s stimulation ($p < 0.001$ in Wilcoxon signed-rank test).

5.3.3 Effects of stimulation on neuronal firing rates

In Heschl's gyrus, only one single unit per session was detected. Considering that both single units were detected on the same channel, have a similar shape, and that the time

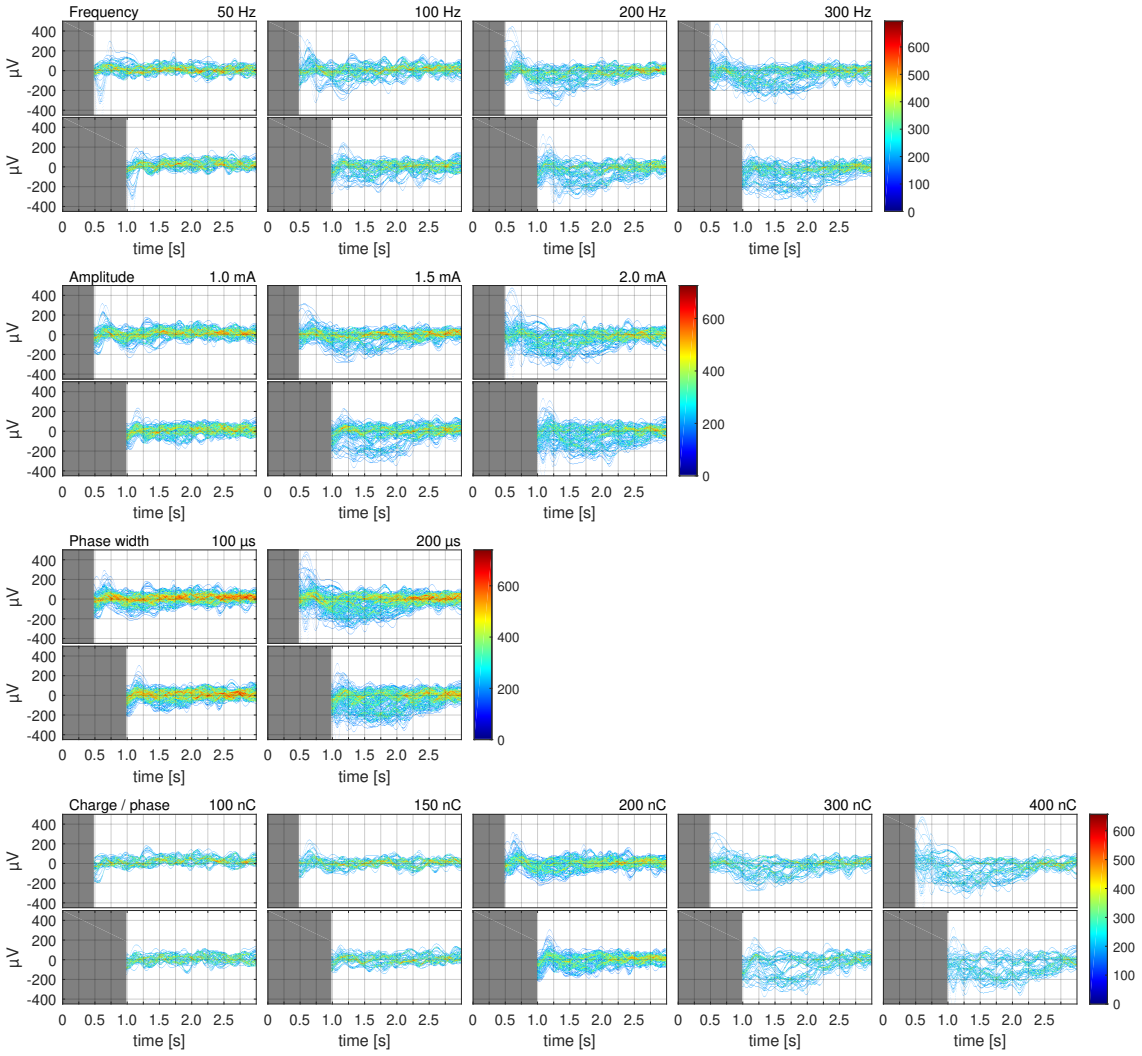

Figure 5.6: **Density plot of event-related potentials**. Each row of graphs includes one median ERP for each of the eight micro-electrodes in Heschl's gyrus during each condition in each of the two sessions. There are twice as many conditions that use 200 nC per phase (1.0 mA for 200 µs and 2.0 mA for 100 µs) as there are conditions that use one of the other values of charge per phase. Hence, for better visualization, density values in the two 200 nC graphs were scaled so that their 99th percentile matches that of the 100 nC plots.

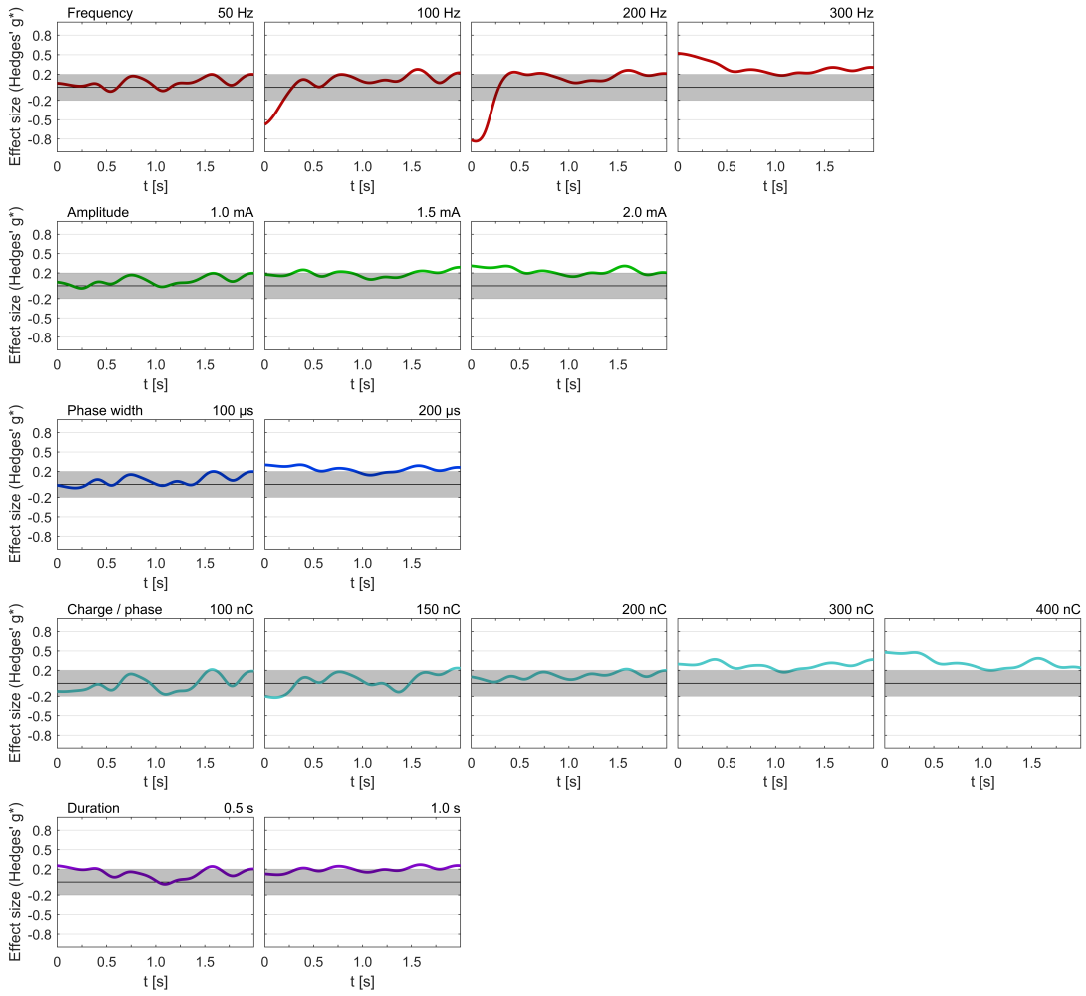

Figure 5.7: **Effects of stimulation parameters on time dependent neuronal firing**. In the presented data, Hedge's g* is nearly identical to Cohen's d. Hence, the threshold values for small (0.2), medium (0.5) and large (0.8) effects are depicted (Cohen 2013). Firing rates were aligned to the end of the pulse train (t = 0 s).

between both sessions was less than an hour, both single units likely originated from the same neuron. Figure 5.7 displays the effect size Hedge's g* of different parameter values on neuronal firing. In a similar manner, Fig. 5.8 depicts the cumulative raster plots for each condition. One trace of a cumulative raster plot includes the spikes from both units in all trials of the respective stimulation condition. For frequencies up to and including 200 Hz, units showed similar responses to stimulation as neurons in the PHC (see Section 4.3.3); a period of inhibition that increases with increasing stimulation frequency. However, at 300 Hz, these units showed a period of increased neuronal activity.

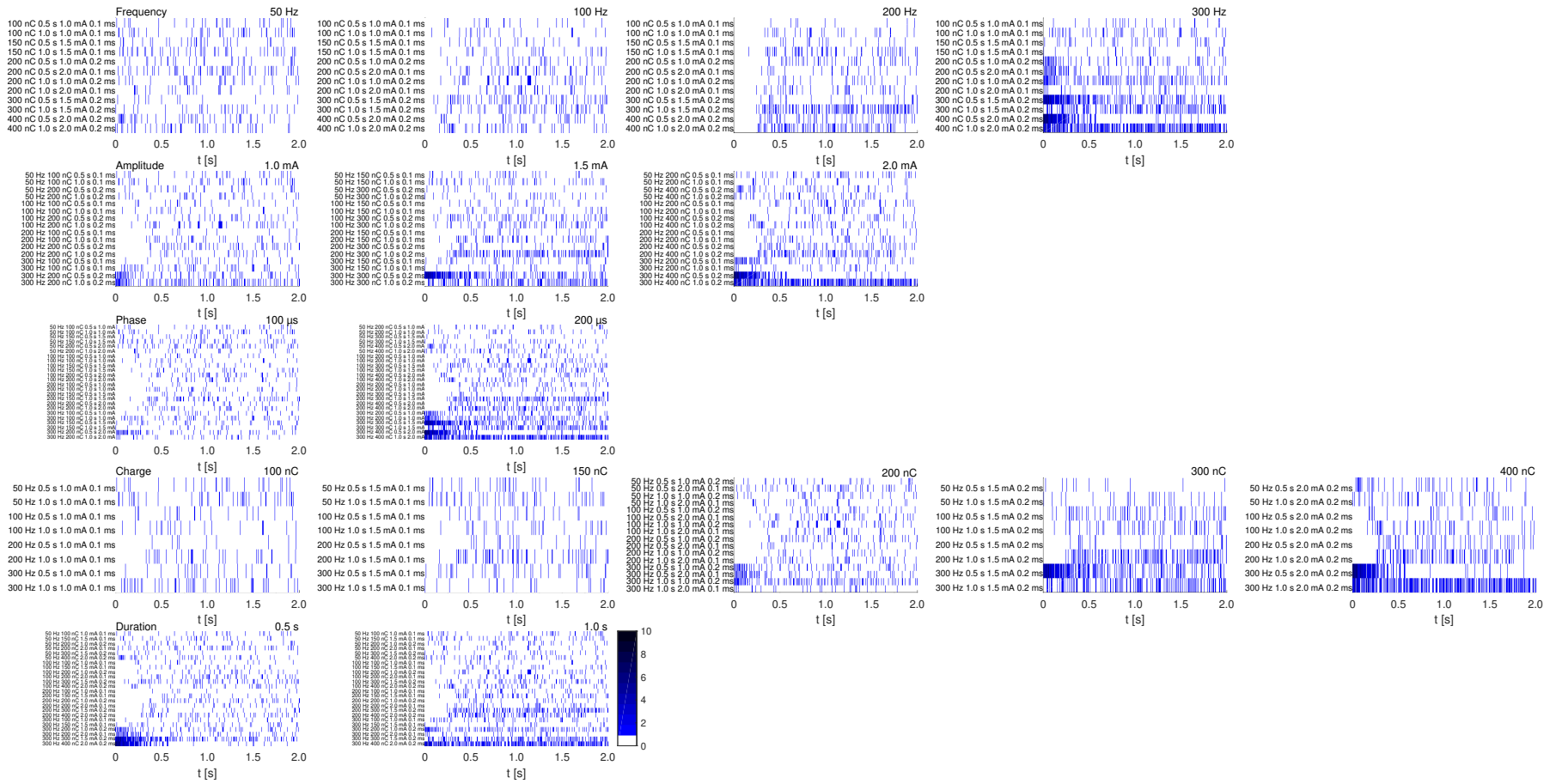

Figure 5.8: **Cumulative raster plots**. Each row represents one stimulation condition and cumulatively encompasses all 20 trials within this condition. Hence, considering the bin size of 1 ms, there could be two or more spikes in the same bin. Bins with more than one spike were colored according to the depicted colormap.

5.4 Discussion

In this chapter, we reported findings from a stimulation-parameter screening of Heschl's gyrus in a patient who experienced auditory verbal hallucinations (AVH) as part of her seizures. Being able to measure LFP and single units in Heschl's gyrus is a rare opportunity. Serino et al. (2014) noted that only 2.6% of their pharmacoresistant epilepsy patients reported AVH (9 out of 352). The number of AVH patients with inconclusive non-invasive diagnostics that hence required invasive presurgical monitoring was even lower at approximately 0.6% (2 out of 352). As far as reported, neither of those patients was implanted in Heschl's gyrus. The scarcity of this patient group is further stressed by the small number of patients reported in other studies presenting depth-electrode data from Heschl's gyrus (e.g., two patients in Mukamel et al. 2005, 2011, three patients in Nir et al. 2007, 2008, and four patients in Bitterman et al. 2008).

5.4.1 Effects on behavioral measures

An exploratory stimulation session revealed that parameters slightly higher than those used in Chapter 4 were capable of evoking AVH. Hence, in comparison to Chapter 4, amplitudes were raised by 0.5 mA, pulse-train durations were raised by 0.5 s, and trial durations were raised by an average of 1.0 s. Longer trial durations were used to prevent AVH from blending together across subsequent trials, given the longer pulse-train durations.

A model of the patient's reports of AVH showed that the most influential parameter was current amplitude, followed by phase width, frequency, and pulse-train duration. Repetition had a negative effect on reports of AVH. This ranking differs from the ranking for evoking phosphenes (reported in Chapter 4), in which frequency was more effective than amplitude and phase width. The reason for this discrepancy might be related to the required increase in stimulation parameters to evoke AVH, discussed in the following.

Penfield reported that he was able to induce AVH by stimulating regions anterior and posterior to Heschl's gyrus but not when stimulating Heschl's gyrus directly. Stimulating Heschl's gyrus would only result in much cruder auditory sensations like tones, buzzing, or knocking (Penfield and Rasmussen 1950; Penfield and Perot 1963). Yet our patient's reports of evoked AVH (see Appendix A.2 and Fig. 5.3) and the location of the stimulation contacts (see Fig. 5.2) convincingly show an induction of AVH triggered by stimulation in Heschl's gyrus.

Penfield used a silver ball electrode that had a smaller surface area than our macro-

contacts (1.5 mm^2 vs. 6 mm^2). He also used smaller currents: 0.05 to 0.5 mA vs. 1.0 to 2.0 mA (Penfield and Perot 1963). In our patient, these smaller currents were likewise unable to evoke AVH. The higher the current, the greater the number of cells that are being excited, a phenomenon called current spread (Tehovnik et al. 2006; Mädler and Coenen 2012). Measurements of current spread show a large variance across studies and subjects (Bagshaw and Evans 1976). The dependance of AVH induction on higher currents could be caused by different phenomena, depending on how far the stimulation's effect spread. A minimum volume of Heschl's gyrus may need to be excited in order to evoke AVH. Considering the hypothesis that AVH are caused by abnormal connectivity of Heschl's gyrus with other areas (Ćurčić-Blake et al. 2017), AVH might only be evoked if enough of these connections are excited simultaneously. Alternatively, if the current spread was sufficiently high, our stimulation might have excited neurons in the adjacent planum temporale, a region that is reportedly able to induce AVH when stimulated (Penfield and Perot 1963). In both cases, the required current spread would explain why amplitude and phase width are more effective than frequency in evoking AVH.

Little information could be derived from the patient's response times. Stimulation parameters only accounted for about 5% of the variance. There were several factors that could have contributed to the variance in her RT. Diagnostics revealed abnormalities in her fine motor skills. Further, during testing, she was sitting cross-legged with the keyboard in her lap and her extended finger (held perpendicular to the keyboard's surface) was hovering over the keyboard at varying distances. When asked if she would prefer a more comfortable position, she declined. Nonetheless, a significant positive effect of pulse-train duration was detected. This could either point to an induction of AVH *after* stimulation, or it could mean that the AVH distracted the patient from responding. The rather long median RT of 2.21 s could also be partially due to the nature of the hallucination. Hearing words or even sentences takes time that is dependent on the words' lengths. Hence, it is not surprising that detecting an AVH takes longer than detecting phosphenes.

5.4.2 Effects on event-related potentials

ERPs of this patient's Heschl's gyrus were of such a small amplitude that we were unable to reliably detect them in individual trials. However, the filtered median LFP revealed a few patterns worth noting. The variance in shape, both across wires and also across conditions was much larger than what we observed in the PHC. After stimulation, the LFP seemed to exhibit an early component (in the first 500 ms) followed by a low

frequency deflection. Especially noticeable is how the early component changed sign depending on the stimulation condition. In most conditions, the majority of wires in Heschl's gyrus recorded a small positive peak during the first 500 ms. Nonetheless, after stimulation with 50 Hz, 2 mA, and 200 µs there was a clear negative peak on almost all wires for both durations. Finally, as any of the stimulation parameters increased, the variance of the LFP across wires increased as well. This could reflect an overall higher complexity of the Heschl network compared to the PHC.

5.4.3 Effects on neuronal firing rates

Similarly to neurons in the PHC, the units in Heschl's gyrus showed increasing inhibition after stimulation with increasing frequencies. This phenomenon is consistent with our hypothesis introduced in Chapter 4, namely, that inhibition was caused by prolonged repetitive excitation. The inhibitory effect could have been mediated by various mechanisms. First, increased neurotransmitter release at the synapse can cause ligand-gated ion channels in the postsynaptic neuron to desensitize due to continued agonist exposure (Keramidas and Lynch 2013). Second, repetitive excitation of a neuron elevates extracellular K^+ ($[K^+]_e$) around the cell membrane. Elevated $[K^+]_e$ may prevent the generation and propagation of an action potential. These phenomena are referred to as depolarization block and functional disconnection (or axonal block), respectively (Bikson et al. 2001, 2003; Shin et al. 2007; Bellinger et al. 2008; Feng et al. 2013). Third, an increased intracellular Na^+ concentration due to increased neuronal activity could cause sodium pumps to generate a prolonged afterhyperpolarization (Gulledge et al. 2013). Lastly, inhibitory synapses could cause inhibitory postsynaptic potentials (IPSP) mediated by $GABA_A$ (Dostrovsky et al. 2000), and $GABA_B$ receptors (Mott et al. 1999).

Whereas in the PHC the charge per phase showed an inhibitory effect, the units measured in Heschl's gyrus increased their firing in response to a higher charge. The difference in response behavior to higher currents between units measured in the PHC and units measured in Heschl's gyrus could be caused by differences in the respective networks. Higher currents excite a larger volume of cells. In Heschl's gyrus, these cells might have been connected to the measured units in a predominantly excitatory fashion, while in the PHC inhibitory connections to the measured units might have dominated.

Similarly to what we reported for the PHC, the most striking contrast was between stimulation frequencies of 200 and 300 Hz. Inhibition was strongest for 200 Hz, but largely absent for 300 Hz. In fact, at 300 Hz, the excitatory effect of charge per phase was most pronounced. This points towards the hypothesis that the charge-dependent

effect was mediated by a neuron's respective balance between inhibitory and excitatory synapses. The absence of the frequency-mediated inhibitory effect at 300 Hz could have been due to desynchronization between excited cells, caused by the relative refractory period of voltage-gated Na^+ channels. Some neurons, depending on their state and relative spatial position to the electrode, might be able to fire after a certain pulse, while for other neurons the pulse might not be strong enough to fire within the relative refractory period, hence diminishing the inhibitory effects of fast repetitive excitation outlined above.

5.4.4 Conclusion

The presented data demonstrate the induction of AVH via stimulation in Heschl's gyrus in a patent suffering from AVH as part of her seizures. It remains open whether the evoked AVH were caused by sufficiently strong excitation of Heschl's gyrus or by current spread to neighboring areas like the planum temporale. While epilepsy patients with AVH who require invasive presurgical monitoring are quite rare (Serino et al. 2014), a multi-patient study could help resolve inconsistencies (Ćurčić-Blake et al. 2017) between fMRI studies (Dierks et al. 1999; Hauf et al. 2013) and reports of intracranial stimulation (Penfield and Perot 1963) about the involvement of Heschl's gyrus in AVH generation.

5.5 References

Bagshaw EV and Evans MH (1976). *Measurement of current spread from microelectrodes when stimulating within the nervous system*. Experimental Brain Research 25.4:391–400.

Bellinger SC, Miyazawa G, and Steinmetz PN (2008). *Submyelin potassium accumulation may functionally block subsets of local axons during deep brain stimulation: a modeling study*. Journal of Neural Engineering 5.3:263–274.

Bikson M, Hahn PJ, Fox JE, and Jefferys JG (2003). *Depolarization Block of Neurons During Maintenance of Electrographic Seizures*. Journal of Neurophysiology 90.4:2402–2408.

Bikson M, Lian J, Hahn PJ, Stacey WC, Sciortino C, and Durand DM (2001). *Suppression of epileptiform activity by high frequency sinusoidal fields in rat hippocampal slices*. The Journal of Physiology 531 (Pt 1):181–191.

Bitterman Y, Mukamel R, Malach R, Fried I, and Nelken I (2008). *Ultra-fine frequency tuning revealed in single neurons of human auditory cortex*. Nature 451.7175:197–201.

Cohen J (2013). *Statistical Power Analysis for the Behavioral Sciences*. Routledge. 579 pp.

Ćurčić-Blake B, Ford JM, Hubl D, Orlov ND, Sommer IE, Waters F, Allen P, Jardri R, Woodruff PW, David O, Mulert C, Woodward TS, and Aleman A (2017). *Interaction of language, auditory and memory brain networks in auditory verbal hallucinations*. Progress in Neurobiology 148:1–20.

David AS (2004). *The cognitive neuropsychiatry of auditory verbal hallucinations: an overview*. Cognitive Neuropsychiatry 9.1:107–123.

Dierks T, Linden DEJ, Jandl M, Formisano E, Goebel R, Lanfermann H, and Singer W (1999). *Activation of Heschl's Gyrus during Auditory Hallucinations*. Neuron 22.3:615–621.

Dostrovsky JO, Levy R, Wu JP, Hutchison WD, Tasker RR, and Lozano AM (2000). *Microstimulation-induced inhibition of neuronal firing in human globus pallidus*. Journal of Neurophysiology 84.1:570–574.

Feng Z, Zheng X, Yu Y, and Durand DM (2013). *Functional disconnection of axonal fibers generated by high frequency stimulation in the hippocampal CA1 region in-vivo*. Brain Research 1509:32–42.

Gulledge AT, Dasari S, Onoue K, Stephens EK, Hasse JM, and Avesar D (2013). *A Sodium-Pump-Mediated Afterhyperpolarization in Pyramidal Neurons*. Journal of Neuroscience 33.32:13025–13041.

Hauf M, Wiest R, Schindler K, Jann K, Dierks T, Strik W, Schroth G, and Hubl D (2013). *Common mechanisms of auditory hallucinations–perfusion studies in epilepsy*. Psychiatry Research: Neuroimaging 211.3:268–270.

Hugdahl K (2015). *Auditory hallucinations: A review of the ERC "VOICE" project*. World Journal of Psychiatry 5.2:193–209.

Keramidas A and Lynch JW (2013). *An outline of desensitization in pentameric ligand-gated ion channel receptors*. Cellular and Molecular Life Sciences 70.7:1241–1253.

Knieling S, Niediek J, Kutter E, Bostroem J, Elger CE, and Mormann F (2017). *An online adaptive screening procedure for selective neuronal responses*. Journal of Neuroscience Methods 291:36–42.

Korsnes MS, Hugdahl K, Nygård M, and Bjørnæs H (2010). *An fMRI study of auditory hallucinations in patients with epilepsy*. Epilepsia 51.4:610–617.

Mädler B and Coenen VA (2012). *Explaining Clinical Effects of Deep Brain Stimulation through Simplified Target-Specific Modeling of the Volume of Activated Tissue*. American Journal of Neuroradiology 33.6:1072–1080.

Mott DD, Li Q, Okazaki MM, Turner DA, and Lewis DV (1999). *GABAB-Receptor-mediated currents in interneurons of the dentate-hilus border*. Journal of Neurophysiology 82.3:1438–1450.

Mukamel R, Gelbard H, Arieli A, Hasson U, Fried I, and Malach R (2005). *Coupling Between Neuronal Firing, Field Potentials, and fMRI in Human Auditory Cortex*. Science 309.5736:951–954.

Mukamel R, Nir Y, Harel M, Arieli A, Malach R, and Fried I (2011). *Invariance of firing rate and field potential dynamics to stimulus modulation rate in human auditory cortex*. Human Brain Mapping 32.8:1181–1193.

Niediek J, Boström J, Elger CE, and Mormann F (2016). *Reliable Analysis of Single-Unit Recordings from the Human Brain under Noisy Conditions: Tracking Neurons over Hours*. PloS One 11.12:e0166598.

Nir Y, Fisch L, Mukamel R, Gelbard-Sagiv H, Arieli A, Fried I, and Malach R (2007). *Coupling between Neuronal Firing Rate, Gamma LFP, and BOLD fMRI Is Related to Interneuronal Correlations*. Current Biology 17.15:1275–1285.

Nir Y, Mukamel R, Dinstein I, Privman E, Harel M, Fisch L, Gelbard-Sagiv H, Kipervasser S, Andelman F, Neufeld MY, Kramer U, Arieli A, Fried I, and Malach R (2008). *Interhemispheric correlations of slow spontaneous neuronal fluctuations revealed in human sensory cortex*. Nature Neuroscience 11.9:1100–1108.

Penfield W and Perot P (1963). *The Brain's Record of Auditory and Visual Experience: A Final Summary and Discussion*. Brain 86.4:595–696.

Penfield W and Rasmussen T (1950). *The cerebral cortex of man: a clinical study of localization of function*. Macmillan. 272 pp.

Serino A, Heydrich L, Kurian M, Spinelli L, Seeck M, and Blanke O (2014). *Auditory verbal hallucinations of epileptic origin*. Epilepsy & Behavior 31:181–186.

Shin DS, Samoilova M, Cotic M, Zhang L, Brotchie JM, and Carlen PL (2007). *High frequency stimulation or elevated K+ depresses neuronal activity in the rat entopeduncular nucleus*. Neuroscience 149.1:68–86.

Shinn AK, Baker JT, Cohen BM, and Öngür D (2013). *Functional connectivity of left Heschl's gyrus in vulnerability to auditory hallucinations in schizophrenia*. Schizophrenia Research 143.2:260–268.

Sweet RA, Dorph-Petersen K.-A, and Lewis DA (2005). *Mapping auditory core, lateral belt, and parabelt cortices in the human superior temporal gyrus*. Journal of Comparative Neurology 491.3:270–289.

Tehovnik EJ, Tolias AS, Sultan F, Slocum WM, and Logothetis NK (2006). *Direct and Indirect Activation of Cortical Neurons by Electrical Microstimulation*. Journal of Neurophysiology 96.2:512–521.

6. Effects of PHC and amygdala stimulation on categorical discrimination

Author	Contribution (CASRAI Contributor Role Taxonomy)
Simeon Knieling[1]	Conceptualization, data curation, formal analysis, investigation (experiments), methodology, software, validation, visualization, writing – original draft, writing – review & editing
Thomas P. Reber[1]	Investigation (experiments), supervision
Jan Bostroem[2]	Investigation (surgery)
Christian E. Elger[1]	Resources
Florian Mormann[1]	Conceptualization, funding acquisition, investigation (surgery, experiments), project administration, resources, supervision

[1] Department of Epileptology, University of Bonn
[2] Department of Neurosurgery, University of Bonn

6.1 Introduction

In Chapter 1 we introduced concept cells and the notion that they could be involved in perception. In a nutshell, concept cells change their firing rate in response to most stimuli representing the concept-cell's preferred concept, but rarely in response to stimuli representing other concepts. Concept cells are found throughout the human medial temporal lobe (MTL) with varying degrees of selectivity and invariance, depending on the respective region (Mormann et al. 2008; Quian Quiroga et al. 2009).

Several studies have shown some form of correlation between concept-cell activity and perception as well as awareness (Quian Quiroga et al. 2005, 2008, 2009; Pedreira et al. 2010; Reber et al. 2017). Here we investigate the causal relationship behind this correlation. It seems almost self-evident that perception is a central process in shaping concept-cell activity: For a representation of a concept to be created, that concept must likely be perceived first (whether by senses or by imagination). Anecdotally, our group once found a concept cell that responded to a colleague in an invariant and selective

manner, less than 4 hours after the patient met our colleague for the first time. Hence, the influence of perception on concept-cell activity seems not just likely but also fast-acting. The less obvious question is if there could be a relationship in the opposite direction, namely if concept-cell activity can alter perception.

A causal relationship between category-selective cells and perception has been demonstrated in other species. Afraz et al. (2006) showed that electrical stimulation near face-selective clusters of neurons in the macaque monkey's inferior temporal (IT) cortex biased monkeys to respond with *face* in a *face* versus *non-face* discrimination task. They found three important aspects to successfully induce a bias. First, the stimulated cluster of cells should have a high face-selectivity. Stimulating clusters that were not selective for faces had no effect. Second, stimulating larger clusters of face-selective cells induced a greater bias. Lastly, stimulation onset should coincide with the cells' natural response latency.

Based on these findings, an ideal target region would include large topographical clusters of cells that respond to semantically similar concepts. However, concept cells in the human MTL do not tend to topographically organize in clusters of semantic similarity (De Falco et al. 2016; Quian Quiroga 2016). The most likely candidate region to incorporate a high density of semantically related cells is the parahippocampal cortex (PHC). The degree of topographical organization in the PHC is high enough to cause an LFP response to stimuli with a spatial layout (scenes and landscapes, see Mormann et al. 2017). Scene selectivity within the PHC is not distributed evenly but increases from anterior to posterior (Litman et al. 2009), culminating in the parahippocampal place area (PPA, see Epstein and Kanwisher 1998). In fact, Mégevand et al. (2014), describes a patient who reported hallucinations of scenes in response to PPA stimulation. Furthermore, when the area in which the PPA typically resides (near the border of parahippocampal and lingual gyrus) is damaged, patients report topographical disorientation (Barrash et al. 2000). The patient H. M. who is known for having most of the other MTL regions bilaterally resected (amygdalae, the entorhinal cortices, and the anterior part of the hippocampi), reported no deficits in perception (Scoville and Milner 1957; Corkin et al. 1997). Hence, we argue that the most likely candidate region of the MTL to be involved in perceptogenesis is the PHC. This assumption is further corroborated by the average response latencies. While the amygdala (397 ms), the hippocampus (394 ms), and the entorhinal cortex (392 ms) have been associated with declarative memory, significantly lower average response latencies (271 ms) and a greater tendency to respond to broader concepts indicate that the PHC is involved in earlier processes (Mormann et al. 2008; Quian Quiroga 2012).

Here we test whether PHC stimulation in humans can alter perception in a forced-choice categorization task. Participants had to discriminate between noisy images of landscapes and animals, while either no stimulation, PHC stimulation, or amygdala stimulation was applied. Neuronal responses to landscapes are more frequently found in the PHC (similar to other scenes, see Mormann et al. 2017), while neuronal responses to animals are more frequently found in the right amygdala (Mormann et al. 2011). Amygdala stimulation was used as a negative control condition, since its long response latency renders the amygdala unlikely to be involved in perceptogenesis.

To be able to gauge the degree of scene selectivity in the stimulated area, an fMRI localizer of the PPA was performed one day prior to implantation. A post-operative computed tomography (CT) scan allowed to estimate the distance between the stimulation contacts and the PPA.

6.2 Materials and Methods

6.2.1 Subjects

The participants in this study were patients suffering from pharmacologically intractable medial temporal lobe epilepsy. Patients underwent invasive presurgical evaluation (see Section 1.2) to localize their epileptic focus and evaluate the expedience of a resection. As part of the invasive presurgical evaluation, patients were implanted with Behnke–Fried depth electrodes (Ad-Tech, Racine, WI) in various areas, including the parahippocampal cortex (PHC) and the amygdala.

Depth electrodes had 8 macro-contacts, each 1.57 mm in length and 1.28 mm in diameter. The two most distal contacts were used for stimulation. Their centers were 3 mm apart. Micro-electrodes were implanted through the hollow depth electrodes. A total of nine wires per depth electrode were implanted; eight recording channels and one uninsulated wire for referencing purposes. Micro-electrodes were 40 µm in diameter and extended approximately 3 to 5 mm from the tip of the depth electrode.

Nine patients agreed to participate in the pilot study. One of them was excluded for mislabeling more than 30% of the well visible stimuli (noise $\leq$ 20%), and three aborted the experiment. The five remaining patients participated in four sessions each. Another seven patients agreed to participate in the main study. One of them was excluded for mislabeling more than 30% of the well visible stimuli (noise $\leq$ 20%). The remaining six patients participated in four sessions each.

Each patient gave written informed consent for the implantation of micro-electrodes,

participation in cognitive paradigms, and electrical stimulation delivered through depth electrodes. The internal review board of the University of Bonn provided approval for all conducted studies and procedures.

6.2.2 fMRI localizer

One day prior to the implantation of depth electrodes, the parahippocampal place area (PPA) was localized using functional magnetic resonance imaging (fMRI). In order to reduce variability between measurements, each patient was measured at the same location in the same 1.5 T scanner (Siemens MAGNETOM Avanto). All measurements were conducted on a Monday around 6:30 pm ($\pm$ 3 h). Repetition time (TR) was set to 2.5 s and echo time (TE) was set to 45 ms.

Design

The fMRI localizer used a block design with three conditions (block types), namely, landscapes, animals, and faces. Each block consisted of 10 trials. A trial encompassed the presentation of a fixation cross (0.25 s), an image (1.0 s), and a black screen (jittered between 0.05 and 1.3 s). Depending on the condition, the image was either a landscape, an animal, or a face. The patient was asked to perform a one-back visual working memory task: When two consecutive images were identical, the patient had to respond with the thumb button of a response grip (a gun-shaped input controller by NordicNeuroLab, Bergen, Norway). In any other case the patient was to respond with the index-finger button. Each block included two one-back repetitions at pseudo-random positions within the block. The entire session encompassed 40 blocks per condition. Block order was chosen pseudo-randomly with two restrictions: First, two consecutive blocks could not be of the same condition. Second, each consecutive block-triplet had to include each of the three conditions. After the fMRI localizer, a T1 structural magnetic resonance image (MRI) was recorded.

Analysis

To estimate the PPA's location, the Matlab toolbox *spm12* was used. The acquired blood-oxygen-level dependent (BOLD) images were realigned, coregistered to the T1 structural MRI, and smoothed using a Gaussian kernel (full width at half maximum was 8 by 8 by 8 mm). The smoothed BOLD signal was used to model a canonical hemodynamic response function (HRF). The modeled HRF was used in a general linear model (GLM) to estimate how much the BOLD signal changes in response to the presented image

category. The difference between the beta (estimated signal change) for the landscape category and the beta for the animal category was used to calculate the t-statistic. To be able to evaluate the spatial extent of the PPA activation maps and to compare them between subjects, we used the AMPLE (activation mapping as percentage of local excitation) technique: The t-value map was thresholded at 60% of the maximum t-value within the PPA cluster (Voyvodic 2006; Voyvodic et al. 2009). To preserve relative differences in hemispheric laterality, the same t-value (the maximum between the left and the right PPA cluster) was used to threshold both (left and right) clusters (Voyvodic 2012). Betas were converted to *percent signal change* using the approach of the ArtRepair software suite (Mazaika 2009). Cohen's d was calculated according to the formula $\frac{2\times t}{\sqrt{df}}$, where df is the number of effective residual degrees of freedom.

6.2.3 Experimental setup

Macro-electrodes were connected to the data acquisition system (Neuralynx ATLAS system) via an ATLAS HC headbox (Neuralynx, Bozeman, MT). The headbox was also connected to the stimulator and permitted continuous recording during electrical stimulation. Two independent channels of a constant current stimulator (STG 4004, Multi Channel Systems, Germany) were utilized. The first channel was connected to the headbox's contacts that corresponded to the two most medial macro-contacts of the right PHC depth-electrode. The second channel was connected to the headbox's contacts that corresponded to the two most medial macro-contacts of the right amygdala depth-electrode. A recording PC was connected to the data acquisition system. The recording PC was running Neuralynx's data acquisition software Cheetah ATLAS (version 1.1.0) or Pegasus (version 2.1.1) to record data received from the ATLAS system.

The paradigm ran on a laptop computer connected to the stimulator's trigger input via a USB DAQ device (Measurement Computing's USB-1208FS). The stimulator was also connected to the recording PC. The connection to the recording PC was used to configure the pulse train delivered by the stimulator upon receiving a trigger input from the laptop. The laptop was connected to the ATLAS system's TTL input via a second DAQ device to send event signatures (such as stimulation onset) from the laptop to the ATLAS system.

Micro-electrodes were connected to the ATLAS system via headstage pre-amplifiers (CHET-10, Neuralynx, Bozeman, MT). The experimental setup is shown schematically in Fig. 6.1.

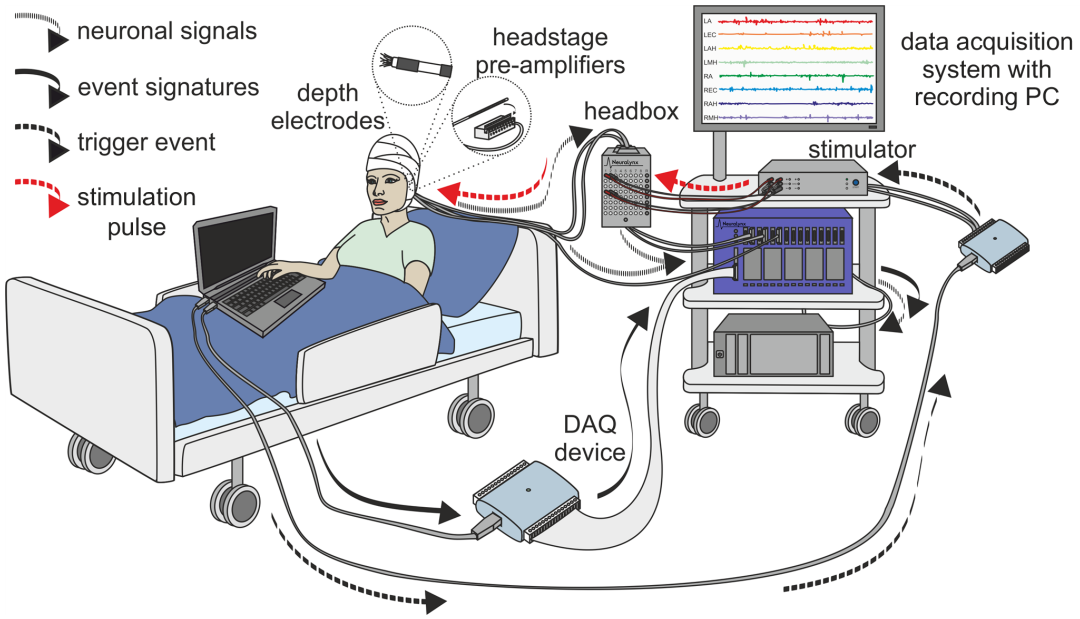

Figure 6.1: **Experimental setup**. See Section 6.2 for details. Figure adapted from Knieling et al. (2017). Permission for publication in this thesis was granted.

6.2.4 Experimental protocol

Pilot study

Before the experiment began, patients were instructed that they would have to categorize noisy images as either a landscape or an animal. In addition, they were asked to make a guess based on their gut feelings or thoughts when they are unable to recognize either category.

The experiment was implemented in Matlab (Mathworks) using the Psychtoolbox library (Brainard 1997; Pelli 1997; Kleiner et al. 2007). A trial comprised the presentation of a fixation cross (jittered between 0.3 and 0.6 s), a pre-stimulus mask (0.2 s), the stimulus image (0.17 s), a post-stimulus mask (0.2 s), and a self-paced forced-choice categorization task (see Fig. 6.2).

Masks were generated by applying various filters to random checkered patterns. Filters included motion blur, Laplacian of Gaussian, and unsharp masking. The stimulus image was a superposition of a random noise image with either a landscape or an animal image. The patient's task was to push the left arrow when the stimulus depicted an animal or the right arrow when the stimulus depicted a landscape.

Images of landscapes and animals have, on average, different low-level visual properties, such as brightness, contrast, and dominating spatial frequencies. Hence, prior to superpositioning, landscape and animal images were converted to grayscale and normal-

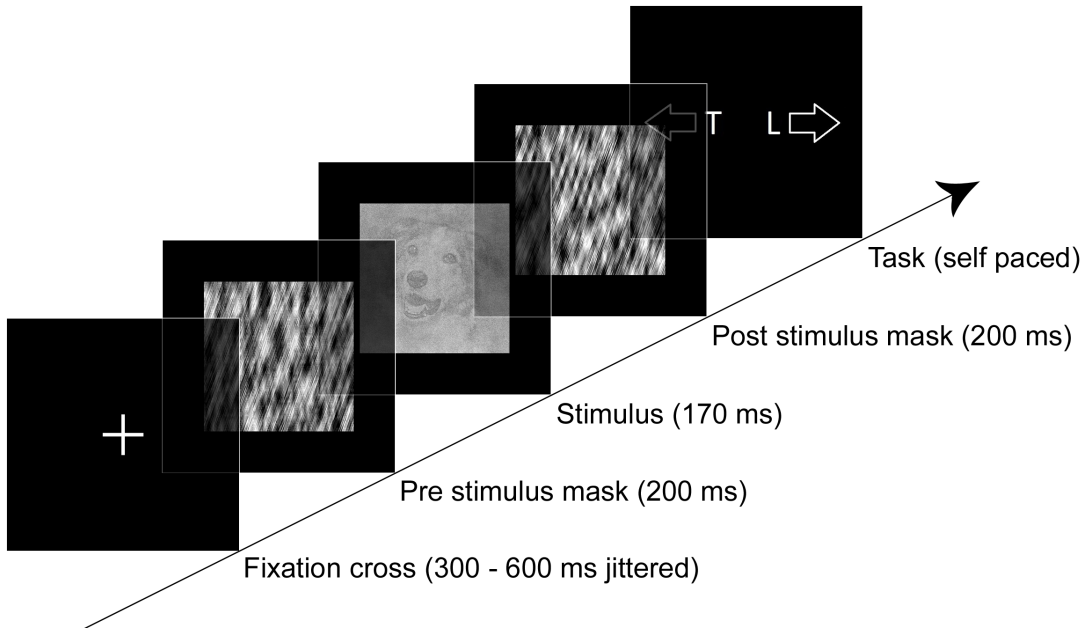

Figure 6.2: **Sequence of events in a trial**. The stimulus image is taken from the pilot study and depicts a superposition of a dog (80%) and random noise (20%).

ized for luminance and contrast using the SHINE toolbox (Willenbockel et al. 2010). Normalizing images for contrast adds a cloud-like noise to the image that made discrimination rather difficult for an untrained subject. Since it was not feasible to train patients in advance, we decided to use a rather long presentation time of 170 ms.

Stimuli were created according to the formula $G_s \times w_s + G_n \times (1 - w_s)$, where G_s are the grayscale values of either an animal or a landscape image, G_n are the grayscale values of a random noise image, and w_s is the weight (opacity) of the animal or the landscape image. The experiment included 114 unique animal images and 114 unique landscape images. For each superposition, w_s was randomly drawn (without replacement) from the vector W_s that included 228 weights. Sixty-eight of the weights in W_s were uniformly distributed between 0.95 and 0.785. Another 60 weights were uniformly distributed between 0.6 and 0.02. The remaining 100 weights were determined in a preliminary study. In the preliminary study, the remaining 100 weights were chosen by the psi method; an adaptive algorithm designed to pick weights that allow for an efficient estimation of both the threshold (i.e., inflection point) and the slope of a psychometric curve (Kontsevich and Tyler 1999; Kingdom and Prins 2016; Prins and Kingdom 2018). For each participant, a histogram of the weights that were chosen by the psi method was generated (bin size $= 0.005$). The average histogram of the 12 students who participated in the preliminary study was used to determine the 100 remaining weights for the pilot study.

The experiment included three conditions: No stimulation, amygdala stimulation, and PHC stimulation. Each of the 228 stimuli as well as 42 pure noise images were presented under each condition for a total of 810 trials per session. A session was divided into 3 consecutive runs. Each run included the presentation of all 270 stimuli in pseudo-random order. For each stimulus, there are six possible orders of which condition could be chosen in which run. Ensuring that each run included an equal amount of each condition, each stimulus was assigned an order drawn randomly (without replacement) from a vector including 270 / 6 = 45 instances of each of the six possible orders.

The micro-stimulation parameters reported to induce a behavioral effect in monkeys for this type of discrimination task would have caused a charge density of 800 $\mu C/cm^2$ at the surface of the platinum-iridium micro-electrodes used at our institution (Afraz et al. 2006). The threshold for faradayic charge transfer for platinum-iridium electrodes is between 50 and 100 $\mu C/cm^2$ (Rose and Robblee 1990). A charge density of 800 $\mu C/cm^2$ could create harmful oxidation and reduction products at the electrode's surface. Hence, stimulation was applied through the macro-contacts of the clinical depth electrodes instead of through the micro-wires. Thereby, a larger cluster of cells can be stimulated in a safer manner. Accordingly, stimulation parameters were based on previous macro-stimulation studies that reported behavioral effects in humans; a current amplitude of 1.5 mA, a pulse width of 200 µs, and a repetition frequency of 50 Hz (Arzy et al. 2006; Rauschecker et al. 2011; Parvizi et al. 2012; Mégevand et al. 2014). For the duration of the stimulation, we chose 120 ms; a compromise between the 54 ms used in Afraz et al. (2006) and the longer durations ($\geq$ 1 s) typically used for macro-stimulation.

Electrical stimulation of the PHC was applied at stimulus onset so that the electrically evoked potential (see, e.g., Chapter 4, Fig. 4.5) had the same latency as the potential evoked by visual stimulation using landscape images (approximately 125 ms after stimulus onset, see Mormann et al. 2017). Amygdala stimulation was applied 120 ms after stimulus onset as the average response latency of neurons in the amygdala is approximately 120 ms longer compared with neurons in the PHC (Mormann et al. 2008).

While positive reinforcement is frequently used in monkey research, we decided not to present feedback of whether or not the participant answered correctly. In case PHC stimulation induced a bias towards choosing the landscape category, repeated negative feedback might have weakened the effect.

After the experiment, patients were interviewed about their response behavior and whether they noticed the stimulation or anything unusual during the experiment.

Main study

After the pilot study, the instructions, the task, the stimuli, and the stimulation parameters were changed. Before the experiment began, patients were instructed that they would have to categorize images that each included the superposition of a semitransparent landscape and a semitransparent animal, based on which image (category) was more prominent.

Stimuli were created by superposing a landscape and an animal image according to the formula $G_l \times w_l + G_a \times (1 - w_l)$, where G_l are the grayscale values of a landscape image, G_a are the grayscale values of an animal image, and w_l is the weight (opacity) of the landscape. Each of the 114 animal and 114 landscape images was randomly paired twice to create a total of 228 superimposed stimulus images. For each superposition, w_l was randomly drawn (without replacement) from the vector W_l, which contained 228 normally distributed ($\mu = 0.5$, $\sigma = 0.16$) weights.

Except for the following changes, the design of a session and a run was kept identical to the pilot study. The number of trials per run decreased from 270 to 228. Duration and frequency of the stimulation were changed to 100 ms and 300 Hz, respectively. The stimulation's timing was changed to match the average latencies that the surrounding neurons respond with: in the amygdala 397 ms and in the PHC 271 ms after stimulus onset (Mormann et al. 2008).

6.2.5 Signal processing

Micro-electrode signals were sampled at 32,768 Hz, band-pass filtered between 0.1 and 9,000 Hz, and inverted before the data were saved to file.

Spikes

Spike detection and sorting was performed using the Combinato software package (Niediek et al. 2016). Several parameters were adjusted to improve the separability of artifacts from genuine action potentials.[1] Subsequent to the automated spike detection and sorting, manual adjustments were made to reject remaining artifacts and to correct for over- and under-clustering using Combinato's graphical user interface (GUI).

Instantaneous neuronal firing rates were calculated for each condition. For each single unit, a histogram of the unit's spike occurrences (relative to stimulus onset) was

[1] In *mask_artifacts.py*, *binlength* was set to 100, *max_spk_per_bin* was set to 150, and *min_dist* was set to 0.75. In *concurrent.py*, *BIN_MS* was set to 1. In *filters.py*, *DETECT_HIGH* was set to 3000. In *options.py*, *RecursiveDepth* was set to 2 and *MinInputSizeRecluster* was set to 500.

created, including all trials of the respective condition. The histogram's weighted average was calculated using a gaussian kernel ($\sigma = 0.1$ s). Instantaneous neuronal firing rates were obtained by multiplying the weighted average with the histogram's sampling rate (1000 Hz) and dividing it by the number of included trials. The standard error of the mean (SEM) was determined via bootstrapping (10,000 repetitions).

6.2.6 Statistical analysis

Statistical analyses were performed in *R*. A logistic regression analysis of the probability to respond with *landscape* was computed using a general linear mixed model (*glmer()* of the *lme4* package) from the binomial family (link = logit). Landscape opacity and condition were declared as fixed effects, while patient ID and stimulus ID were declared as random effects. Confidence intervals for odds ratios were estimated via bootstrapping, using 10,000 repetitions (*confint.merMod()* from the *lme4* package).

Response latency was modeled using a general linear mixed model of the Gamma family (link = inverse). Ambiguity, landscape opacity, and condition were declared as fixed effects, while stimulus ID was declared as random effect.

6.3 Results

6.3.1 Pilot study

Group results of the pilot study are presented in Table 6.1. Naturally, landscape opacity had a large effect on categorizing a landscape stimulus as a landscape. Stimulation of either the amygdala or the PHC showed no effect on categorization. Similar results were found for the animal stimuli (data not shown). Animal opacity had a large positive effect on categorizing an animal stimulus as an animal, while stimulation had no effect.

During piloting of this study, patients reported issues with the difficulty and ambiguity of the task. Out of 9 potential candidates, 4 patients were unable to perform the task correctly. The 5 remaining patients in the pilot study all reported that they were unsure how to respond to stimuli when they saw nothing but noise. Most of them used a fixed mental strategy, unlikely to be influenced by stimulation. Some strictly alternated left and right when they did not recognize a stimulus, others strictly chose the opposite category of the previous recognized stimulus.

Table 6.1: Generalized linear mixed model of the effect of PHC stimulation on landscape discrimination: Results of the pilot study.

			95% CI for odds ratio			
Fixed effects	**b**	**SE(b)**	**lower**	**odds ratio**	**upper**	**p**
Model: Pseudo $R^2 = .10^{HL} / .12^{CS} / .17^{N}$			Model χ^2 (5) = 1177.86 ***			
Intercept	−0.65	0.098				***
Landscape opacity	2.79	0.12	13.02	16.35	20.72	***
Stim. right amygdala	−0.028	0.057	0.87	0.97	1.09	0.63
Stim. right PHC	0.013	0.057	0.90	1.01	1.14	0.82
Random effects	**Groups**	**Variance**				
Patient ID (intercept)	5	0.011				
Stimulus ID (intercept)	115	0.12				

Patients = 5, observations = 9360. *** $p < 0.001$.
^{HL} Hosmer–Lemeshow
^{CS} Cox–Snell
^{N} Nagelkerke

6.3.2 Main study

After the pilot study, the task was changed to reduce ambiguity. Instead of adding noise to either a landscape or an animal, a landscape and an animal were superimposed using varying landscape opacities. The new task was to identify the more dominant image category. This change coincided with the first results of the stimulation-parameter study reported in Chapter 4. Hence, the stimulation frequency was increased, to have a stronger influence on the stimulated region.

Group results of the main study are presented in Table 6.2. Qualitatively, the results of the main study were similar to those of the pilot study. Neither amygdala nor PHC stimulation had an effect on the decision which category was more prominently represented in the stimulus. The effect of landscape opacity on choosing landscape increased considerably compared to the pilot study. This increase is likely caused by the change in stimulus composition. In the pilot study, a landscape opacity of zero would result in a random noise stimulus and cause the participant to make a random guess. In the main study, a landscape opacity of zero would result in a distinct animal stimulus and (disregarding lapses) cause the participant to respond with animal.

Table 6.2: Generalized linear mixed model of the effect of PHC stimulation on landscape discrimination: Results of the main study.

			95% CI for odds ratio			
Fixed effects	**b**	**SE(b)**	**lower**	**odds ratio**	**upper**	**p**
Model: Pseudo R^2 = .54 ^{HL} / .52^{CS} / .70 ^{N}				Model χ^2 (5) = 12160.34		***
Intercept	−6.64	0.29				***
Landscape opacity	13.16	0.29	2.66×10^5	5.21×10^5	8.69×10^5	***
Stim. right amygdala	0.033	0.055	0.93	1.03	1.15	0.55
Stim. right PHC	−0.063	0.055	0.84	0.94	1.05	0.25
Random effects	**Groups**	**Variance**				
Patient ID (intercept)	6	0.36				
Stimulus ID (intercept)	4485	2.59				

Patients = 6, observations = 16416. *** $p < 0.001$.
^{HL} Hosmer–Lemeshow
^{CS} Cox–Snell
^{N} Nagelkerke

6.3.3 Patient #08

Considering intersubject variability in brain anatomy and electrode trajectories, we also looked at each patient individually. In one patient (#08), PHC stimulation significantly biased the decision towards landscapes. Neither PHC nor amygdala stimulation showed an effect in any of the other patients. Patient #08's results are shown in Table 6.3.

A Friedman test ($p = 0.0090$) with post hoc Wilcoxon signed-rank tests ($p = 0.87$ for amygdala vs. no stimulation, $p = 0.0071$ for PHC vs. no stimulation, $p = 0.0097$ for amygdala vs. PHC stimulation) also showed a significant effect of PHC stimulation on patient #08. However, given that we found this effect in only one patient, we conducted several plausibility analyses.

A regression of #08's responses illustrates the effect's dependency on landscape opacity (see Fig. 6.3). The effect size peaks around the threshold of the psychometric curve (the point at which the response probability equals 0.5) of the PHC-stimulation condition. Depending on the regression kernel's bandwidth, the difference in response probability at the peak is approximately 7% to 10%.

A histogram of #08's response times is shown in Fig. 6.4. A general linear model (GLM) revealed several factors that influenced #08's response times (see Table 6.4): Ambiguity (meaning how close the stimulus was to a landscape opacity of 0.5) had the largest positive effect, followed by landscape opacity, followed by PHC stimulation.

Table 6.3: Generalized linear mixed model of the effect of PHC stimulation on landscape discrimination of patient #08.

			95% CI for odds ratio			
Fixed effects	**b**	**SE(b)**	**lower**	**odds ratio**	**upper**	**p**
Model: Pseudo R^2 = .67 ^{HL} / .60 ^{CS} / .80 ^{N}			Model χ^2 (4) = 2484.31 ***			
Intercept	−10.51	0.65				***
Landscape opacity	18.93	1.17	$2.26_{\times 10^7}$	$1.66_{\times 10^8}$	$4.10_{\times 10^9}$	***
Stim. right Amy.	0.024	0.16	0.76	1.02	1.39	0.88
Stim. right PHC	0.42	0.16	1.12	1.52	2.08	**
Random effects	**Groups**	**Variance**				
Stimulus (intercept)	884	5.64				

Patients = 1, observations = 2736. ** p < 0.01, *** p < 0.001.
^{HL} Hosmer–Lemeshow
^{CS} Cox–Snell
^{N} Nagelkerke

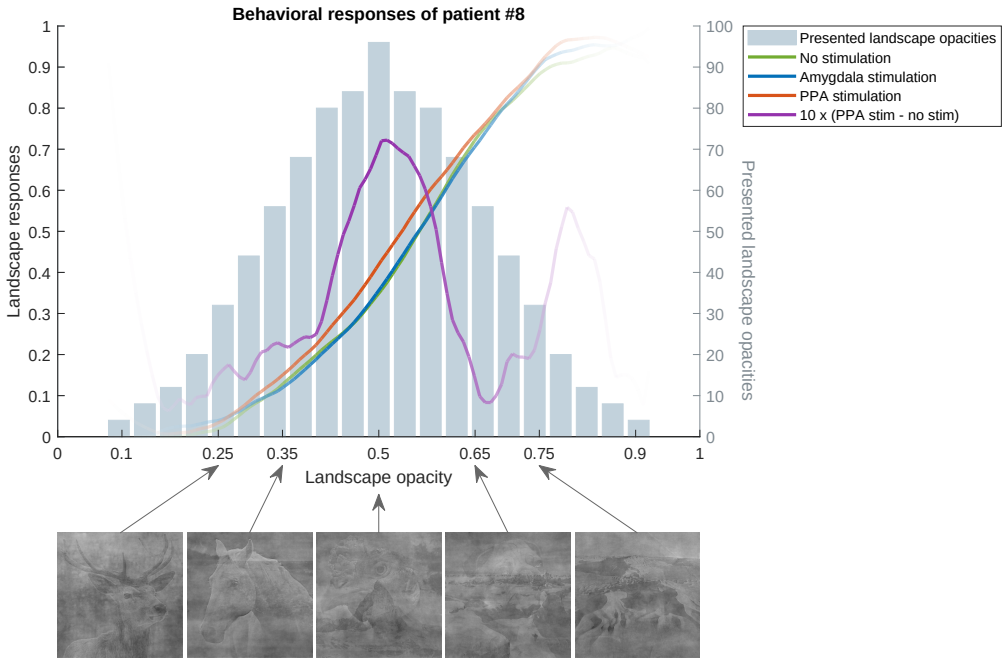

Figure 6.3: **Results of patient #08**. Visually-weighted Nadaraya–Watson kernel regression (Hsiang 2013) of #08's responses (bandwidth = 0.1). The purple line is the regression of the difference between PHC stimulation and no stimulation multiplied by 10 for better visualization. It peaks approximately at the threshold (i.e., inflection point)of the psychometric curve. The histogram depicts the distribution of presented landscape opacities.

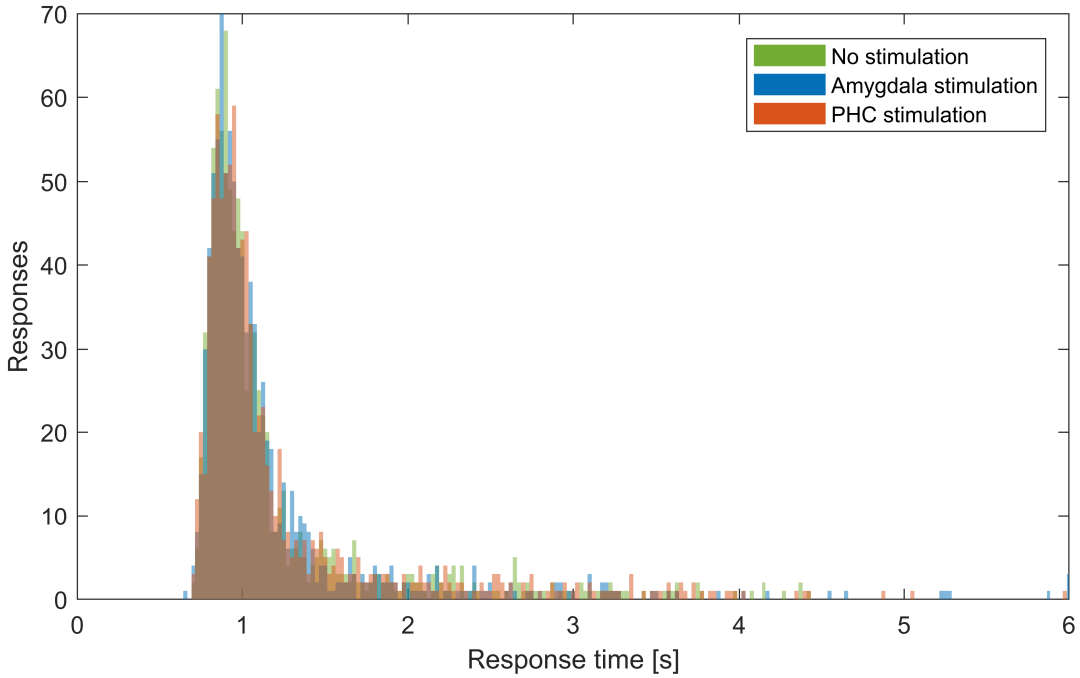

Figure 6.4: **Histogram of #08's response times**.

Amygdala stimulation had no detectable effect.

A regression of #08's response times illustrates their dependency on landscape opacity (see Fig. 6.5). The patient responded latest around the threshold of her psychometric curve, about 70 ms sooner to well distinguishable landscapes, and about 115 ms sooner to well distinguishable animals. PHC stimulation increased her response time to trials with higher landscape opacities. For the visually-weighted regression in Fig. 6.5A, response times were capped at 1.25 s to prevent the regression from being distorted by large response times. To examine if this manipulation of the data caused artificial effects in the regression, we computed the same regression on the ranks of the unaltered response times (see Fig. 6.5B). We also tested removing all three presentations of all stimuli with a response time greater than 1.5 s in any of the three conditions from the regression (data not shown). The effect of PHC stimulation on response times was still more prominent for higher landscape opacities.

Patient #08's neuronal firing rates in the PHC are shown in Fig. 6.6. At 300 Hz stimulation, signal distortions considerably impaired spike detection. Hence, the duration of the pulse train was cut out. Similar to the results of the study we reported in Chapter 4 (see Fig. 4.8), PHC stimulation was followed by a period of prolonged inhibition of neuronal firing (which was also observed in other patients). Amygdala stimulation had no noticeable effect on PHC neurons.

In order to evaluate if a PHC electrode is located close to tissue involved in processing

Table 6.4: Generalized linear mixed model of the effect of PHC stimulation on response times of patient #08.

Fixed effects	**b**	**SE(b)**	**p**
Model: Pseudo R^2 = .48 ^{HL} / .08 ^{CS} / .50 ^{N}	Model χ^2 (6) = 227.78 ***		
Intercept	1.23	0.051	***
Ambiguity †	−0.26	0.050	***
Landscape opacity	−0.21	0.061	***
Stim. right PHC	−0.028	0.011	* (0.011)
Stim. right Amy.	0.0080	0.011	0.88
Random effects	**Groups**	**Variance**	
Stimulus (intercept)	884	0.039	

Patients = 1, observations = 2736. * $p < 0.05$, *** $p < 0.001$.
^{HL} Hosmer–Lemeshow
^{CS} Cox–Snell
^{N} Nagelkerke
† Ambiguity $= 1 - 2 \times abs(w_l - 0.5)$, where w_l is landscape opacity.

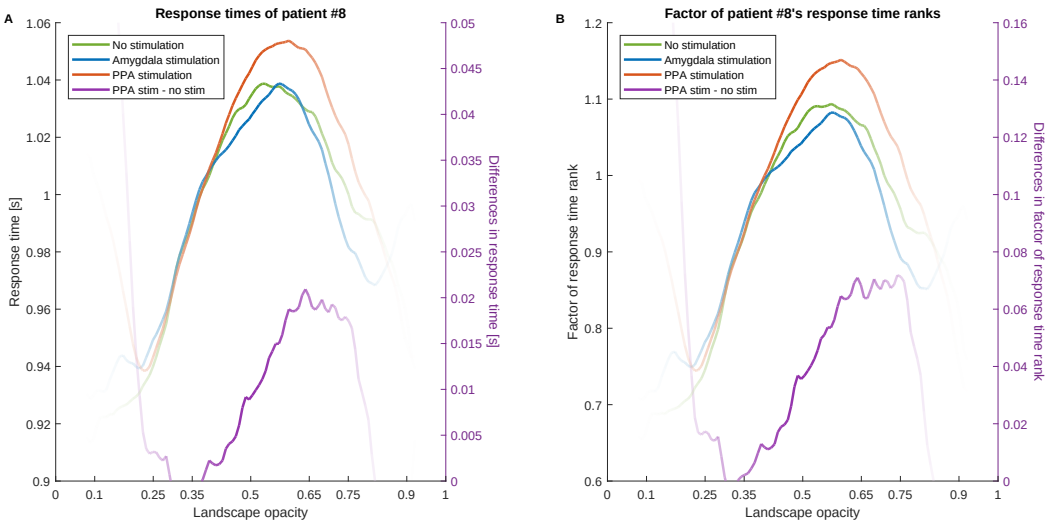

Figure 6.5: **Differences in #08's response times**. Visually-weighted Nadaraya–Watson kernel regression (Hsiang 2013) of #08's response times (bandwidth = 0.1). The purple line is the regression of the difference in response times between PHC stimulation and no stimulation. **A**: Regression of response times that have been capped at 1.25 s. **B**: Regression of the ranks of the response times divided by the average rank.

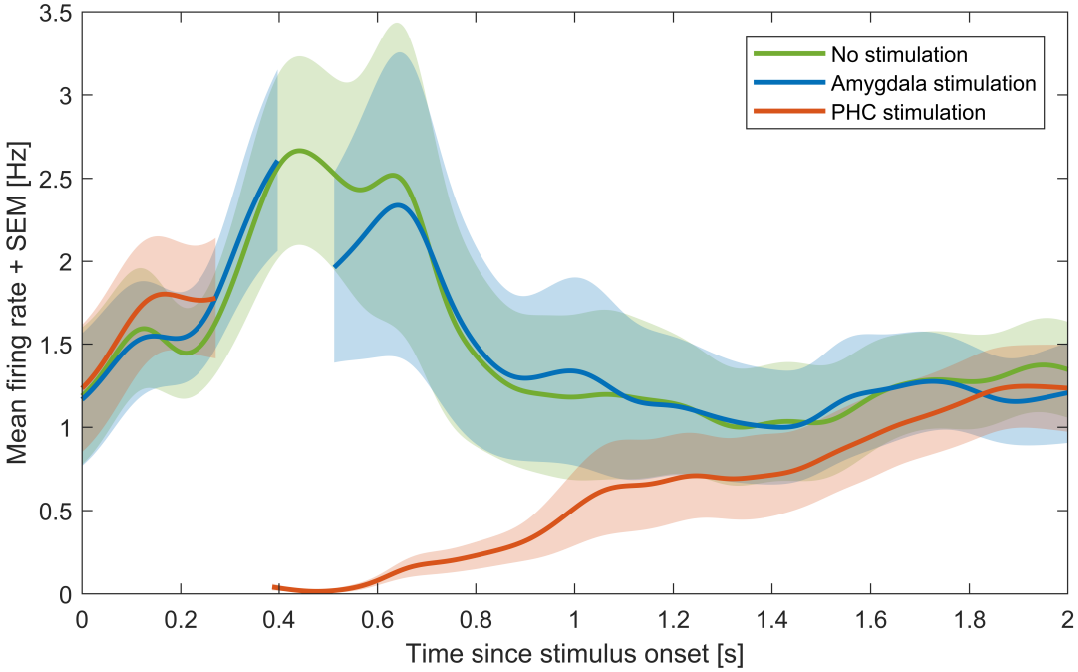

Figure 6.6: **Firing rates of #08's PHC neurons**. Firing rates were aligned to stimulus onset (t = 0 s). Shadows represent the standard error of the mean (SEM) across 18 units. The stimulation period was cut out, because spikes could not be reliably detected during 300 Hz stimulation.

landscapes, we ran an fMRI localizer one day prior to the implantation of depth electrodes. Figure 6.7 shows the position of #08's right PHC electrode. Both stimulation contacts are almost entirely inside her PPA's fMRI cluster.

6.3.4 Patient comparison

In Table 6.5 we compare patients based on their fMRI localizer results and their lapses during the stimulation study. Comparing ROI sizes and activation strengths between measurements or even subjects is difficult due to the large variability introduced by different scanners, experiments, experimental durations, repetition times, temperatures, and of course individual brain anatomy. We minimized variability by using the same scanner at the same location for each of our patients. Measurements were conducted during the same day of the week at around the same time (± 3 h). The number of blocks per condition and the number of trials per block were the same, although the overall duration varied minimally due to randomly jittered durations of the black screen between trials. To determine the extent of the ROI we used the AMPLE technique, which produces highly reproducible spacial patterns across measurements and subjects, while maintaining relative differences in hemispheric laterality (Voyvodic et al. 2009; Voyvodic

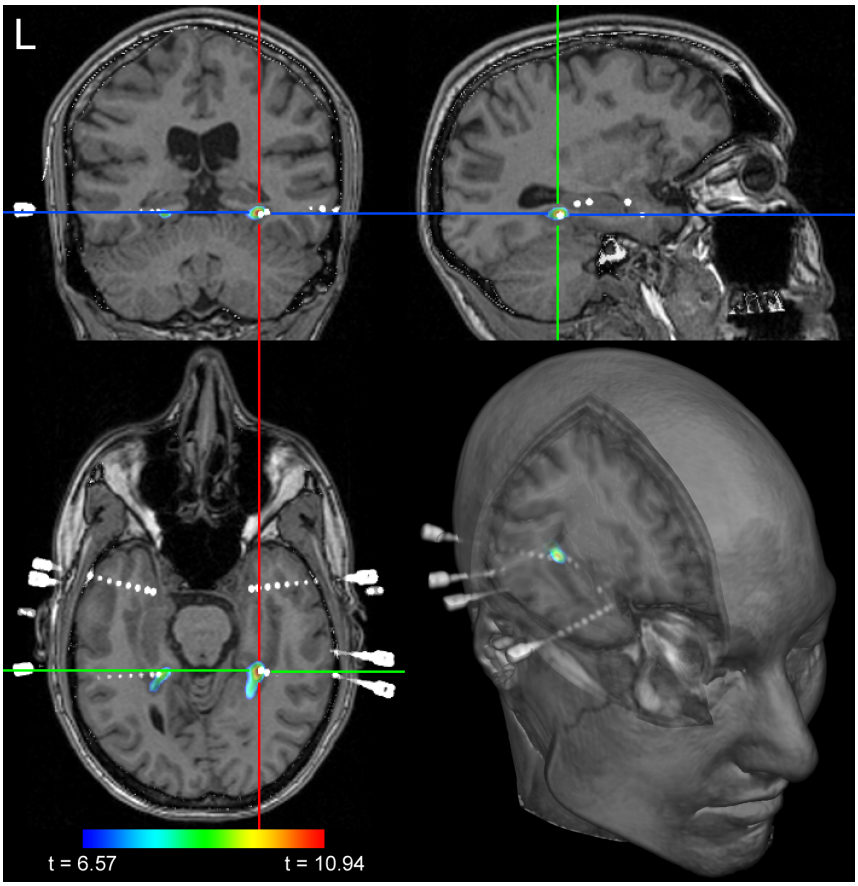

Figure 6.7: **Position of #08's right PHC electrode relative to her right PPA's fMRI cluster**.

2012). Peak-activation magnitudes are reported in percent signal change (PSC).

Note that despite using AMPLE, there is still considerable variability in PPA sizes across subjects. In part, this is caused by differences in hemispheric laterality. For example, in patient #03, right PPA activation was almost absent, especially compared to left PPA activation. Hence, no voxel in the right hemisphere surpassed the AMPLE threshold.

Patient #08 had the largest relative right PPA (0.97 ‰ of brain volume), which was almost twice as large as the next largest subject's. Furthermore, the distance between the stimulation contacts and the peak of activation was shorter than in any of the other subjects (3 mm). Her lapse rate (2.98%) was among the lowest, indicating careful attention to the task.

After the experiment, patients were asked if they had noticed the stimulation or something unusual during some of the trials. In the pilot study, one patient (#05) noticed something but thought it was a malfunctioning light. She only made the connection to the stimulation after the experiment, when (to her) the light was no longer flickering

Table 6.5: Differences in fMRI clusters and experimental performance between patients.

Patient ID	Size [‰]	Cohen's d	PSC	Distance [mm]	Lapses [%]
#01	n/a	n/a	n/a	n/a	9.07
#02	0.53	0.56	0.74	14.80	6.37
#03	0.0	n/a	n/a	n/a	3.68
#04	0.33	0.37	0.48	6.51	15.44
#05	0.25	0.51	0.77	4.93	4.90
#06	0.41	0.48	0.67	5.72	11.90
#07	0.072	0.42	0.56	8.86	9.52
#08	0.97	0.74	0.64	3.02	2.98
#09	0.35	0.35	0.41	5.16	2.38
#10	0.067	0.79	0.86	10.10	7.74
#11	0.54	0.68	0.60	7.51	1.79

Results of the pilot study are depicted on a white background while results of the main study are depicted on a gray background. Size is given in ‰ of subject's brain volume. Distance marks the distance from the electrode's center of mass to the PSC maximum within the right PPA fMRI cluster. Lapses states the percent of miscategorized trials for landscape opacities above 0.8 or below 0.2. No fMRI localizer was performed with #01, and no right PPA cluster was found in #03.

PSC Percent signal change

(see Chapter 4). In the main study, one patient (#09) reported that she noticed the stimulation (see Chapter 4).

6.4 Discussion

In this study we investigated the influence of PHC and amygdala stimulation on a categorical discrimination task. As expected, we found no evidence that short stimulation of the amygdala had an effect on discriminating between animals and landscapes. For short PHC stimulation, results are more ambivalent.

At the group level, we found no evidence that PHC stimulation had an effect on discriminating between animals and landscapes. However, after comparing our patients' post-operative CT scans with their pre-operative fMRI activation maps, we found that in most cases, electrodes were not located in an area of increased scene selectivity. Afraz et al. (2006) reported that category selectivity of the stimulated tissue was a prerequisite for inducing a behavioral bias. They further noted that the size of the category-selective tissue was a predictor for the effect size of the induced bias.

When looking at each patient's results individually, there was no patient whose categorical discrimination was affected by amygdala stimulation. However, there was one

patient whose categorical discrimination was affected by PHC stimulation. She showed a significant increase in landscape responses. In accordance with the findings of Afraz et al. (2006), she was also the patient that had the largest PPA fMRI cluster (using AMPLE), and her PHC electrode was closer to the PPA cluster's peak activation than in any of the other patients. She also had a low lapse rate, indicating that she was actively attending the experiment.

While the effect size of PHC stimulation was small (odds ratio = 1.52), it was nevertheless highly significant ($p = 0.0072$). Further investigation revealed that the effect depended on the ambiguity of the stimulus. The effect was largest (an increase in response probability of 7% to 10%) at the threshold of her psychometric curve (when her probability to respond with landscape was about 50%). It is plausible that an effect to influence a decision would have its highest impact when subjective uncertainty is at its highest.

Her response time, too, was dependent on landscape opacity. She responded fastest (about 920 ms) to well-distinguishable animals, about 45 ms slower to well-distinguishable landscapes, and about 115 ms slower around the threshold of her psychometric function (when her uncertainty was highest). It is known that response times to animals are shorter than to scenes (Crouzet et al. 2012); a phenomenon that could be caused by evolutionary pressure (New et al. 2007). Patient #08's response times increased in response to PHC stimulation. Interestingly, this effect seems to have been restricted to stimuli in which a landscape was the more prominent image.

Note that none of our patients reported visual hallucinations of scenes as described by Mégevand et al. (2014). One reason could be that in most of our patients, stimulation contacts were not inside the PPA. Another reason could be that our stimulation durations were much shorter by comparison. However, we also tested equally long durations with some of our patients. The only patient who reported a visual percept other than a simple phosphene (see Chapter 4) was #11. She reported that her visual field drifted apart vertically, possibly similar to a vertical binocular disparity. A transcript can be found in Appendix A.3.

In summary, while we found only one patient who was affected by PHC stimulation, we found no evidence that would cast doubt on the validity of her results. The stimulation electrode was located in landscape-selective tissue. Stimulation delivered through these contacts altered local firing rates, which coincided with a higher likelihood of her categorizing a stimulus as a landscape. Based on our discussion in Chapter 4 (see Section 4.4.3), we hypothesize that during stimulation (at least in the beginning of the pulse train), a large number of axons and possibly somas were excited, followed by a

longer lasting (about 1.5 s) inhibition of neuronal activity. This temporary inhibition of the PPA (an area that processes landscapes) could have caused the increased response time to ambiguous stimuli with a predominant landscape component.

6.5 References

Afraz S.-R, Kiani R, and Esteky H (2006). *Microstimulation of inferotemporal cortex influences face categorization*. Nature 442.7103:692–695.

Arzy S, Seeck M, Ortigue S, Spinelli L, and Blanke O (2006). *Induction of an illusory shadow person*. Nature 443.7109:287.

Barrash J, Damasio H, Adolphs R, and Tranel D (2000). *The neuroanatomical correlates of route learning impairment*. Neuropsychologia 38.6:820–836.

Brainard DH (1997). *The Psychophysics Toolbox*. Spatial Vision 10.4:433–436.

Corkin S, Amaral DG, González RG, Johnson KA, and Hyman BT (1997). *H. M.'s Medial Temporal Lobe Lesion: Findings from Magnetic Resonance Imaging*. Journal of Neuroscience 17.10:3964–3979.

Crouzet SM, Joubert OR, Thorpe SJ, and Fabre-Thorpe M (2012). *Animal Detection Precedes Access to Scene Category*. PLoS ONE 7.12.

De Falco E, Ison MJ, Fried I, and Quian Quiroga R (2016). *Long-term coding of personal and universal associations underlying the memory web in the human brain*. Nature Communications 7:13408.

Epstein R and Kanwisher N (1998). *A cortical representation of the local visual environment*. Nature 392.6676:598–601.

Hsiang S (2013). *Visually-Weighted Regression*. SSRN Scholarly Paper ID 2265501. Rochester, NY: Social Science Research Network.

Kingdom FAA and Prins N (2016). *Psychophysics: A Practical Introduction*. 2 edition. Amsterdam: Academic Press. 346 pp.

Kleiner M, Brainard D, and Pelli D (2007). "What's new in Psychtoolbox-3?" Talk. ECVP. Arezzo, Italy.

Knieling S, Niediek J, Kutter E, Bostroem J, Elger CE, and Mormann F (2017). *An online adaptive screening procedure for selective neuronal responses*. Journal of Neuroscience Methods 291:36–42.

Kontsevich LL and Tyler CW (1999). *Bayesian adaptive estimation of psychometric slope and threshold*. Vision Research 39.16:2729–2737.

Litman L, Awipi T, and Davachi L (2009). *Category-specificity in the Human Medial Temporal Lobe Cortex*. Hippocampus 19.3:308–319.

Mazaika P (2009). *Percent Signal Change for fMRI*. ArtRepair Software Documentation. Stanford Medicine.

Mégevand P, Groppe DM, Goldfinger MS, Hwang ST, Kingsley PB, Davidesco I, and Mehta AD (2014). *Seeing scenes: topographic visual hallucinations evoked by direct electrical stimulation of the parahippocampal place area*. The Journal of Neuroscience: The Official Journal of the Society for Neuroscience 34.16:5399–5405.

Mormann F, Dubois J, Kornblith S, Milosavljevic M, Cerf M, Ison M, Tsuchiya N, Kraskov A, Quian Quiroga R, Adolphs R, Fried I, and Koch C (2011). *A category-specific response to animals in the right human amygdala*. Nature Neuroscience 14.10:1247–1249.

Mormann F, Kornblith S, Cerf M, Ison MJ, Kraskov A, Tran M, Knieling S, Quian Quiroga R, Koch C, and Fried I (2017). *Scene-selective coding by single neurons in the human parahippocampal cortex*. Proceedings of the National Academy of Sciences of the United States of America 114.5:1153–1158.

Mormann F, Kornblith S, Quian Quiroga R, Kraskov A, Cerf M, Fried I, and Koch C (2008). *Latency and selectivity of single neurons indicate hierarchical processing in the human medial temporal lobe*. The Journal of Neuroscience: The Official Journal of the Society for Neuroscience 28.36:8865–8872.

New J, Cosmides L, and Tooby J (2007). *Category-specific attention for animals reflects ancestral priorities, not expertise*. Proceedings of the National Academy of Sciences of the United States of America 104.42:16598–16603.

Niediek J, Boström J, Elger CE, and Mormann F (2016). *Reliable Analysis of Single-Unit Recordings from the Human Brain under Noisy Conditions: Tracking Neurons over Hours*. PloS One 11.12:e0166598.

Parvizi J, Jacques C, Foster BL, Witthoft N, Withoft N, Rangarajan V, Weiner KS, and Grill-Spector K (2012). *Electrical stimulation of human fusiform face-selective regions distorts face perception*. The Journal of Neuroscience: The Official Journal of the Society for Neuroscience 32.43:14915–14920.

Pedreira C, Mormann F, Kraskov A, Cerf M, Fried I, Koch C, and Quian Quiroga R (2010). *Responses of human medial temporal lobe neurons are modulated by stimulus repetition*. Journal of Neurophysiology 103.1:97–107.

Pelli DG (1997). *The VideoToolbox software for visual psychophysics: transforming numbers into movies*. Spatial Vision 10.4:437–442.

Prins N and Kingdom FAA (2018). *Applying the Model-Comparison Approach to Test Specific Research Hypotheses in Psychophysical Research Using the Palamedes Toolbox*. Frontiers in Psychology 9.

Quian Quiroga R (2012). *Concept cells: the building blocks of declarative memory functions*. Nature Reviews Neuroscience 13.8:587–597.

Quian Quiroga R (2016). *Neuronal codes for visual perception and memory*. Neuropsychologia. Special Issue: Functional Selectivity in Perceptual and Cognitive Systems - A Tribute to Shlomo Bentin (1946-2012) 83:227–241.

Quian Quiroga R, Kraskov A, Koch C, and Fried I (2009). *Explicit Encoding of Multimodal Percepts by Single Neurons in the Human Brain*. Current Biology 19.15:1308–1313.

Quian Quiroga R, Mukamel R, Isham EA, Malach R, and Fried I (2008). *Human single-neuron responses at the threshold of conscious recognition*. Proceedings of the National Academy of Sciences 105.9:3599–3604.

Quian Quiroga R, Reddy L, Kreiman G, Koch C, and Fried I (2005). *Invariant visual representation by single neurons in the human brain*. Nature 435.7045:1102–1107.

Rauschecker AM, Dastjerdi M, Weiner KS, Witthoft N, Chen J, Selimbeyoglu A, and Parvizi J (2011). *Illusions of visual motion elicited by electrical stimulation of human MT complex*. PloS One 6.7:e21798.

Reber TP, Faber J, Niediek J, Boström J, Elger CE, and Mormann F (2017). *Single-Neuron Correlates of Conscious Perception in the Human Medial Temporal Lobe*. Current biology: CB 27.19:2991–2998.e2.

Rose TL and Robblee LS (1990). *Electrical stimulation with Pt electrodes. VIII. Electrochemically safe charge injection limits with 0.2 ms pulses*. IEEE transactions on bio-medical engineering 37.11:1118–1120.

Scoville WB and Milner B (1957). *Loss of Recent Memory After Bilateral Hippocampal Lesions*. Journal of Neurology, Neurosurgery, and Psychiatry 20.1:11–21.

Voyvodic JT (2006). *Activation mapping as a percentage of local excitation: fMRI stability within scans, between scans and across field strengths*. Magnetic Resonance Imaging 24.9:1249–1261.

Voyvodic JT (2012). *Reproducibility of single-subject fMRI language mapping with AMPLE normalization*. Journal of magnetic resonance imaging : JMRI 36.3:569–580.

Voyvodic JT, Petrella JR, and Friedman AH (2009). *fMRI activation mapping as a percentage of local excitation: consistent presurgical motor maps without threshold adjustment*. Journal of magnetic resonance imaging: JMRI 29.4:751–759.

Willenbockel V, Sadr J, Fiset D, Horne GO, Gosselin F, and Tanaka JW (2010). *Controlling low-level image properties: the SHINE toolbox*. Behavior Research Methods 42.3:671–684.

A. Transcripts of patients' stimulation-induced perceptions

The following tables reproduce interviews of patients regarding their evoked perceptions as a result of intracranial electrical stimulation. Interviews were conducted during or after exploratory stimulation sessions. In the english translation, slight adjustments were made to improve readability. The german originals are mostly unedited. Hence, they contain grammatical errors and other mistakes frequently observed in a regular conversation. Additional information is given in italics. Patient statements are highlighted with a gray background.

A.1 Phosphenes induced by stimulation in the PHC, close to the optic radiation.

The following transcripts regard Chapter 4.

Table A.1: Interview with patient #01 - english translation.

Person	**Statement**
FM	Please describe your perception.
#01	Whenever stimulation is applied, my left eye has slightly impaired vision. It is of slight reddish color. First I thought it came from the ceiling lights, because looking into a light for too long also impairs vision for a bit. But this *(the stimulation induced percept)* is all the time. It's flickering for about a second, then it's gone, then it's back, then gone again. In a constant rhythm.
Comment	*The interview was conducted during a preliminary stimulation-parameter screening, during which stimulation was applied every 2 to 3 seconds.*
FM	And can you still see and recognize things?
#01	Yes, I can see everything.
FM	You see everything as usual with the exception that it flickers?

This table continues on the next page.

Table A.1: Interview with patient #01 - english translation. (continued)

Person	**Statement**
#01	Yes, it just flickers, but only on the left side.
FM	Is it only on the left eye?
#01	Yes, only on the left eye.
FM	And if you close your left eye and keep the right one open?
#01	It's still flickering. Even with the left eye closed.
FM	Meaning it's not on the left eye but in the left field of view in both eyes, correct?
#01	Yes, that might be it.
FM	Yes.
#01	Yes, it's still flickering.
FM	And if you close the right eye?
#01	And open the left one?
FM	Exactly. It probably still appears only on the left side, correct?
#01	Yes, not on the right side, but on the left.
FM	Ok. This means it's on both eyes but only on the left side.
#01	Yes.
#01	We just compared, right?
SK	Yes.
#01	I was asked to say something, whenever I saw it. Now a bit. Now.
FM	But, for example, you can see the door to your right out of the corner of your eye, without looking directly at it?
#01	Yes. Yes, I can see that.
FM	And if someone were to enter, you could see them?
#01	Yes, I would.
FM	Even during stimulation? And you said it's reddish?
#01	I feel like it's a bit reddish. If I had to assign a color to the flickering. Slightly.
FM	Ok. Could you please tell us again when you notice it?
#01	Ok.
Comment	*We compared the temporal occurrence of stimulation artifacts in the recording to her reports. The monitor was facing away from the patient, so the signal was not visible to them.*
#01	A bit just now.
#01	Now a bit.
#01	Again a bit.
#01	Now.
#01	Now.
FM	Excellent. Thank you very much.
Comment	*A stimulation artifact was observed just prior to each report.*

FM = Prof. Dr. Dr. Florian Mormann. SK = Simeon Knieling

Table A.2: Interview with patient #01 - german original.

Person	**Aussage**
FM	Beschreiben Sie mal was Sie merken.
#01	Ja, also, ich merke, wie der Kollege auch schon gesagt hat, immer wenn ich Stimulation bekomme, auf dem linken Auge, em, ja, ne leichte Sehstörung ist das. Es ist leicht rötliche Farbe irgendwie, aber ich dachte es kommt erst weil die Lichter am scheinen waren *(zeigt auf die Lampen in der Decke)* und wenn man zu lange ins Licht guckt, dann flackert das ja so ein Bisschen nach. Aber das ist die ganze Zeit. Ja, das ist immer für so eine Sekunde kommt das, flackert das auf, dann ist weg, dann kommt's wieder, dann kommt's wieder.
Kommentar	*Das Interview wurde während eines preliminären Stimulationsparameter Screenings durchgeführt, in dem alle 2 bis 3 Sekunden ein Stimulus appliziert wurde.*
FM	Und können Sie dabei noch sehen, können Sie dabei noch Dinge erkennen?
#01	Ja, ich sehe alles.
FM	Sie sehen alles normal, es flackert nur?
#01	Ja, es flackert nur, und nur hier auf der Seite *(zeigt auf ihr linkes Auge)*.
FM	Nur auf der Seite. Ist es nur auf dem Auge oder?
#01	Ja, nur auf dem Auge. Ja.
FM	Wenn Sie jetzt mal das linke Auge zu machen und das andere auf lassen.
#01	Dann kommt das trotzdem.
FM	Dann kommt das trotzdem.
#01	Auch bei dem zuen Auge sozusagen.
FM	Heißt, es ist nicht auf dem linken Auge, sondern es ist auf der linken Seite der beiden Augen?
#01	Ja, das kann sein. Nochmal hier *(zeigt auf ihre linke Seite)*.
FM	Genau.
#01	Ja, das kommt trotzdem.
FM	Wenn Sie jetzt das andere Auge zu machen.
#01	Das linke wieder auf?
FM	Genau. Dann kommt es wahrscheinlich nur nach links, ne? Und nicht da wo ich bin *(FM stand auf der rechten Seite des Bettes)*.
#01	Das ist nicht immer da. Ich muss abwarten *(wahrscheinlich folgten zu der Zeit ein paar unterschwellige Stimulationen hintereinander)*.
#01	Ja, jetzt kommt's. Genau, bei Ihnen nicht *(zeigt auf die rechte Seite, auf der FM steht)*. Aber da wieder *(zeigt auf ihre linke Seite)*.
FM	Ok. Genau. Das heißt, es ist auf beiden Augen, aber immer nur nach links gerichtet.
#01	Ja, ja. Wir haben eben schon mal verglichen *(zeigt auf SK)*, nicht war?
SK	Ja.

Diese Tabelle wird auf der nächsten Seite fortgesetzt.

Table A.2: Interview with patient #01 - german original. (continued)

Person	**Aussage**
#01	Immer wann ich das sehe, sollte ich sagen und, jetzt zum Beispiel. Jetzt ein bisschen. Jetzt.
FM	Und Sie können aber die Tür zum Beispiel, ohne das Sie jetzt direkt da drauf gucken, trotzdem sehen aus den Augenwinkeln *(die Tür war auf der linken Seite)*?
#01	Ja. Ja, ja, das sehe ich.
FM	Und wenn jemand reinkommen würde, würden Sie den sehen?
#01	Ja würde ich auch.
FM	Auch wenn es in dem Moment ist *[wenn stimuliert wird]*. Und Sie sagen es ist rötlich?
#01	Ich hab das Gefühl es ist ein Bisschen rötlich. Wenn man jetzt die Farbe beschreiben müsste, wie das flackert. So leicht.
FM	Ja. Und dann sagen Sie doch nochmal wann es da ist.
#01	Ok.
Kommentar	*Wir verglichen das Auftreten von Stimulationsartefakten in der Aufzeichnung mit den Berichten der Patientin. Die Rückseite des Monitors war zur Patientin gerichtet, so dass sie das Signal nicht sehen konnte.*
#01	Ein bisschen gerade.
#01	Jetzt ein bisschen.
#01	Nochmal ein bisschen.
#01	Jetzt.
#01	Jetzt.
FM	Super, vielen Dank.
Kommentar	*Allen Berichten über auftretende Phosphene ging ein Stimulationsartefakt mit kurzem Abstand voraus.*

FM = Prof. Dr. Dr. Florian Mormann. SK = Simeon Knieling

Table A.3: Interview with patient #02 - english translation.

Person	**Statement**
FM	Please describe what you feel or perceive.
#02	I see a flicker above my left eye, about here *(circles her hand around her upper left field of view)*.
FM	A flicker like a flash or lightning?
#02	Like a drop that splashes in every direction.
FM	Ok.
#02	It's not just one spike like lightning. It spreads towards different directions.

This table continues on the next page.

Table A.3: Interview with patient #02 - english translation. (continued)

Person	**Statement**
FM	And does it have a color?
#02	Bright, just bright, like sunlight. Bright sunlight. Or a camera's flash. Just bright.
FM	Do you also see it with your eyes closed?
#02	I don't know.
FM	May we try that? Would you close your eyes please?
Comment	*Patient closes her eyes.*
Comment	*Stimulation was applied.*
SK	Did you perceive this?
#02	No.
SK	Those were the same stimulation parameters for which you reported a percept earlier. I'll try slightly different parameters now.
Comment	*Stimulation was applied.*
#02	Could you repeat the stimulation?
Comment	*Stimulation was applied.*
#02	Yes, I perceived that. But it was very short and without paying attention I might have missed it.
SK	Now I will increase the stimulation's duration.
Comment	*Stimulation was applied.*
#02	Yes, it's above my left eye. As if it is behind my eyelid.
FM	Great, you can open your eyes now. Now we would like to conduct the experiment during which you'll have to press a key whenever you have this percept.
#02	Ok, great.
FM	Great.
Comment	*During a later exploratory session she refined her description of the percept:*
#02	Like when you take a brush with paint and swing it. Splashes of paint scatter across the wall.

FM = Prof. Dr. Dr. Florian Mormann. SK = Simeon Knieling

Table A.4: Interview with patient #02 - german original.

Person	**Aussage**
FM	So, dann schildern Sie doch mal, was Sie empfinden dabei; was Sie merken.
#02	Über dem linken Auge, hier oben irgendwo *(kreist mit der Hand über ihr linkes oberes Gesichtsfeld)*, sehe ich ein Zucken. Flackern.
FM	Flackern. So wie ein Lichtblitz? Oder?

Diese Tabelle wird auf der nächsten Seite fortgesetzt.

Table A.4: Interview with patient #02 - german original. (continued)

Person	**Aussage**
#02	Ja wenn man, als wenn man 'n Tropfen fallen lässt und der dann in alle Richtungen sich verteilt.
FM	Ach so.
#02	Also es ist nicht nur ein Zacken, wie bei einem Blitz sondern schon so in verschiedene Richtungen.
FM	Ja.
#02	Ja.
FM	Und, hat das eine bestimmte Farbe?
#02	Hell. Einfach helles; wie Sonnenlicht. Helles Sonnenlicht. Oder wenn man irgendwie fotografiert wird, Blitzlicht. So. Einfach nur hell.
FM	Sehen Sie das auch, wenn Sie die Augen zu machen?
#02	Das weiß ich nicht.
FM	Sollen wir das mal ausprobieren? Machen Sie mal die Augen zu.
Kommentar	*Patientin schließt die Augen.*
Kommentar	*Stimulation wird appliziert.*
SK	Haben Sie etwas gemerkt?
#02	Nein.
SK	Ok, das war die Parameterkombination, bei der Sie das erste mal etwas gemerkt haben. Ich gehe jetzt mal zu einer anderen. Jetzt.
#02	Machen Sie noch mal.
Kommentar	*Stimulation wird appliziert.*
#02	Ja. Hab ich gemerkt. Es war zwar nur ganz kurz und wirklich mit Aufmerksamkeit, sonst hätt man es nicht gemerkt.
SK	Ich stimuliere jetzt nochmal länger.
Kommentar	*Stimulation wird appliziert.*
#02	Ja. Dann ist es hier überm linken Auge. Wie, wenn es hinter dem Augenlid wäre.
FM	Prima, dann können Sie die Augen wieder auf machen. Und dann würden wir jetzt die Testung machen, wo Sie jedes mal eine Taste drücken wenn Sie etwas merken.
#02	Gut. In Ordnung.
FM	Prima.
Kommentar	*Während einer späteren explorativen Testung verfeinerte die Patientin ihre Beschreibung der Phosphene:*
#02	[*Es*] war eher wie son Farbklecks, wenn man Farbkleckse hinhaut *(sie bewegt ihren Arm als würde sie mit einem Pinsel Farbe an die Wand spritzen)*, der dann so spritzt, an die Seiten.

FM = Prof. Dr. Dr. Florian Mormann. SK = Simeon Knieling

Table A.5: Interview with patient #03.

Person	**Statement**
Comment	*There is no transcript of patient #03. She described her percept as a white flickering. Her description was otherwise comparable to that of patient #01.*

A.2 AVH induced by stimulation in Heschl's gyrus.

The following transcripts regard Chapter 5.

Table A.6: Interview with patient #01 - english translation.

Person	Statement
FM	Please describe what you perceive when we stimulate.
#01	Just now, I had the feeling as if someone tells me to turn right at the next light. Like in driving school.
FM	For that long?
#01	Yes, for that long. Then there was nothing. Then just a tone.
FM	A tone? High or low? How would you describe the tone?
#01	I can't really describe it. And then, after a while, the driving school thing again.
FM	Ok. And they were whole sentences? Meaning multiple words that made sense together?
#01	Yes *(nodding)*. And there were also names. Last names. Ms. so and so. But it was more like from back in school. At one point it might have been from elementary school.
FM	That's interesting. And you said sometimes there were tones. Pure tones like from a musical instrument or noise?
#01	For example during the elementary school thing it was a women's voice.
FM	And did you feel like you know or recognize these voices?
#01	I'm not so sure.
FM	Ok, thank you.

This table continues on the next page.

FM = Prof. Dr. Dr. Florian Mormann. SK = Simeon Knieling

Table A.7: Interview with patient #01 - german original.

Person	**Aussage**
FM	Gut, dann beschreiben Sie mal, wie die Empfindungen sind, die Sie haben, wenn wir stimulieren.
#01	Gerade kam vor allem, so hatte ich das Gefühl, mir würde jemand, wie in der Fahrschule, sagen, an der nächsten Ampel rechts abbiegen.
FM	Auch so lange?
#01	Auch wirklich so, wirklich so lange. Dann kam mal zwischendurch gar nichts. Dann kam einfach nur ein Ton.
FM	Ein Ton, hoch, tief? Wie würden Sie sagen ist der Ton?
#01	Kann ich gar nicht so beschreiben. Und dann kam nach einiger Zeit halt wieder diese Fahrschulsache.
FM	Ok. Und das waren ganze Sätze, also mehrere Wörter, die zusammen Sinn ergaben?
#01	Ja *(nickend)*. Was aber auch kam war Namen, also direkt den Nachnamen. Frau so und so. Aber es war mehr so aus Schulzeiten noch. Einmal war ich mir echt nicht sicher ob es nicht sogar in der Grundschule war.
FM	Das ist interessant. Und die Töne, also manchmal waren es Töne, waren das eher reine Töne, wie von einem Musikinstrument oder Geräusche?
#01	Zum Beispiel bei der Sache mit der Grundschule war es eine Frauenstimme.
FM	Und hatten Sie das Gefühl, dass Sie die Stimmen kennen oder erkennen?
#01	Ich bin mir nicht so ganz sicher.
FM	Ok, danke.

FM = Prof. Dr. Dr. Florian Mormann. SK = Simeon Knieling

A.3 Perceptual hallucinations induced by stimulation in the PHC.

The following transcripts regard Chapter 6.

Table A.8: Interview with patient #11 - english translation.

Person	**Statement**
SK	Ok, I'll try 0.5 seconds now.
Comment	*Stimulation was applied.*
SK	Did you experience a percept?
#11	*She shakes her head.*
SK	Ok, next we'll try 1 second. At 2 mA, 200 Hz and 200 µs.
Comment	*Stimulation was applied.*
#11	That was strange. The painting. Like they were closing. One painting and another. I can't explain it.
Comment	*The patient points to the painting on the wall and moves her palms vertically towards each other, as if her vision was recovering from a vertical binocular disparity.*
FM	So you saw the painting on the wall twice?
#11	Yes, I closed my eyes and when I opened them again, there were two paintings *(she gestured the vertical displacement again)*. Now I see as usual. When I open my eyes, there is just one painting. But during stimulation, there were two paintings when I opened my eyes. Now everything is ok. It was just during those two times when you stimulated.
SK	Were the paintings beside each other or on top of each other?
#11	On top of each other *(she holds her hands on top of each other at a certain distance, not overlapping)*.
SK	On top.
#11	Yes, like this *(she moves her hands vertically towards each other and back again)*. I can only explain it how I see it.
FM	You're doing very well.
#11	Without stimulation, everything is normal.
SK	Let's see if the percept changes when we alter the stimulation parameters. Next I'll try 1.5 mA for 2 seconds.

This table continues on the next page.

Table A.8: Interview with patient #11 - english translation. (continued)

Person	**Statement**
#11	Ok.
SK	Now.
Comment	*Stimulation was applied.*
#11	No *(she shakes her head)*.
SK	You didn't perceive anything?
#11	No.
SK	Ok, next we'll try with 2 mA again.
#11	Now the left side became darker. My vision was normal on the right side but on the left it was slightly darker.
SK	Yes. We are currently stimulating the right side.
#11	The right side was ok, but the left side was darker. But just slightly.
SK	Yes.
FM	This is not unexpected.
SK	Exactly. And the double image, did you see that again?
#11	No, that was ok.
SK	Ok. We'll try 3 seconds next.
#11	Oh now, I have the funny second painting thing again *(she repeats her previous hand gesture)*.
SK	Now there was a second painting on top again?
#11	Yes.
SK	Ok.
#11	In my native language I might be able to explain it a bit better. It's the first time that I'm having a percept like that. Now I look and it's normal. A normal painting. Independent of whether I have my eyes open or closed. But during stimulation. I don't know why. The left side was a bit darker. But now both sides are ok. During stimulation it was a bit darker. But only on the left. On the right side, everything was ok.
SK	Ok, let's try it again with the same parameters.
Comment	*Stimulation was applied.*
SK	Did you have the same percept?
#11	Now I don't know what I have. Too much today.
Comment	*The patient still seems in a good mood and it appears as if she is not physically exhausted but more at a loss of words due to the language barrier. Hence we continue.*
SK	But you definitely perceived something?
#11	Yes, I believe it was the double painting thing again. Without the darkening. But with the paintings a bit.
SK	Ok, next we'd like to try bilateral stimulation with those same parameters.
Comment	*Short break while setting up for bilateral PPA stimulation.*
SK	Now.

This table continues on the next page.

Table A.8: Interview with patient #11 - english translation. (continued)

Person	Statement
Comment	*Stimulation was applied.*
#11	Now it was faster. First painting and second painting. But it was peculiarly fast. I had just closed my eyes and then there were two paintings. Not just one like right now. There was one, I closed my eyes and when I opened them again, there were two paintings. Normally this is not possible *(she laughs amused)*. Normally, there should just be one painting. Yes, and it was too fast. When you clicked, it happened immediately. You clicked and immediately two paintings.
FM	Let's do it again.
Comment	*Stimulation was applied.*
#11	Yes, this is a funny and new experience *(laughing)*.
FM	Next, try to keep your eyes open during stimulation.
Comment	*Stimulation was applied.*
#11	Oh, with open eyes, the painting was turned around *(she spins her left and right index finger around each other in a circle)*. I can't explain it.
FM	The painting turned around?
#11	Yes, like.
SK	*(While handing her a piece of paper)* If this is the painting, can you show us what happened?
#11	Like turned around *(she turns the paper 180° about the horizontal axis)*. And the same happened with eyes closed. I opened them and there were two paintings. Now I kept my eyes open and the painting was like on the other side. My eye didn't do that. The painting did that.
SK	Now keep your eyes closed please.
Comment	*Stimulation was applied.*
SK	Did you experience any percept?
#11	Too dark. I didn't see anything.
FM	Now try to look at me.
Comment	*Stimulation was applied.*
#11	It was the same *(pointing at FM)*
FM	What happened?
#11	Two people *(laughing)*.
FM	You saw me twice?
#11	Yes.
SK	Again on top of each other, or beside each other?
#11	No, from bottom to top. Like, take this hand and immediately there is a second hand *(she gestured vertical displacement again)*. It was immediate. For example, you take two cards and put them behind each other. You pull one card down and immediately you'll see the other card below. One is gone and you see the other.
SK	An it happened immediately?

This table continues on the next page.

Table A.8: Interview with patient #11 - english translation. (continued)

Person	**Statement**
#11	Yes.
SK	Or did you observe the movement?
#11	No, it was so fast that I can only speculate.
FM	Suddenly it was different.
#11	Yes, it was automatic. But I want to see normal *(laughs)*.
FM	Don't worry, these effects are not persistent.
SK	Now we would try a slightly higher amplitude for which other authors reported that their patient saw scenes outside the patient room. We'll stimulate for two seconds.
Comment	*Stimulation was applied.*
FM	Did you feel anything?
#11	*(She shakes her head)*.
FM	No?
#11	No.
SK	Nothing at all?
#11	No.
SK	We'll try that one more time.
Comment	*Stimulation was applied.*
#11	*(Laughing)* I see running water in the painting.
FM	Water running down the painting?
#11	Yes, it's like. What is the word for it. People are standing and some are walking. What's it called?
FM	Moving?
#11	Yes, there is movement in the painting.
SK	Do you still see the running water?
#11	No.
FM	Could you look at me while we do it again?
#11	Yes.
Comment	*Stimulation was applied.*
#11	It was so fast. Its not like now, when I see normal. Its always this additional image. The movement. So fast. Now, everything is ok. I just heard the mouse click and it was immediate. No time, no nothing. Immediately another image. It's the first time I'm seeing something like that.
FM	Yes, it is very rare and very special.
#11	For example, in the painting, they all stand still but they move during stimulation. There are three "people" in the painting. Something like people, or a cat or I don't know.
Comment	*The painting was rather abstract, but it has three entities in it.*
FM	Yes, maybe. I also don't know what they are supposed to be.

This table continues on the next page.

Table A.8: Interview with patient #11 - english translation. (continued)

Person	**Statement**
#11	It wasn't like it is now. There was a bit of movement.
FM	And when you looked at me? Was there any movement?
#11	No, there was just the two images thing.
SK	Ok, let's try it again while looking at the painting. Is there movement again?
Comment	*Stimulation was applied.*
#11	*(While pointing at the picture and smiling)* Yes. The painting was beautiful. It's a pity I don't have a camera in my eyes, so I could take a picture. Then we could compare now and when you stimulate.
FM	And what was different? How did the painting change when we stimulated?
#11	There was movement and the painting was a bit more beautiful.
FM	What about the painting was more beautiful?
#11	It was faster. The two image thing *(she showed the vertical image displacement with her hands, similar to before)*.
SK	But there was nothing new added to the painting?
#11	No.
FM	There were these three entities?
#11	Yes.
SK	Ok, now lets change from bilateral stimulation to just the left side.
Comment	*Short break while setting up for left PPA stimulation.*
SK	Please look at the painting again.
Comment	*Stimulation was applied.*
SK	Did you experience the same percept?
#11	No *(shakes her head)*.
FM	You didn't feel anything?
#11	No.
SK	Ok, now let's try it again while looking at Prof. Mormann.
#11	Yes, it was the same. The two image thing.
SK	Ok, same as before, no difference?
#11	No.
FM	And with the same, you mean how the image was displaced?
#11	Yes.
FM	So it was not the same as usual.
#11	*(Laughs)* Yes, its different from usual. I prefer to see one person. But it is a new experience for me.
FM	Should we conclude here?
SK	There is one last thing I'd like to test. Using a lower frequency.
Comment	*Short break while changing the frequency to 50 Hz.*
SK	We are going to repeat the stimulation with a lower frequency now. If you have the same percept, it might change now. Maybe the separation is slower or starts flickering or something like that. Let's see.

This table continues on the next page.

Table A.8: Interview with patient #11 - english translation. (continued)

Person	**Statement**
Comment	*Stimulation was applied.*
SK	Did you perceive that?
#11	No.
SK	Let's try this bilaterally.
Comment	*Short break while setting up for bilateral PPA stimulation.*
Comment	*Stimulation was applied.*
SK	And now?
#11	Yes, now it was kind of slow. The two image thing. So slow. One and then the other *(again, she shows the vertical dissociation with her hands)* but slow. There was one image and the other image moved downwards *(she shows how the image moved downwards and then back up again)*.
SK	The second image moved downwards?
#11	Yes *(nodding)*.
FM	And it moved slower?
#11	Yes.
Comment	*Stimulation was changed to 25 Hz.*
Comment	*Stimulation was applied.*
SK	And now?
#11	No, nothing.
SK	I'll try again.
Comment	*Stimulation was applied.*
SK	Nothing?
#11	No *(shaking her head)*.
Comment	*Stimulation was changed to 4 seconds.*
Comment	*Stimulation was applied.*
SK	And now?
#11	No, everything was fine.
SK	Alright, so at 50 Hz it was slower and at 25 Hz it was gone. Even if we use the same number of pulses, meaning stimulating for 4 instead of 2 seconds. I think we can conclude at this point.
FM	Great.

FM = Prof. Dr. Dr. Florian Mormann. SK = Simeon Knieling

Table A.9: Interview with patient #11 - german original.

Person	**Aussage**
SK	Ok, ich probiere nochmal die halbe Sekunde, und zwar jetzt.
Kommentar	*Stimulation wird appliziert.*
Diese Tabelle wird auf der nächsten Seite fortgesetzt.	

Table A.9: Interview with patient #11 - german original. (continued)

Person	**Aussage**
SK	Haben Sie da etwas gemerkt?
#11	*Schüttelt mit dem Kopf.*
SK	Dann gehen wir mal auf eine Sekunde. Bei 2 mA, 200 Hz und 200 µs. Für eine Sekunde, jetzt.
Kommentar	*Stimulation wird appliziert.*
#11	Es war so komisch. Die Bilder. Wie zumachen. Die eine Bilder mit zweite Bilder. Ich kann das nicht so erzählen.
Kommentar	*Patientin zeigt auf das Bild an der Wand und bewegte ihre Hände vertikal aufeinander zu.*
FM	Also das Bild was an der Wand hängt war zwei mal da?
#11	Ja, so wie, ich mache Auge zu, offen und das Bild war zwei mal *(sie bewegte erneut ihre Hände vertikal aufeinander zu)*. So wie, jetzt ich sehe normal, egal ob ich zu mache oder auf, ein Bild. Aber in dieser Zeit *(während der Stimulation)*. Ich habe zu gemacht und offen, war zwei Bilder. Jetzt ist alles ok. Das war nur diese zwei mal. Diese, komische Zeit. Aber jetzt ist alles ok.
SK	Und die Bilder, waren die nebeneinander oder übereinander.
#11	Übereinander *(sie hält ihre Hände mit gewissem Abstand senkrecht übereinander)*.
SK	Übereinander.
#11	Ja, so wie eine, wie zweite so gehen *(sie bewegt ihre Hände vertikal aufeinander zu und wieder weg)*. Wie eine wie zweite. So ich kann das erklären, keine Ahnung wie. So wie ich das sehe.
FM	Das machen Sie gut.
#11	Ohne das *(die Stimulation)*, ist alles ok. Ich sehe normal.
SK	Ja, sie haben das gleiche gerade auch bei 1.5 mA beschrieben, als wir eine Sekunde stimuliert haben, ich gehe jetzt nochmal zurück auf 1.5 und diesmal probieren wir 2 Sekunden und schauen mal ob sich das was Sie dann spüren, also das was Sie dann sehen, ob sich das dann verändert.
#11	Ok.
SK	Jetzt.
Kommentar	*Stimulation wird appliziert.*
#11	Nein *(schüttelt den Kopf)*.
SK	Sie haben jetzt gar nichts gemerkt?
#11	Nein.
SK	Ok, dann probieren wir das nochmal mit 2 mA.
Kommentar	*Stimulation wird appliziert.*
#11	Jetzt war so, die eine Seite, diese Seite, Links? Ja. Die war so wie. Ein bisschen dunkler. Hier *(zeigt nach rechts)* ich habe normal gesehen, aber hier *(zeigt nach links)* ein bisschen dunkel. Die linke Seite.
SK	Aja. Wir stimulieren auf der rechten Seite.

Diese Tabelle wird auf der nächsten Seite fortgesetzt.

Table A.9: Interview with patient #11 - german original. (continued)

Person	**Aussage**
#11	Ja, rechte Seite war alles ok, normal. Aber diese, die linke war bisschen so, dunkel. Aber nur ein bisschen.
SK	Ja.
FM	Das passt.
SK	Genau. Und das mit dem Doppelbild, hatten Sie das wieder, oder?
#11	Nein, da war alles ok.
SK	Ok, dann probieren wir noch einmal das gleiche für 3 Sekunden aus. Und zwar jetzt.
Kommentar	*Stimulation wird appliziert.*
#11	Oh jetzt ich habe so komisch in die drücken die Auge, die komische zweite Bilder *(sie bewegt erneut ihre Hände vertikal voneinander weg)*.
SK	Jetzt ist wieder das Bild über dem Bild da?
#11	Ja.
SK	Ok.
#11	Ja, ich kann nicht so gut Deutsch. In meiner Muttersprache könnte ich das ein bisschen besser vielleicht erklären. Ich habe das erste mal so. Jetzt ich gucke, ist normal. Normal Bild. Egal ob ich mache zu oder offen. Aber diese *(zeigt auf Stimulator)*. Keine Ahnung warum. So wie mit diese eine Seite *(links)* war ein bisschen dunkel. Auch jetzt, ich gucke, beide Seite ist alles ok. In diese Zeit *(zeigt zum Stimulator)* war nur ein bisschen. Ein bisschen war dunkel. Nur diese Seite *(links)*. Diese Seite *(rechts)* ist alles ok.
SK	Ok, das würden wir jetzt nochmal probieren. Und zwar jetzt.
Kommentar	*Stimulation wird appliziert.*
SK	Und hatten Sie das gleiche wieder?
#11	Jetzt ich habe keine Ahnung was ich habe. Zu viel Heute.
Kommentar	*Die Stimmung der Patientin scheint weiterhin positiv. Sie erscheint nicht physisch erschöpft sondern eher etwas frustriert über die Sprachbarriere die es ihr erschwert ihre Erfahrung zu kommunizieren.*
SK	Also sie haben definitiv etwas gemerkt?
#11	Ja. Ich glaube da war das gleiche mit diesen Bildern. Mit der dunkel, nein. Dunkel war nur das eine Mal. Aber mit den Bildern ist ein bisschen.
SK	Ok, dann würde ich sagen, probieren wir es jetzt mal bilateral mit ansonsten gleichen Parametern.
Kommentar	*Kurze Pause während wir auf bilaterale PPA Stimulation umstellen.*
SK	Jetzt.
Kommentar	*Stimulation wird appliziert.*
#11	Jetzt war so schneller. Ein Bild wie zweite Bild. Aber da war so, komisch schnell. Ich habe nur Augen zu gemacht und da waren ein, zwei Bilder. Nicht nur eine, so wie jetzt aber eine; ich habe zu, offen *(Augen geschlossen und wieder geöffnet)*; und war ein und zwei *(Bilder)*.

Diese Tabelle wird auf der nächsten Seite fortgesetzt.

Table A.9: Interview with patient #11 - german original. (continued)

Person	**Aussage**
#11	Normalerweise das geht nicht *(lacht amüsiert)*. Normalerweise müsste nur ein Bild kommen. Ja und da war zu schnell. Der *(schaut auf SK)* hat nur gesagt mache und automatisch. Haben Sie gemacht und automatisch zwei Bilder.
FM	Machen wir noch einmal.
Kommentar	*Stimulation wird appliziert.*
#11	Ja das ist, schöne neue Sache *(lacht)*.
FM	Versuchen Sie mal die Augen aufzuhalten dabei.
Kommentar	*Stimulation wird appliziert.*
#11	Oh, ich habe offen Auge und der Bild war so umdrehen *(dreht linken und rechten Zeigefinger gegeneinander im Kreis)*. So. Ich kann das nicht *[beschreiben]*. So wie.
FM	Das Bild hat sich umgedreht?
#11	Ja. So wie.
SK	Wenn das Ihr Bild ist *(reicht der Patientin ein Blatt Papier)*.
#11	So wie umgedreht *(die Patientin dreht das Papier 180° um die horizontale Achse)*. Und so gleiche war mit den Augen zu. Ich habe offen und es waren zwei Bilder. Jetzt ich habe die *(Augen)* immer offen und das Bild war so wie; das hat nicht mein Auge gemacht sondern das Bild hat das gemacht. So wie andere Seite.
SK	Jetzt lassen Sie mal die Augen die ganze Zeit geschlossen.
Kommentar	*Stimulation wird appliziert.*
SK	Haben Sie jetzt etwas gemerkt?
#11	Zu dunkel, ich sehe nichts.
FM	Dann gucken Sie jetzt mal mich an.
Kommentar	*Stimulation wird appliziert.*
#11	Das war gleich *(zeigt auf FM)*.
FM	Was ist passiert?
#11	Dann diese zwei Foto. Zwei Personen *(lacht)*.
FM	Sie haben mich auf einmal doppelt gesehen?
#11	Ja.
SK	Und war das jetzt auch so, dass Sie ihn übereinander gesehen haben oder nebeneinander.
#11	Ne, das war von unten nach oben. So wie. Nehmen Sie ein Bild und sofort. Nehmen Sie diese Hand *(zeigt es mit ihren Händen)* und sofort kommt die zweite Hand. Das war so automatisch. Hast du eine genommen und eine rein da kann so schneller machen. Sum Beispiel ich nehme sind zwei Karten in eine Karte aber kannst du so machen *(zeigt mit Ihren Händen, dass die Karten in diesem Beispiel hintereinander sind)*. Nimmst du eine Karte und zweite Karte siehst du. Eine ist weg und zweite siehst du *(bewegt ihre vordere Hand nach unten weg)*.
SK	Und ging das sofort?
#11	Ja.
SK	Oder haben Sie gesehen, wie sich das verschoben hat?

Diese Tabelle wird auf der nächsten Seite fortgesetzt.

Table A.9: Interview with patient #11 - german original. (continued)

Person	**Aussage**
#11	Nein. Das ist so schnell, da kann ich nur so denken.
FM	Auf einmal war es so.
#11	Ja, da kann anderes nichts machen. Nur so. Aber das war auch automatisch. Ich habe nur geguckt und automatisch war. Aber ich will normal sehen *(lacht)*.
FM	Keine Angst, sie sehen auch gleich wieder normal.
SK	Wir würden es jetzt einmal etwas stärkere Parameter probieren, bei denen andere Autoren berichteten, das ein Patient plötzlich eine Szene gesehen hat. Die nichts mit dem zu tun hatte, was eigentlich im Raum war. Das würden wir jetzt mal ausprobieren, auch für zwei Sekunden etwas stärker. Und zwar jetzt.
Kommentar	*Stimulation wird appliziert.*
FM	Haben Sie da was gemerkt?
#11	*(Schüttelt mit dem Kopf)*.
FM	Ne?
#11	Nein.
SK	Gar nichts?
#11	Nein.
SK	Wir probieren das noch ein mal. Jetzt.
Kommentar	*Stimulation wird appliziert.*
#11	*(Lacht)* Ich sehe in diese Bild Wasser, das so die läuft.
FM	Das Wasser runter läuft?
#11	Ja, das so wie da. Wie heißt das. Da stehen alles. Andere die laufen. Wie heißt das?
FM	Bewegen sich?
#11	Ja, die bewegen da in diese Bild.
SK	Sehen Sie das fließen jetzt immer noch?
#11	Nein.
FM	Können Sie jetzt noch einmal mich angucken und wir machen das noch einmal?
#11	Ja.
Kommentar	*Stimulation wird appliziert.*
#11	Das war so schnell. Das kommt immer was. Das ist nicht so wie jetzt ich sehe hier normal nur ist immer was, immer diese Bild dazu. Das Bewegen. Diese. So schnell. Jetzt ist alles ok. Machen Sie, ich habe nur gehört diesen gedrückt *(den Mausclick beim Drücken auf den Stimulationsbutton)* und es war automatisch. Ohne Zeit, ohne nichts. Automatisch war andere Bild. Das ist das erste mal, dass ich sehe sowas.
FM	Das ist was ganz seltenes, was besonderes.
#11	Zum Beispiel hier, die stehen alle und in dieser Zeit nur bewegen *(während der Stimulation)*. Da sind drei "Leute". Das ist so, Leute und eine Katze oder, keine Ahnung.
Kommentar	*Das Bild an der Wand ist recht abstrakt aber drei Entitäten sind darauf zu erkennen*

Diese Tabelle wird auf der nächsten Seite fortgesetzt.

Table A.9: Interview with patient #11 - german original. (continued)

Person	**Aussage**
FM	Ja vielleicht, ich weiß auch nicht *(was die Figuren auf dem Bild sein sollen)*.
#11	Und da hat bisschen bewegen. Da war nicht so wie jetzt. Bisschen bewegen.
FM	Und bei mir? Hat sich da was bewegt?
#11	Ne da war nur die Bild *(zeigt erneut das Doppelbild mit den Händen)* schnell.
SK	Ok, versuchen wir es noch einmal mit dem Bild. Das Sie auf das Bild schauen und ob sich das dann nochmal bewegt.
Kommentar	*Stimulation wird appliziert.*
#11	Ja *(zeigt auf das Bild und lächelt)*. Ja die Bild war so schön. Das ist blöd, dass ich keine Kamera habe hier *(zeigt vor ihre Augen und lacht)*. Dann könnte ich ein Foto machen und sehen so wie jetzt ist und so wie vorher ist.
FM	Und was war anders? Wie ist das Bild wenn wir stimulieren?
#11	Wie hier *(zeigt auf das Bild)*. Da war so schöner. Da bewegen und bisschen schöner diese Bild war. War bisschen anderes.
FM	Und was war schöner daran?
#11	Die schneller, die Bild, wir haben geguckt, diese Bild *(zeigt erneut die vertikale Separierung des Bildes)*. So Bild schneller machen. Eine nehmen und zweite gucken.
SK	Aber in dem Bild ist nichts neues hinzugekommen oder?
#11	Nein.
FM	Es waren diese drei Gestalten?
#11	Ja das was da. Ja.
SK	Ja gut, dann probieren wir noch einmal links alleine.
Kommentar	*Kurze Pause während wir auf linke PPA Stimulation umstellen.*
SK	Schauen Sie jetzt nochmal auf das Bild.
Kommentar	*Stimulation wird appliziert.*
SK	Hatten Sie jetzt die gleiche Empfindung?
#11	Nein *(schüttelt mit dem Kopf)*.
FM	Sie haben gar nichts gemerkt?
#11	Nein.
SK	Ok, dann schauen Sie doch nochmal auf den Prof. Mormann. Dann probieren wir es noch einmal.
#11	Ja, da war das gleiche. Diese Bild *(Verschiebung)*.
SK	Ok, also es gab da keine Unterschiede.
#11	Nein.
FM	Also das gleiche, damit meinen Sie, dass sich das Bild verschoben hat?
#11	Ja.
FM	Also es war schon was anderes als normal.
#11	*(Lacht)* Ja, das ist was anderes. Besser ich sehe normal eine Person. Aber das ist für mich auch was neues.
FM	Dann sind wir fertig oder?

Diese Tabelle wird auf der nächsten Seite fortgesetzt.

Table A.9: Interview with patient #11 - german original. (continued)

Person	**Aussage**
SK	Eine letzte Sache. Ich würde gerne die Frequenz reduzieren.
Kommentar	*Kurze Pause während wir die Frequenz auf 50 Hz ändern.*
SK	Also wir machen das jetzt noch einmal mit einer geringeren Wiederholungsrate. Also eventuell, wenn Sie das gleiche wieder sehen, könnte es sein, dass diese Separierung langsamer kommt, oder vielleicht flickert oder so. Schauen Sie mal. Jetzt.
Kommentar	*Stimulation wird appliziert.*
SK	Haben Sie da was gemerkt?
#11	Nein.
SK	Machen wir es jetzt nochmal beidseitig.
Kommentar	*Kurze Pause während wir auf bilaterale PPA Stimulation umstellen.*
Kommentar	*Stimulation wird appliziert.*
SK	Und jetzt?
#11	Ja jetzt war so langsam. Diese Bild für Bild. Ich habe vorher gesagt, diese Bilder. So langsam. So, eine für eine. Eine, dazu die zweite *(zeigt nochmal sehr deutlich mit den Händen die vertikale Dissoziation des Bildes)* aber da war langsam. Die eine kommt für eine *(zeigt wie das eine Bild langsam das andere überlagert, wie als würde man zwei Ebenen, die vertikal verschoben sind, wieder aufeinander schieben)*. Ich habe gesehen war eine und die zweite nach unten *(zeigt erneut wie das eine Bild sich nach unten bewegt um danach wieder zu einem Bild zu fusionieren)*.
SK	Die zweite bewegte sich dann nach unten?
#11	Ja *(kopfnickend)*.
FM	Und sie hat sich langsamer bewegt?
#11	Ja.
Kommentar	*Stimulation wurde auf 25 Hz geändert.*
Kommentar	*Stimulation wird appliziert.*
SK	Und jetzt?
#11	Nein. Nichts.
SK	Ich probiere es noch einmal.
Kommentar	*Stimulation wird appliziert.*
SK	Gar nichts?
#11	Nein *(kopfschüttelnd)*.
Kommentar	*Stimulation wurde auf 4 Sekunden geändert.*
Kommentar	*Stimulation wird appliziert.*
SK	Und jetzt?
#11	Ne, es war auch alles ok. Alles ok war es.
SK	Alles klar. Also bei 50 Hz war es dann langsamer. Bei 25 Hz war gar nichts mehr. Selbst wenn wir die gleiche Anzahl an Pulsen nehmen. Also jetzt anstatt 2, 4 Sekunden. Ok, dann sind wir durch.
FM	Prima.

FM = Prof. Dr. Dr. Florian Mormann. SK = Simeon Knieling

B. Acknowledgements

First, I would like to acknowledge each patient's bravery to undergo neurosurgery for diagnostic purposes and their selflessness to participate in scientific experiments to further our understanding of the human brain.

Second, I would like to thank Gert Dehnen and the monitoring unit of the Department of Epileptology for connecting the patients, monitoring their signals, and continuously improving signal quality.

Next, I would like to express a special thank you to Esther F. Kutter for her help in visualizing the setup schematics seen in Fig. 4.1, Fig. 5.1, and Fig. 6.1.

I am particularly grateful to Thomas P. Reber, Sina Mackay, Johannes E. Niediek, Gert Dehnen, and Alexander Unruh Piñeiro for their valuable comments and suggestions during the drafting of this thesis.

Moreover, I would like to thank everyone in the Mormann group for providing such a kind, friendly, and helpful work environment.

Furthermore, I'd like to express my appreciation to Florian Mormann for the opportunity to work in his group and for his valuable comments and suggestions during the drafting of this thesis.

In addition, I would like to extend my gratitude to Horst Bleckmann for taking the time to be the second reviewer in my doctorate committee. I enjoyed and appreciated his teachings and insights since the first semester of my Master's studies.

Finally, I'd like to thank my parents Ines and Ulrich Knieling as well as the rest of my family for their unwavering support.